8-2016

# Control-oriented modeling, validation, and analysis of a natural gas engine architecture

Chaitanya Panuganti
*Purdue University*

**PURDUE UNIVERSITY**
**GRADUATE SCHOOL**
**Thesis/Dissertation Acceptance**

This is to certify that the thesis/dissertation prepared

By Chaitanya Panuganti

Entitled
CONTROL-ORIENTED MODELING, VALIDATION, AND ANALYSIS OF A NATURAL GAS ENGINE ARCHITECTURE

For the degree of    Master of Science in Mechanical Engineering

Is approved by the final examining committee:

Gregory M. Shaver
Chair

Peter H. Meckl

Li Qiao

To the best of my knowledge and as understood by the student in the Thesis/Dissertation Agreement, Publication Delay, and Certification Disclaimer (Graduate School Form 32), this thesis/dissertation adheres to the provisions of Purdue University's "Policy of Integrity in Research" and the use of copyright material.

Approved by Major Professor(s):    Gregory M. Shaver

Approved by:    Jay P. Gore                                    7/18/2016
               Head of the Departmental Graduate Program              Date

CONTROL-ORIENTED MODELING, VALIDATION, AND ANALYSIS OF A

NATURAL GAS ENGINE ARCHITECTURE

A Thesis

Submitted to the Faculty

of

Purdue University

by

Chaitanya Panuganti

In Partial Fulfillment of the

Requirements for the Degree

of

Master of Science in Mechanical Engineering

August 2016

Purdue University

West Lafayette, Indiana

Dedicated to my parents and sister.

## ACKNOWLEDGMENTS

I would like to express my gratefulness to my adviser, Dr. Gregory M. Shaver, for his guidance throughout my research and coursework. I also wish to acknowledge Caterpillar Inc. for the support, active involvement, and the expertise they have provided since the beginning of the project. I would also like to thank my committee members, Dr. Peter H. Meckl and Dr. Li Qiao, for their feedback on my thesis. Finally, I'd like to thank my family for their support.

## TABLE OF CONTENTS

# LIST OF TABLES

## LIST OF FIGURES

Figure                                                                                      Page

# SYMBOLS

| | |
|---|---|
| $\omega$ | engine speed |
| $P_{im}$ | intake manifold pressure |
| $P_{bm}$ | boost manifold pressure |
| $P_{em}$ | exhaust manifold pressure |
| $\omega_{tc}$ | turbocharger speed |
| $L_{wg}$ | wastegate valve lift |
| $V_{wg}$ | wastegate valve velocity |
| $W_{thr}$ | throttle valve mass flow |
| $W_{byp}$ | bypass valve mass flow |
| $W_{fuel}$ | fuel mass flow |
| $J$ | engine inertia |
| $R, R_{im}, R_{bm}, R_{em}$ | specific gas constant of air |
| $V_{im}$ | intake manifold volume |
| $V_{em}$ | exhaust manifold volume |
| $V_{bm}$ | boost manifold volume |
| $T_{bm}$ | boost manifold temperature |
| $LF$ | load factor |
| $C_{trq}$ | engine torque gain |
| $\eta_v$ | volumetric efficiency |
| $\eta_{therm}$ | thermal efficiency |
| $Q_{LHV}$ | lower heating value of natural gas |
| $V_D$ | engine displacement volume |
| $AFR$ | air-fuel ratio |
| $T_{im}$ | intake manifold temperature |
| $Trq_L$ | torque load on the engine |

| | |
|---|---|
| $T_{max}$ | maximum expected torque load on engine |
| $W_{cyl}$ | cylinder mass flow |
| $W_{comp}$ | compressor mass flow |
| $\rho_a$ | ambient air density |
| $d_c$ | compressor blade diameter |
| $\gamma$ | ambient air specific heat ratio |
| $T_a$ | ambient air temperature |
| $c_{p,a}$ | ambient air specific heat capacity |
| $a_1, a_2, a_3, a_4$ | nonlinear compressor mass flow coefficients |
| $g_1, g_2, g_3$ | linear compressor mass flow coefficients |
| $W_{turb}$ | turbine mass flow |
| $T_{em}$ | exhaust manifold temperature |
| $b_1, b_2, b_3, b_4, b_5, b_6, b_7, b_8$ | nonlinear turbine mass flow coefficients |
| $P_a$ | ambient air density |
| $C_1, C_2$ | linear turbine mass flow coefficients |
| $W_{wg}$ | wastegate mass flow |
| $CD$ | coefficient of discharge |
| $d_{wg}$ | wastegate valve diameter |
| $A_{wg}$ | wastegate valve flow area |
| $\rho_{is}$ | isentropic gas density at the throat of wastegate |
| $\gamma_{exh}$ | exhaust gas specific heat ratio |
| $U_{is}$ | isentropic velocity at throat of wastegate |
| $f_1$ | linear wastegate mass flow coefficient |
| $P_{comp}$ | compressor power |
| $\eta_{comp}$ | compressor efficiency |
| $h_1, h_2, h_3$ | linear compressor power coefficients |
| $P_{turb}$ | turbine power |
| $\eta_{turb}$ | turbine efficiency |
| $c_{p,exh}$ | exhaust gas specific heat capacity |

| | |
|---|---|
| $e_1, e_2$ | linear turbine power coefficients |
| $b_{tc}$ | turbocharger damping |
| $I_{tc}$ | turbocharger inertia |
| $\eta_{mech}$ | turboshaft mechanical efficiency |
| $m_{wg}$ | wastegate diaphragm mass |
| $A_d$ | wastegate diaphragm area |
| $k_{wg}$ | wastegate spring constant |
| $F_P$ | wastegate spring pretension force |
| $b_{wg}$ | wastegate diaphragm damping coefficient |
| $\alpha$ | engine angular acceleration |
| $Trq_{eng}$ | torque produced by engine |
| $M_{im}$ | mass of gas in intake manifold |
| $M_{bm}$ | mass of gas in boost manifold |
| $M_{em}$ | mass of gas in exhaust manifold |
| $Trq_{turb}$ | turbine torque on turboshaft |
| $Trq_{comp}$ | compressor torque on turboshaft |
| $\alpha_{tc}$ | turbocharger angular acceleration |
| $x_1$ | engine speed state variable |
| $x_2$ | intake manifold pressure state variable |
| $x_3$ | boost manifold pressure state variable |
| $x_4$ | exhaust manifold pressure state variable |
| $x_5$ | turbocharger speed state variable |
| $x_6$ | wastegate valve lift state variable |
| $x_7$ | wastegate valve velocity state variable |
| $x_8$ | fuel-air ratio state variable |
| $u_1$ | throttle valve mass flow input variable |
| $u_2$ | bypass valve mass flow input variable |
| $u_3$ | fuel mass flow input variable |
| $w$ | load factor |

# ABBREVIATIONS

AFR       air-fuel ratio

FAR       fuel-air ratio

MIMO      multi-input multi-output

SISO      single-input single-output

RGA       relative gain array

MPC       model predictive controller

PID       proportional-integral-derivative controller

ECU       engine control unit

ECM       engine control module

CNG       compressed natural gas

VGT       variable-geometry turbocharger

EGR       exhaust-gas recirculation

QFT       quantitative feedback theory

ABSTRACT

Panuganti, Chaitanya M.S.M.E., Purdue University, August 2016. Control-Oriented Modeling, Validation, and Analysis of a Natural Gas Engine Architecture. Major Professor: Gregory M. Shaver, School of Mechanical Engineering.

In order to improve performance and meet increasingly tight emissions regulations, engine manufacturers must improve algorithms used to control the engine. One possible strategy is to utilize centralized control algorithms that take into account the coupled interactions between inputs and outputs. Implementing a centralized control strategy often requires some kind of dynamic model of the system, which is a primary motivation for modeling efforts in this thesis. In a methodical fashion, this thesis derives a control model for a natural gas engine architecture and validates this control model against reference data in simulation. Additionally, this thesis performs control-oriented analysis on a state-space model provided by Caterpillar to determine the engine's suitability to decentralized control. Based on the results of the control-oriented analysis, the thesis demonstrates how a decentralized control framework can be implemented.

The first study declares a set of seven state variables that characterize the operation of the engine. The engine of interest runs on natural gas and is used in power generation applications. Additionally, this study models all mass flow rates and power terms as functions of the selected state variables. These models are then validated against truth-reference data. This study also explicitly states the assumptions and simplifications that correspond to each of the models.

The second study derives dynamic equations for each of the seven state variables via a first-principles approach. The dynamic state equations contain expressions for mass flow rates and power that were modeled in the first study. This study then numerically validates the entire state-space model by exercising control inputs from

reference data on it. Together, the seven state equations effectively serve as a control model that can be used for controller synthesis. The goal of the first two studies is to demonstrate a procedure for obtaining a control model for an engine architecture, not to obtain a high-fidelity simulation model.

The third study demonstrates control-oriented analysis on a state-space model provided by Caterpillar. The relative gain array (RGA) is used to show that the system is well-suited is for decentralized control. This study implements a decentralized control structure on the state-space model provided by Caterpillar and validates, in simulation, its ability to achieve reference tracking for desired outputs.

# 1. INTRODUCTION

The applications of internal combustion engines are vast and serve various aspects of society's needs. Both consumers and retailers rely upon these engines in areas ranging from transportation to power generation. There are various fuels that power internal combustion engines including gasoline, diesel, natural gas, and blends of these fuels. No matter what kind of fuel is used in an engine, its chemical potential energy can only be harnessed by combustion, and to do so there are two main types of combustion engines. Compression ignition (CI) engines rely upon high pressures to auto-ignite a fuel-air mixture, while spark ignition (SI) engines rely upon a spark plug to initiate the combustion process. Fuels such as diesel and dual-fuel blends have lower octane numbers and are easier to auto-ignite, so they are often used in CI engines. Fuels such as gasoline and natural gas have higher octane numbers and are harder to auto-ignite, so they are used in SI engines.

Other considerations for engine manufacturers are constraints imposed by consumer demand and governmental agencies. Consumers demand engines that perform well but are fuel-efficient so that they save money on fuel costs. Governmental agencies set emissions regulations that a manufacturer must meet. Natural gas is often regarded as a "clean fuel". Its advantages include high energy density compared to gasoline, and cleaner combustion properties from an emissions standpoint. The storage and availability of natural gas are issues from a consumer perspective, but not in stationary off-highway applications like power generation.

## 1.1 Motivation

In power generation applications, two important requirements are generating enough power to meet electricity needs and ensuring the engine speed is maintained

to produce current at the mains frequency, as mentioned in [1]. The controllers in an engine must be able to meet those requirements but also abide by respective federal emissions requirements. Control problems in the engine are often multifaceted. As mentioned in [2], a control problem that focuses on governing engine speed may have to meet lower level control constraints such as air-fuel ratio (AFR) targets. This means engine control problems that have a primary objective may very well feature secondary goals.

For example, in a throttle-governed automobile driven by a consumer, the driver pushes down on the gas pedal with the goal of increasing speed. Inside the engine, there are many secondary objectives that must be met to facilitate acceleration. There are also constraints that impose limits on how the engine operates while accelerating. This simple example illustrates the importance of control algorithm design in the context of vehicles, and more specifically engines. A primary motivation for this thesis is control-oriented modeling and analysis of a natural gas engine architecture with the high-reaching goal of control algorithm design.

## 1.2    Background Literature

Engine control problems are often multiple-input multiple-output (MIMO) in nature. Inputs are actuators that an engine control module (ECM) has direct control over, and outputs are control objectives. In MIMO systems, there can be a great deal of coupling between inputs and output as mentioned in [3]. The degree of coupling can often influence the type of control strategy that is selected. The three main categories of control structures include decentralized controllers, decoupling controllers, and coupled controllers. This section explains the control structures in detail and highlights the various engine control strategies used in academia and industry for the following control problems: managing air-handling, regulating fueling, and engine speed control.

### 1.2.1 Control Structures

**Decentralized Controller**

In decentralized control frameworks, each input is used to independently control one target output [4]. Such control structures feature an independent controller on every input-output pair, as shown in Figure 1.1. This works well for plants with minimal coupling interaction. In such plants, every input primarily affects one output, and has minimal effect on other outputs. The advantage of decentralized controllers is that they are easier to tune, particularly in industrial applications. In [5], researchers design a feedback-based spark timing controller. It is considered decentralized in the sense that spark timing is solely used to maximize fuel efficiency. Traditional spark timing controllers use an open-loop map to generate the maximum brake torque spark timing, but this paper uses five combustion phase indicators and a PI controller to optimize the spark timing.
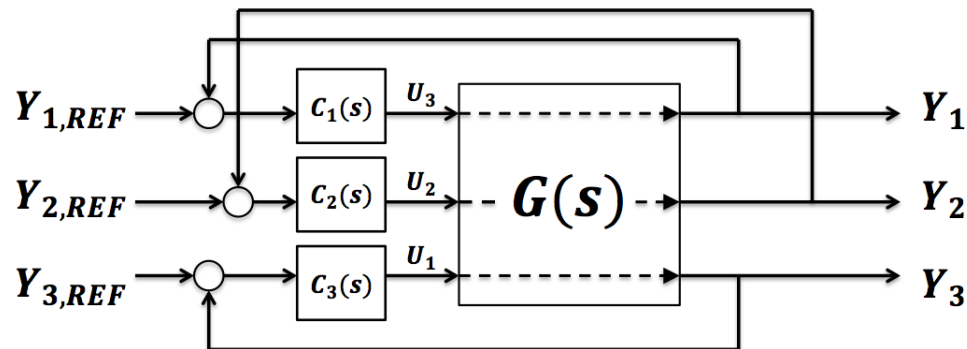


Figure 1.1. Example of decentralized control structure.

**Decoupling Controller**

Decoupled control frameworks use a decentralized control structure after mathematically decoupling plant dynamics, as shown in Figure 1.2. The plant dynamics

of a transfer matrix, $G(s)$, can sometimes be decoupled by means of a decoupling matrix. There are three main types of decoupling strategies discussed in [4]:

1. Dynamic decoupling: $G(s)$ is decoupled at all frequencies, $s = j\omega$.

2. Steady-state decoupling: The plant is decoupled at a frequency of zero.

3. Approximate decoupling: The plant is decoupled at a selected frequency, often the bandwidth frequency.

While appealing in theory, decoupling controllers can be difficult to implement.
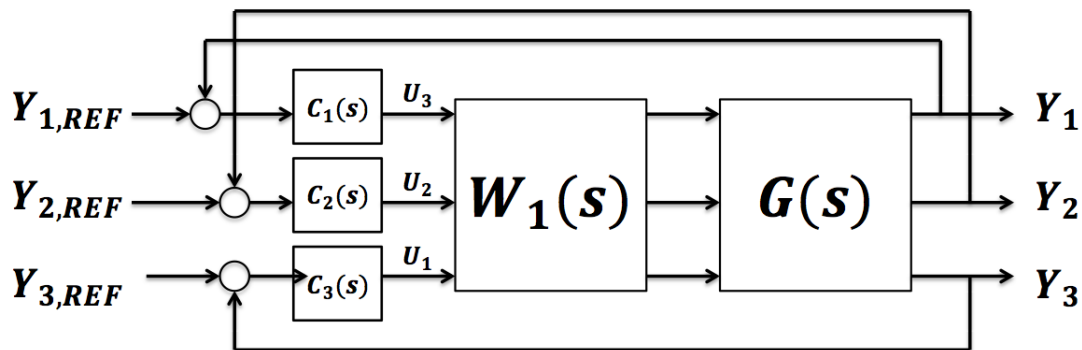


Figure 1.2.  Example of decoupled control structure with pre-compensator $W_1$.

Reference [6] summarizes a patent on a decoupling control framework for air-handling in a diesel engine. The engine architecture of this reference features an exhaust throttle valve, exhaust-gas recirculation (EGR), and a variable-geometry turbocharger (VGT). In diesel engines, the EGR and VGT are often key features of the air-handling system. The EGR valve allows exhaust gases to go back into the cylinders, which lowers combustion temperatures and reduces nitrous-oxide (NOx) emissions. In a turbocharger, a turbine is driven by exhaust gases and causes the compressor to induct more air on the intake side. A VGT can be altered geometrically, effectively allowing for control over charge flow into the boost manifold. For a fixed EGR valve position in the engine architecture of [6], a controller would ideally

use the exhaust throttle valve to control EGR mass flow and use the VGT to control charge flow. In reality, the air-handling system is quite coupled. The exhaust throttle valve position can affect charge flow, and the VGT can affect EGR mass flow rate. Figure 1.3 is a schematic from [7], and it shows an example of an engine architecture with high pressure EGR and a turbocharger. Researchers in [6] effectively
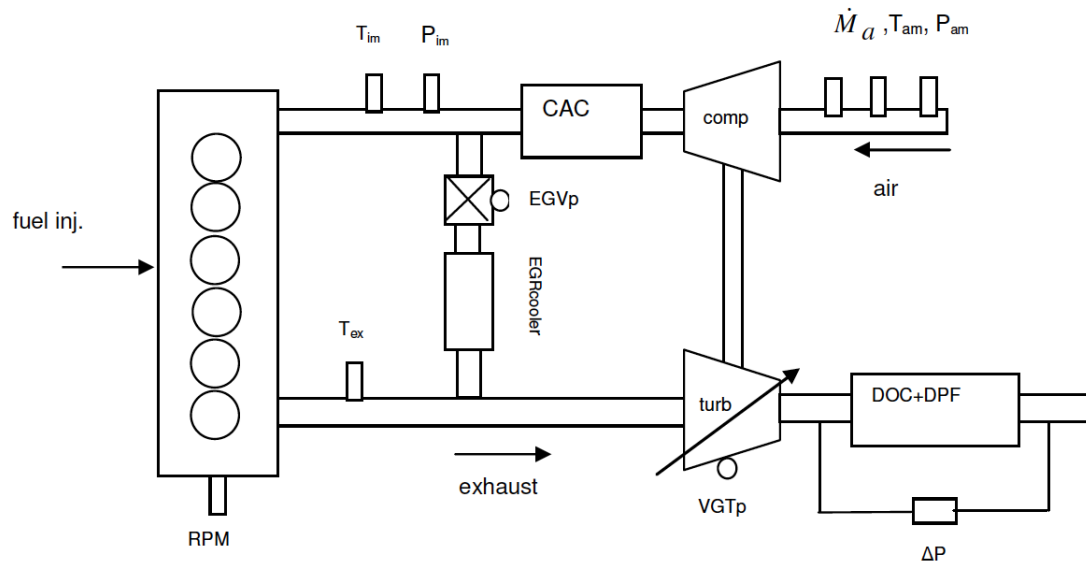


Figure 1.3. Engine architecture of reference [7] with turbocharger and EGR.

design a transformed coordinate system in which, for a given EGR valve position, transformed EGR fraction is decoupled from VGT position and transformed charge flow is decoupled from exhaust throttle position. Controller design is then done in this transformed coordinate system to allow for the implementation of a decentralized controller. Figure 1.4 shows a block diagram from the patent that is representative of the coordinate transform manager within the controller.
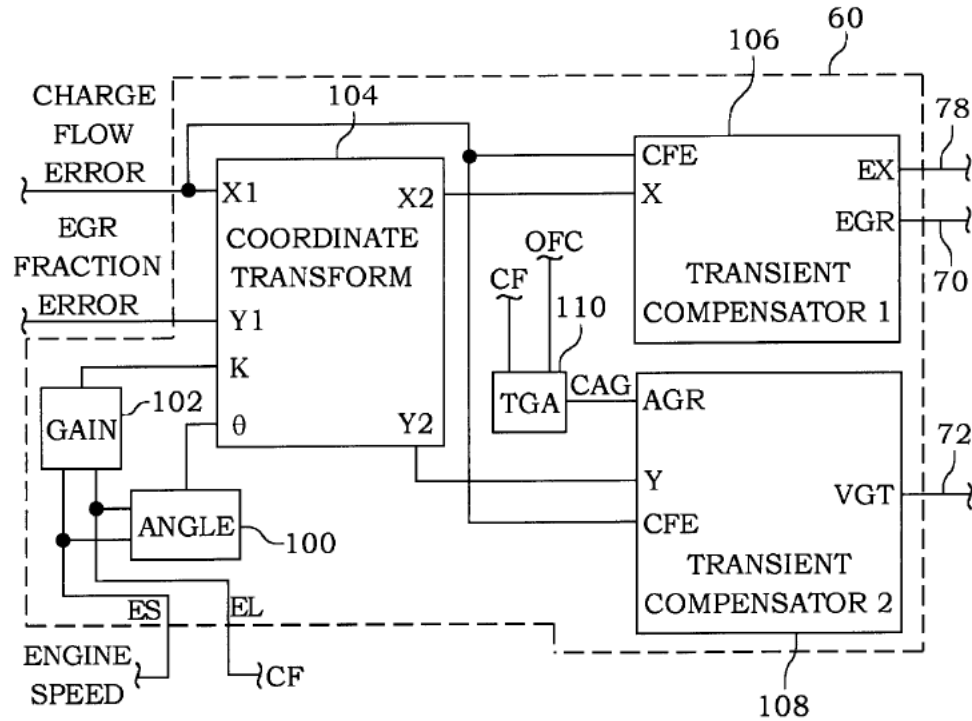
Figure 1.4. EGR-VGT transform manager of reference [6].

## Coupled Controller

In coupled control structures, a central controller take into the account the interactions of various input-output pairs to coordinate the actuators, as represented by Figure 1.5. In the engine, air-handling systems are often quite coupled and may benefit from control strategies that can handle interaction between input-output channels. For example, in reference [3], a sliding mode controller is utilized to control EGR and boost pressure by taking into account the coupling between input-output channels. Coupled control structures such as optimal controllers and sliding mode controllers may be necessary to capture the physics of a highly coupled system during steady-state and transient operation. However, coupled controllers are more difficult to tune in the field and may not be as intuitive as a decentralized controller that features independent controllers for each input-output channel.
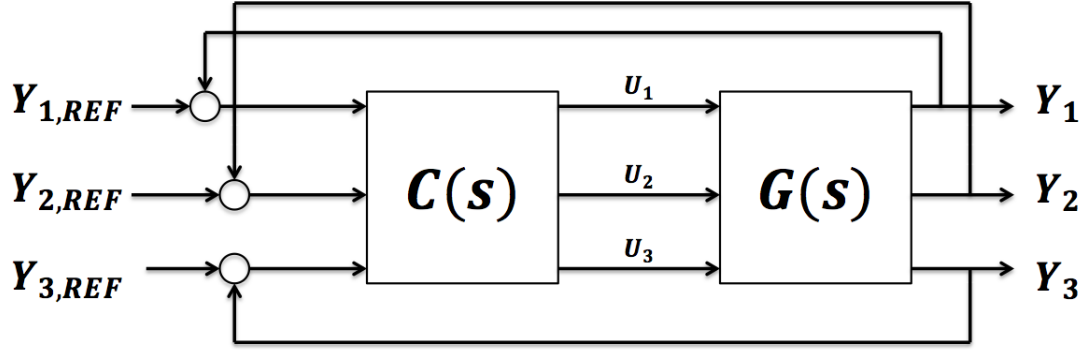
Figure 1.5.  Example of centralized control structure.

## 1.2.2   Air-Handling Control

Air-handling control involves regulating charge flow past valves and pressures in manifolds. Key architectural components seen in engines, particularly diesel engines, include turbochargers and EGR systems. There can also be throttle valves on the intake and exhaust side, bypass valves for the compressor, and wastegate valves for the turbocharger. As mentioned in [8], the EGR mass flow has a significant impact on the turbocharger operation. This is because EGR mass flow bypasses the turbine and flows towards the intake manifold, thus lowering the boost pressure differential. EGR flow also lowers turbocharger speed because less exhaust gases are routed to drive the turbine. It is clear that the air-handling problem features highly coupled dynamics, therefore academic literature often features decoupling or coordinated control strategies rather than directly applying decentralized control.

In reference [9], researchers design a controller to manage air-handling in a diesel engine architecture that features a fixed geometry turbocharger, EGR system, and intake throttle. The target outputs in this paper are the intake manifold pressure and total air mass flow rate into the compressor. The control inputs are the EGR valve and throttle valve. Since there is inherent coupling between these inputs and outputs, decentralized control strategies may not be optimal. The researchers use model predictive control (MPC), an optimal control method that can deal with various

output targets and is suitable for MIMO systems as mentioned in the paper. Before controller synthesis, the researchers obtain a black box input-output ARX model via system identification and transform it to a state-space form. The researchers then synthesize the MPC and also include a disturbance observer to account for modeling error. The researchers claim their MPC controller, which takes into account the coupled dynamics of the system, achieves target values for the output 2.5 to 8 times faster than a conventional controller.

Reference [7] utilizes a decoupling control strategy to manage EGR rate and boost pressure in a turbocharged diesel engine. The researchers implement a decoupling matrix, $W(s)$, which allows them to pair VGT to boost pressure and EGR valve to EGR fraction. Quantitative feedback theory (QFT) is then applied to obtain a diagonal controller for the compensated plant, $P(s) = G(s)W(s)$. The diagonal controllers are expressed in PI form using QFT. The researchers find that the decoupled controller achieves superior reference step tracking for EGR rate and boost pressure when compared to a coupled controller.

### 1.2.3 Fueling Control

Fuel mass flow is often used as a control input to regulate targets such as AFR for emissions purposes. A lower level controller manipulates actuators such as valves or injectors to achieve a desired fuel flow rate. Researchers in [10] utilize a PID compensator for fueling control in a retrofitted compressed natural gas (CNG) engine. The engine of interest in this paper was originally a gasoline engine, but it has been converted to run on natural gas. The engine control unit (ECU) uses a model predictive feed-forward controller to regulate AFR with a fuel pulse-width signal intended for a gasoline engine. The retrofitted PID controller converts the gasoline fuel pulse-width signal generated by the ECU to an equivalent pulse-width for CNG. This application is considered decentralized because fueling is used to control AFR via a map based strategy, and feedback control is used for pulse-width conversion.

In direct injection systems, injection pressure is used as a proxy for fuel mass flow metering. Researchers in [11] use a model predictive controller for a novel electronic CNG injection system. The researchers first use a physics-based approach to obtain nonlinear state equations for rail pressure and control chamber pressure. They then linearize and discretize the nonlinear state equations about various operating points and synthesize a model predictive controller. The input to the controller is a reference pressure and the output is the solenoid valve lift. The control system in the paper reduces pressure of the CNG stored in the tank and delivers it to a common rail where it is injected into the cylinders.

Physics-based approaches to fueling control require knowledge of fuel flow dynamics in the engine. Black box approaches are one way of obtaining input-output relationships for a plant. Researchers in [12] utilize neural networks to obtain a model for the fuel control system of a CNG engine. AFR is the primarily control objective in this paper, and fueling is the control input used to regulate it. There are two controllers used in the paper, one is a feed-forward map-based controller and the other is a neural network based PI controller. Both controllers generate a fuel pulse signal as their outputs. The feed-forward controller takes throttle and engine speed data as inputs, while the feedback controller takes the error between reference and actual AFR as an input. The researchers find success in AFR reference tracking during throttle and torque transients. Researchers in [13] utilize auto-regressive artificial neural networks (ANN) to obtain a complete model for input-output relationships on emissions, manifold dynamics, and actuator dynamics. They then apply a nonlinear model predictive controller (MPC) and achieve better performance and fewer emissions when compared to a feed-forward controller.

In reference [14] a model predictive controller (MPC) is developed to regulate lambda, or AFR. In this case, the control model is obtained via system identification. More specifically, pseudo-random binary signals (PRBS) are applied to obtain a black box model between fuel injection duration and lambda. During MPC formulation, the throttle valve is treated as a disturbance variable, and there are constraints on

weighted control inputs and outputs. When step disturbance changes in the throttle are exercised, the researchers find that the MPC maintains reference lambda better than a PI controller.

### 1.2.4 Engine Speed Control

Engine speed control is of particular interest to natural gas engines used in power generation applications. As mentioned in [1], during power generation, engine speed must be maintained such that current is produced at the mains frequency. In such applications, engine speed is a primary control objective along with meeting the power demanded by the grid, but secondary control objectives such as AFR and emissions requirements should be met as well. For example, researchers in [1] design a speed controller for a natural gas power supply engine. The architecture features a fixed geometry turbocharger with a compressor bypass valve, indirect fueling upstream of the compressor, intake throttle valve, and spark ignition. The authors employ a physics-based approach to modeling, and utilize a mean-value engine model to express the system in linearized state-space form. They then synthesize an H-infinity controller based on the state-space formulation. The goal of the H-infinity controller is to find a controller that minimizes the H-infinity norm, meaning it is a controller that relies on optimization. The researchers find that the H-infinity controller maintains engine speed better than a PID controller during transient changes in power load.

Researchers in [15] also take a model-based approach to tackling the engine speed control problem. Unlike in [1] where a physics-based approach is used to obtain a control model, researchers in this paper utilize system identification (harmonic generation) on their engine architecture which features a throttle valve and spark ignition. They use the system identification process to develop a truncated Volterra series, a type of model used to capture nonlinear behavior. They then obtain a nonlinear model-based controller by inverting the nonlinear plant dynamics of the Volterra series in the frequency domain. The inversion is done based on an approximate for-

mula for nonlinear plants. Additionally, they augment this model-based controller with an adaptive component that utilizes an instrumental variables approach. The researchers of [15] express their controller design in the frequency domain and utilize additional poles and filters on the controller to ensure closed-loop stability. Because voltage to the throttle valve is the only input that the nonlinear model-based controller controls affects, it is implied that this engine is throttle-governed, meaning fueling is dependent on throttle position. The researchers validate their nonlinear model-based adaptive controller on a 4.6 L 8-cylinder Ford engine. They find that the nonlinear model-based adaptive controller tracks step changes in desired engine speed well with comparable performance to a similarly design linear model-based controller. This paper highlights the fact that in a throttle-governed engine, an engine speed controller can be formulated by managing air-handling and having a lower level controller provide the desired fueling.

### 1.2.5  Literature Review Takeaway

This literature review highlights various approaches to different control problems present in an engine. For engines used in power generation, there are higher level control problems such as controlling engine speed and meeting load-torque demand. There are also lower level control problems such as managing air-handling to achieve a desired EGR fraction and boost pressure. The key takeaway is that while there are numerous coupled control strategies, they are model-based and require some kind of model that captures dynamics between inputs and outputs. More specifically, a linear state-space model of an engine is required to formulate some of the coordinated control strategies mentioned in the literature review. Therefore, a primary motivation of this thesis is deriving a state-space model of an engine so that there is the capability to synthesize coordinated control strategies.

## 1.3  Application of Interest

The application of interest is a Caterpillar G3500 series natural gas engine. This SI engine architecture features a twin-turbocharger and a passive wastegate valve. The actuators that an ECU can control directly are throttle valve position, bypass valve position, fuel injection, and spark timing. Since this engine is used in power generation applications on electrical grids, it is imperative that the desired engine speed is maintained at steady-state and maintained as well as possible during transient load-torque changes. Figure 1.6 shows a schematic provided by Caterpillar for the G3500 engine architecture, while Figure 1.7 shows a representative picture of the G3500 engine and generator set.
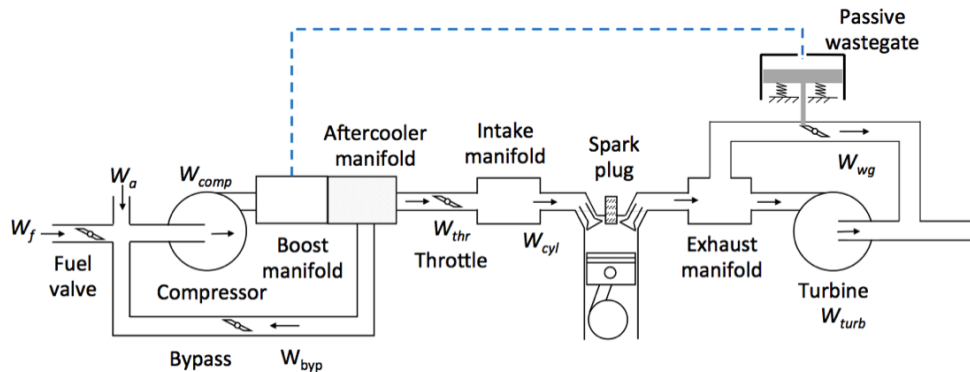


Figure 1.6.  Schematic of the Caterpillar G3500 engine architecture.
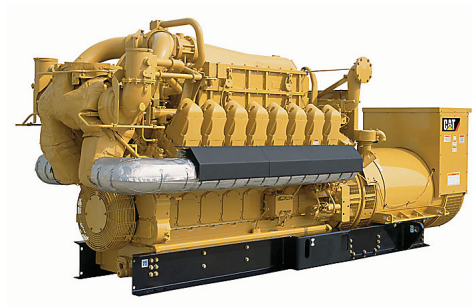


Figure 1.7.  Caterpillar G3500 engine generator set.

## 1.4  Thesis Contributions

The specific contributions of this thesis pertain to physics-based modeling and control-oriented analysis of the Caterpillar G3500 engine architecture and are discussed in the subsections below. Note that the subsections below also represent an outline of the thesis.

### 1.4.1  Power and Mass Flow Modeling Validation

The power and mass flow modeling and validation efforts of this thesis consist of the following:

1. Declare state variables that are later used in the formulation of a complete state-space model that characterizes engine dynamics.

2. Model engine torque gain $(C_{trq})$ as a function of state variables and validate this expression using reference data.

3. Model cylinder mass flow $(W_{cyl})$ as a function of state variables and validate this expression using reference data.

4. Model compressor mass flow $(W_{comp})$ as a function of state variables and validate this expression using reference data.

5. Model turbine mass flow $(W_{turb})$ as a function of state variables and validate this expression using reference data.

6. Model wastegate mass flow $(W_{wg})$ as a function of state variables and validate this expression using reference data.

7. Model compressor power $(P_{comp})$ as a function of state variables.

8. Model turbine power $(P_{turb})$ as a function of state variables.

### 1.4.2   State-Space Modeling Validation

The state-space equation formulation and validation efforts of the thesis consist of the following:

1. Derive a dynamic equation for engine speed $(x_1)$ by using a physics-based approach.

2. Derive a dynamic equation for intake manifold pressure $(x_2)$ by using a physics-based approach.

3. Derive a dynamic equation for boost manifold pressure $(x_3)$ by using a physics-based approach.

4. Derive a dynamic equation for exhaust manifold pressure $(x_4)$ by using a physics-based approach.

5. Derive a dynamic equation for turbocharger speed $(x_5)$ by using a physics-based approach.

6. Derive a dynamic equation for wastegate valve lift $(x_6)$ by using a physics-based approach.

7. Derive a dynamic equation for wastegate valve velocity $(x_7)$ by using a physics-based approach.

8. Formulate a nonlinear state-space model with all flow and power terms expressed as nonlinear functions of state variables.

9. Formulate a simplified nonlinear state-space model with all flow and power terms (except $W_{cyl}$) expressed as linear functions of state variables.

10. Linearize the simplified nonlinear model about an equilibrium point to obtain a linear engine model in conventional state-space form.

11. Validate and compare all three models against truth-reference data obtained by performing a closed-loop GT-Power/Simulink simulation.

### 1.4.3 Control-Oriented Analysis

The control-oriented analysis efforts of this thesis consist of the following:

1. Transfer matrix formulation of a linearized state-space model provided by Caterpillar.

2. Relative gain array (RGA) formulation on the model provided by Caterpillar.

3. RGA number analysis versus frequency to determine the best input-output configuration for decentralized control.

4. RGA element magnitude and phase analysis versus frequency.

5. PI controller analysis based on intuition gained by RGA analysis.

# 2. PHYSICS-BASED MODELING AND VALIDATION OF THE NATURAL GAS ENGINE

As discussed in the previous chapter, coordinated control strategies are of potential interest because they take into account the coupling between all inputs and outputs of a system. However, in order to utilize coordinated control strategies, it is often necessary to obtain a control-oriented model for the system, which in this case is the natural gas engine. While a control-oriented model does not need to be as accurate as a high-fidelity simulation model, it should capture transient behavior of the system fairly well. One way of obtaining a control-oriented state-space model is by means of system identification, such as in [7]. In this method, state variables may or may not represent physical quantities, and the model derivation is "data driven". Another option is utilizing first-principles to obtain a physically-based model. This study focuses on a first-principles approach to obtain a state-space model. More specifically, this chapter explicitly defines all state variables, input variables, and disturbance variables. Additionally, this chapter models all relevant terms as functions of the state-space variables and validates the individual expressions against GT-Power truth-reference data.

## 2.1 GT-Power truth-reference Data

Before any modeling efforts were undertaken, truth-reference data was obtained via a co-simulation on a closed-loop GT-Power/Simulink model for the Caterpillar G3500 natural gas engine. Caterpillar provided Purdue University with both the GT-Power model of the engine and the Simulink engine controller. Since the engine is used in power generation applications, the disturbance it encounters is varying load factor. The load factor is a fraction of the maximum load-torque demand. A closed-

loop simulation was performed consisting of load factor step changes from 0 to 1.0 and back down to 0 in increments of 0.1. The Simulink controller determined control inputs to maintain engine speed and other control targets during the simulation. During this simulation all pertinent engine data was collected into a MATLAB work space. The data consisted of various mass flows, pressures, temperatures, speeds, efficiency values, and thermophysical properties of gases.

## 2.2 State-Space Variable Nomenclature

In order to obtain a control model in state-space form, state variables, control inputs, and disturbances must be explicitly denoted for the engine of interest. Caterpillar provided a set of dynamic equations describing the engine, and these equations are the basis for state-space model formulation.

### 2.2.1 Original Dynamic Equations

The initial set of equations provided by Caterpillar includes differential equations for engine speed, intake manifold pressure, boost manifold pressure, and exhaust manifold pressure. The equations are shown below.

$$\dot{\omega} = \frac{1}{J}[C_{trq}P_{im} - Trq_L] \tag{2.1}$$

$$\dot{P}_{im} = \frac{R_{im}T_{im}}{V_{im}}[W_{thr} - W_{cyl}] \tag{2.2}$$

$$\dot{P}_{bm} = \frac{R_{bm}T_{bm}}{V_{bm}}[W_{comp} - W_{thr} - W_{byp}] \tag{2.3}$$

$$\dot{P}_{em} = \frac{R_{em}T_{em}}{V_{em}}[W_{cyl} - W_{turb} - W_{wg}] \tag{2.4}$$

While this model serves as a foundation for formulation of the state-space equations, there are several components that it lacks, including:

- A model for compressor mass flow, $W_{comp}$.

- A model for turbine mass flow, $W_{turb}$.

- A model of volumetric efficiency, $\eta_v$.

- A model of gas temperature in the exhaust manifold, $T_{em}$.

- A model of thermal efficiency, $\eta_{therm}$, as a function of spark timing.

- An equation for wastegate valve dynamics.

- An equation for turbocharger dynamics.

The locations of the mass flow terms and the manifold volumes are shown in Figure 1.6.

## 2.2.2 Addressing Missing Model Components

The operating range of interest for controller design corresponds to load factors between 0.7 and 1.0. A load factor is the fraction of the maximum load that the engine must generate to meet the demand set by the electrical grid. Table 2.1 summarizes how missing model components are addressed:

Table 2.1. Strategy for addressing missing model components

| Missing Components | Min. Value | Max. Value | Strategy |
|:---:|:---:|:---:|:---:|
| $W_{comp}$ | - - - - - | - - - - - | $\text{fcn}(P_{bm}, \omega_{tc})$ |
| $\eta_{comp}$ | 0.7794 | 0.7937 | $\eta_{comp} = \text{const.}$ |
| $W_{turb}$ | - - - - - | - - - - - | $\text{fcn}(P_{em})$ |
| $\eta_{turb}$ | 0.7539 | 0.7840 | $\eta_{turb} = \text{const.}$ |
| $\eta_v$ | 0.7223 | 0.7575 | $\eta_v = \text{const.}$ |
| $\eta_{therm}$ | N/A | N/A | $\eta_{therm} = \text{const.}$ |
| $T_{em}$ | 910.68K | 943.98K | $T_{em} = \text{const.}$ |

As shown in Table 2.1, the strategy for compressor mass flow is to make it a function of boost pressure and turbocharger speed based on previous work at Purdue

University in [16]. The strategy for turbine mass flow is to make it a function of exhaust manifold pressure based on turbine map data. In the operating range of interest, the truth-reference data values of compressor efficiency, turbine efficiency, and volumetric efficiency do not vary significantly. Therefore, in the control model the efficiency values are set to their averages in the operating range: $\eta_{comp} = 0.79$, $\eta_{turb} = 0.77$, and $\eta_v = 0.74$. The GT-Power truth-reference data does not contain information on thermal efficiency, so a value of $\eta_{therm} = 0.4$ is selected for this natural gas engine. The value of exhaust manifold temperature does not vary significantly in this operating range, so it is set to the average truth-reference value of $T_{em} = 933.6\text{K}$ in the control model. More generally, all temperature parameters that do not vary significantly in the operating range of interest are set to their respective mean values in the truth-reference data:

- Intake manifold temperature: $T_{im} = 340.2\text{K}$

- Boost manifold temperature: $T_{bm} = 445.0\text{K}$

### 2.2.3 State-Space Variables

Seven state variables, three control inputs, and one disturbance variable are chosen to create a state-space model for the engine. The state variables are selected to characterize the physics of the engine and include $x_1 :=$ engine speed (rad/s), $x_2 :=$ intake manifold pressure (Pa), $x_3 :=$ boost manifold pressure (Pa), $x_4 :=$ exhaust manifold pressure (Pa), $x_5 :=$ turbocharger shaft speed (rad/s), $x_6 :=$ wastegate valve lift (mm), and $x_7 :=$ wastegate valve velocity (m/s). The input variables are $u_1 :=$ throttle valve mass flow (kg/s), $u_2 :=$ bypass valve mass flow (kg/s), and $u_3 :=$ fuel mass flow (kg/s). The single disturbance in the state-space model is $w :=$ load factor. Figure 2.1 shows a schematic of the engine provided by Caterpillar with locations of state and inputs variables.
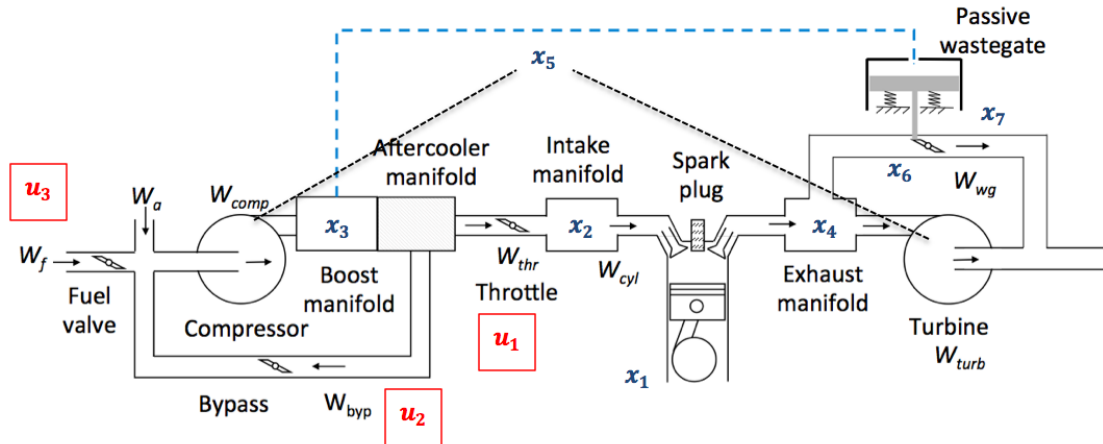
Figure 2.1.  G3500 engine schematic with state and input variables.

It is important to note that the modeling efforts in this study assume direct control over mass flows for the three control inputs.  In reality, an engine controller would have direct control over valve positions, so a lower level controller for target mass flows may be required depending on the control strategy.  Assuming direct control of flows, however, is a common practice.  When this assumption is made, a higher level controller determines a mass flow input to control a target variable, and a lower level controller works to provide the desired mass flow input. Balekai, et al. design a closed-loop EGR controller for a diesel engine in [19].  They utilize an outer control loop to control EGR fraction with EGR mass flow rate and an inner control loop to control the EGR mass flow rate with EGR valve position.  Figure 2.2 below is representative of a nested control structure with inner and outer control loops that would be necessary when assuming direct control over mass flows.
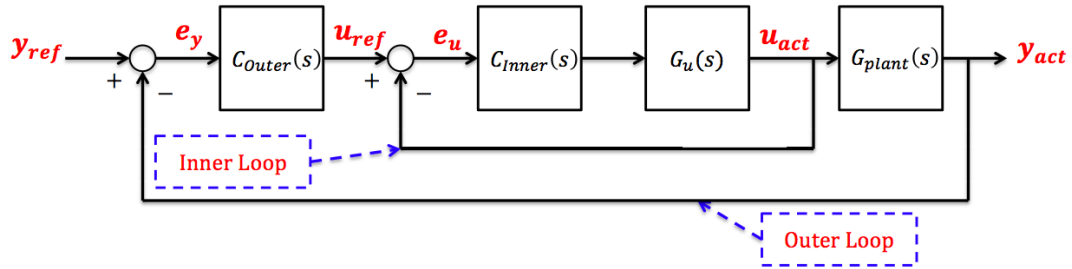
Figure 2.2. Example of nested controller with inner and outer control loops.

Before formulating a set of nonlinear state equations and linearizing them about an equilibrium point, all terms in the original dynamic equations are made explicit functions of state, input, and disturbance variables. This includes the following mass flow terms from the original differential equations: $W_{cyl}$, $W_{comp}$, $W_{turb}$, $W_{wg}$, $W_{thr}$, and $W_{byp}$. These mass flow terms are expressed as functions of state variables and validated in the following sections of this chapter. The engine torque gain, $C_{trq}$, is also made a function of state and input variables. Additionally, the compressor and turbine power terms are expressed as functions of state variables, because the final set of state-space equations takes into account turbocharger speed and wastegate dynamics. The load-torque term, $Trq_L$, in Equation (2.1) is a straightforward function of load factor and maximum expected load-torque:

$$Trq_L = T_{max}w \qquad (2.5)$$

## 2.3 Cylinder Mass Flow Modeling

The cylinder mass flow rate term appears in Equation (2.2) and Equation (2.4) in the dynamic equations for intake manifold pressure and exhaust manifold pressure. It is modeled using the speed density equation [17]. Assumptions for the cylinder mass flow equation in this model include constant intake manifold temperature and constant volumetric efficiency, per Table 2.1.

### 2.3.1 Cylinder Mass Flow Equation

The cylinder mass flow equation is based on the speed density equation and is expressed as follows:

$$W_{cyl}(\omega, P_{im}) = \frac{\omega P_{im} \eta_v V_D}{2RT_{im}} \tag{2.6}$$

This can be written explicitly in terms of state variables $x_1$ and $x_2$:

$$W_{cyl}(x_1, x_2) = \frac{x_1 x_2 \eta_v V_D}{2RT_{im}} \tag{2.7}$$

### 2.3.2 Cylinder Mass Flow Equation Validation

The cylinder mass flow expression is validated by substituting GT-Power values of $x_1$ and $x_2$ into Equation (2.7) and comparing it with GT-Power value of $W_{cyl}$ at every time step. There is a maximum steady-state error of 3.3% in the operating range of interest, which is load factors between 0.7 and 1.0.
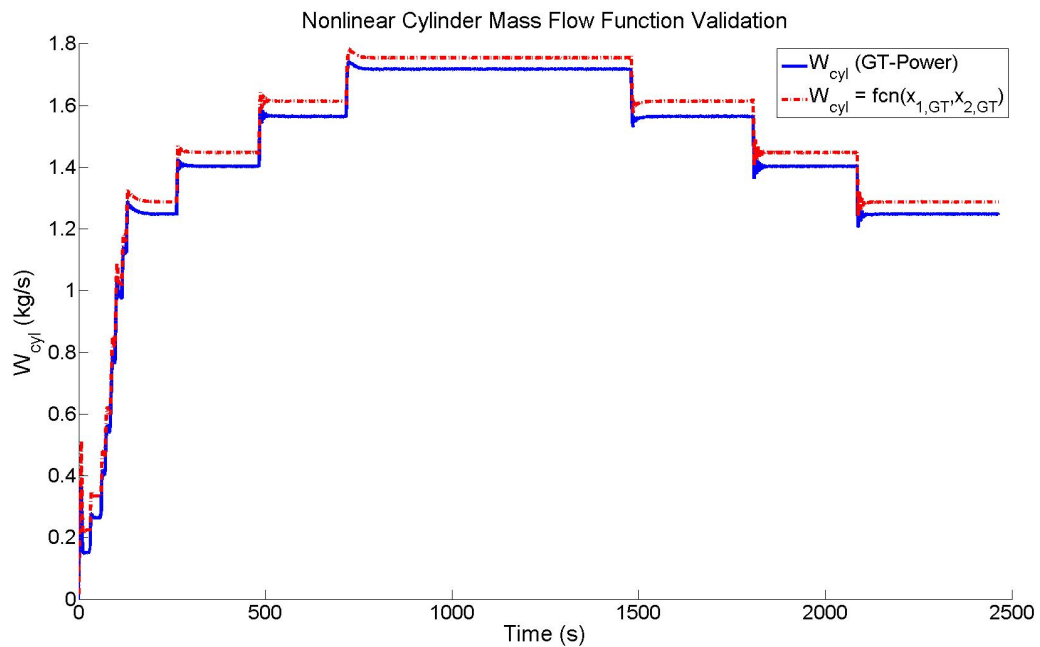


Figure 2.3. Cylinder mass flow expression validation.

## 2.4 Engine Torque Gain Modeling

The engine torque gain term appears in the dynamic equation for engine speed, Equation (2.1). Multiplying the engine torque gain by the intake manifold pressure gives the gross torque generated by the engine. When the total engine torque is greater than the load-torque, the engine speed will be increasing. Assumptions for the engine torque gain equation include constant volumetric efficiency, constant thermal efficiency, and constant intake manifold temperature.

### 2.4.1 Engine Torque Gain Equation

The equation for engine torque gain was provided by Caterpillar and is expressed as:

$$C_{trq} = \frac{\eta_v \eta_{therm} Q_{LHV} V_D}{4\pi RT_{im}(AFR + 1)} \tag{2.8}$$

The air-fuel ratio (AFR) in the cylinder can be approximated by the following equation,

$$AFR = \frac{W_{cyl} - W_f}{W_f} \tag{2.9}$$

which assumes the fueling transport delay for this engine architecture is negligible. Keeping in mind that cylinder mass flow is a function of $x_1$ and $x_2$, and that fuel mass flow is the input $u_3$, AFR is a function of states and inputs, $AFR = fcn(x_1, x_2, u_3)$. The engine torque gain equation can therefore be written explicitly in terms of state variables and inputs:

$$C_{trq}(x_1, x_2, u_3) = \frac{\eta_v \eta_{therm} Q_{LHV} V_D}{4\pi RT_{im}(AFR(x_1, x_2, u_3) + 1)} \tag{2.10}$$

### 2.4.2 Engine Torque Gain Equation Validation

The engine torque gain expression is validated against reference data corresponding to load factors between 0.7 and 1.0. Validation is done by substituting truth-reference GT-Power values of $x_1$, $x_2$, and $u_3$ into Equation (2.10) and comparing it with the truth-reference value of $C_{trq}$ at every time step, as shown in Fig. 2.4.
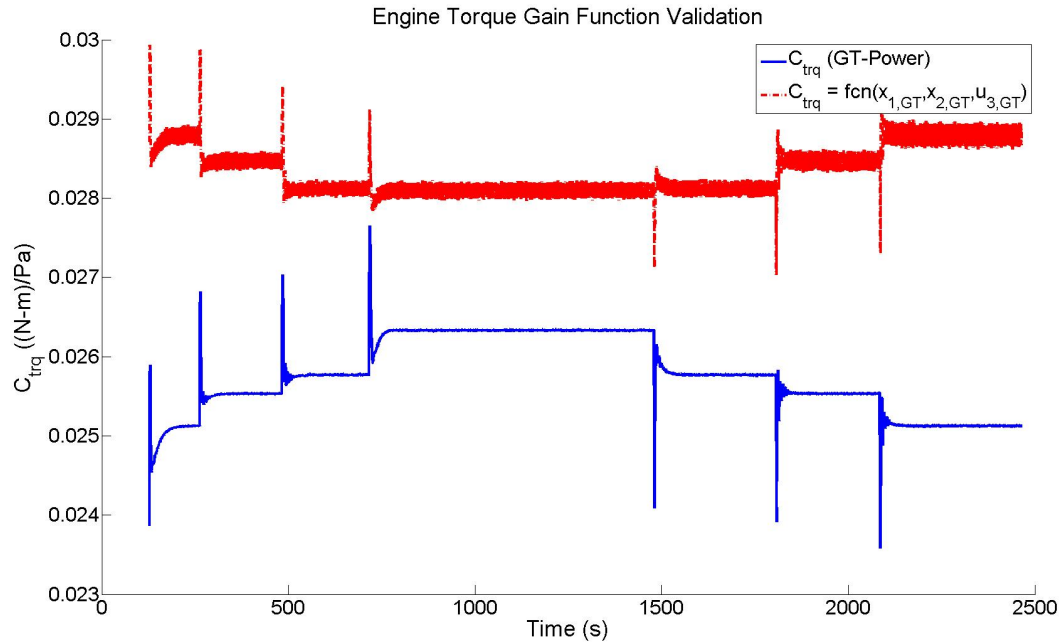
Figure 2.4. Engine torque gain expression validation.

In Fig. 2.4, the load factor on the engine begins at 0.7 and undergoes step changes in increments of 0.1 until it reaches 1.0. The load factor then undergoes step decrements of 0.1 until it is back to 0.7. The engine torque gain model matches the reference data better when load factor is higher. At a load factor of 0.7, there is less than 16% steady-state error and at a load factor of 1.0 there is less than 8% steady-state error. A likely source of this error is the assumption of constant thermal efficiency in the operating range of interest. Based on the validation results, the engine torque gain model of Equation (2.10) is not considered satisfactory and instead a constant value of $C_{trq} = 0.0256$ is assumed. This constant-value assumption has a maximum of 2.9% steady-state error with respect to the reference data. In effect, this simplification means assuming a constant AFR, which means there must be a low level controller that can manage fueling ($u_3$) to maintain the constant AFR value.

## 2.5 Compressor Mass Flow Modeling

The compressor mass flow rate term, $W_{comp}$ appears in Equation (2.3) and is not defined as an explicit function of state variables in the original set of equations provided by Caterpillar. Compressor mass flow rate can be modeled as a function of boost manifold pressure ($x_3$) and turbocharger speed ($x_5$) [16]. As the exhaust gases drive the turbine, the turbocharger speed increases and the compressor inducts more airflow thereby increasing boost pressure. Assumptions for the compressor mass flow rate model include constant ambient air density, constant ambient air temperature, constant ambient air pressure, constant specific heat ratio for ambient air, constant specific heating value (constant-pressure) for ambient air, compressor inlet pressure equal to ambient air pressure, an approximated compressor blade tip diameter, isentropic compression, and constant compressor efficiency.

### 2.5.1 Nonlinear Compressor Mass Flow Equation

The compressor mass flow equation from [16] is highly nonlinear and is written in terms of state variables as:

$$W_{comp}(x_3, x_5) = 2 * [\frac{\pi}{4}\rho_a d_c^2 (\frac{1}{\gamma R T_a})^{\frac{\gamma-1}{2\gamma}} (\frac{\pi}{60}d_c x_5)^{\frac{2\gamma-1}{\gamma}}]*$$
$$(a_1 X^3 + a_2 X^2 + a_3 X + a_4) \tag{2.11}$$

where the term $X$ is,

$$X(x_3, x_5) = \frac{c_{p,a}T_a((\frac{x_3}{P_a})^{\frac{\gamma-1}{2\gamma}} - 1)}{\frac{1}{2}(\frac{\pi}{60}d_c x_5)^2} \tag{2.12}$$

The regression coefficients in the Equation (2.11) are obtained by regression on the compressor map provided by Caterpillar. The equation from the reference is multiplied by a factor of two to account for the twin turbochargers in the G3500 engine architecture.

## 2.5.2 Nonlinear Compressor Mass Flow Equation Validation

The compressor mass flow term of Equation (2.11) is validated against reference data corresponding to load factors between 0.0 and 1.0. The operating range of interest for present modeling purposes is for load factors between 0.7 and 1.0. However, the nonlinear compressor mass flow is validated against the entire operating range since it is based on compressor map data. Validation is done by substituting truth-reference values of $x_3$ and $x_5$ into the nonlinear compressor mass flow expression and comparing it with the GT-Power truth-reference value of $W_{comp}$ at every time step, as shown in Fig. 2.5.
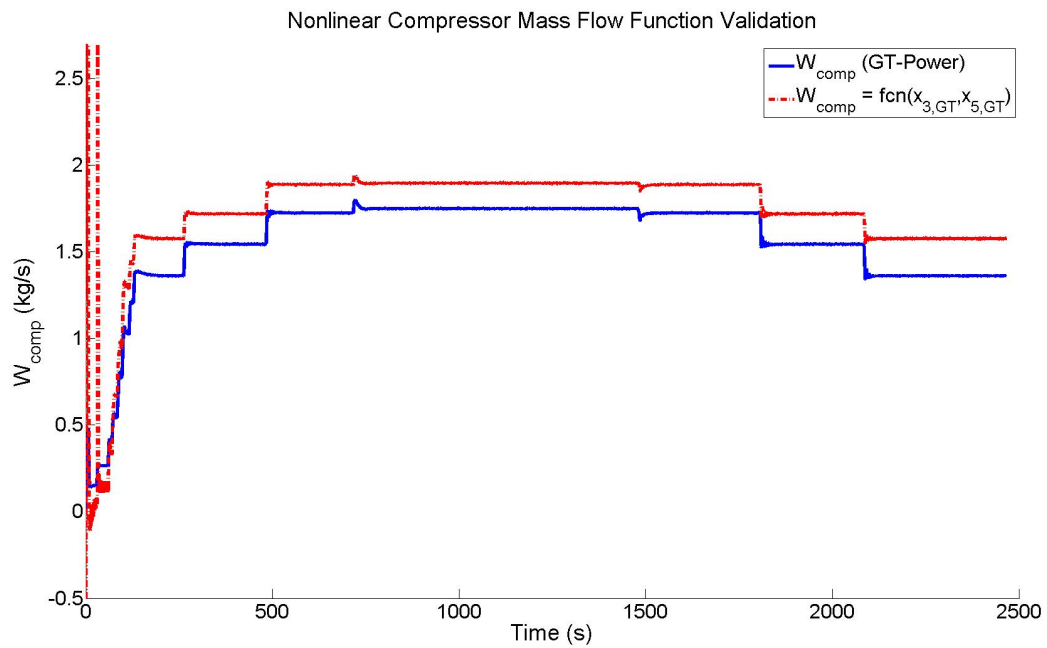


Figure 2.5. Nonlinear compressor mass flow expression validation.

In Fig. 2.5 the load factor on the engine starts at a value of 0.0 and undergoes step changes in increments of 0.1 until it reaches 1.0. The engine then experiences step decrements in load factor down to a value of 0.7. Overall the nonlinear compressor mass flow model of Equation (2.11) matches the reference data well in steady-state,

with a maximum of 16.1% steady-state error in the operating range of interest. The nonlinear compressor mass flow model also captures transient behavior well at most load factor step changes, except at the beginning of the simulation where the model displays significant transient spikes compared to the reference. A possible cause of this is inaccuracy of Equation (2.11) for low turbocharger speeds during engine start-up. Despite this inconsistency, the nonlinear compressor mass flow model is considered satisfactory because of its acceptable steady-state error in the entire operating range and accurate transient behavior particularly for load factors between 0.7 and 1.0.

### 2.5.3  Linear Compressor Mass Flow Equation

By using a physics-based approach, compressor mass flow was expressed as a highly nonlinear function of boost manifold pressure and turbocharger speed. Though the expression is an accurate one, it makes it more challenging to solve for an equilibrium point when linearizing a set of nonlinear state equations. Therefore, compressor mass flow is made a linear function of $x_3$ and $x_5$ as follows:

$$W_{comp} = g_1 x_3 + g_2 x_5 + g_3 \tag{2.13}$$

The coefficients $g_1$, $g_2$, and $g_3$ are obtained by means of regression on the truth-reference data in the operating range of interest. To be clear the linear expression is valid in the operating range of interest, while the nonlinear expression is valid for the whole operating range.

### 2.5.4  Linear Compressor Mass Flow Equation Validation

The linear compressor mass flow model of Equation (2.13) is validated in the same way as the nonlinear model, except now the model is only tested against reference data corresponding to load factors between 0.7 and 1.0. The validation of the linear compressor mass flow model is presented in Fig. 2.6. As shown, the linear compressor mass flow equation captures transient behavior very well and has minimal steady-state

error ($e_{ss} < 1.5\%$) in the specific operating range of interest. Note that $e_{ss}$ denotes steady-state error. Both linear and nonlinear equations accurately capture transient behavior during load factor step changes. The linear model has lower steady-state error in the relevant operating range. This is because the nonlinear model is based on first-principles where compressor mass flow is expressed as a function of $x_3$ and $x_5$, while the linear model is based on a regression fit.
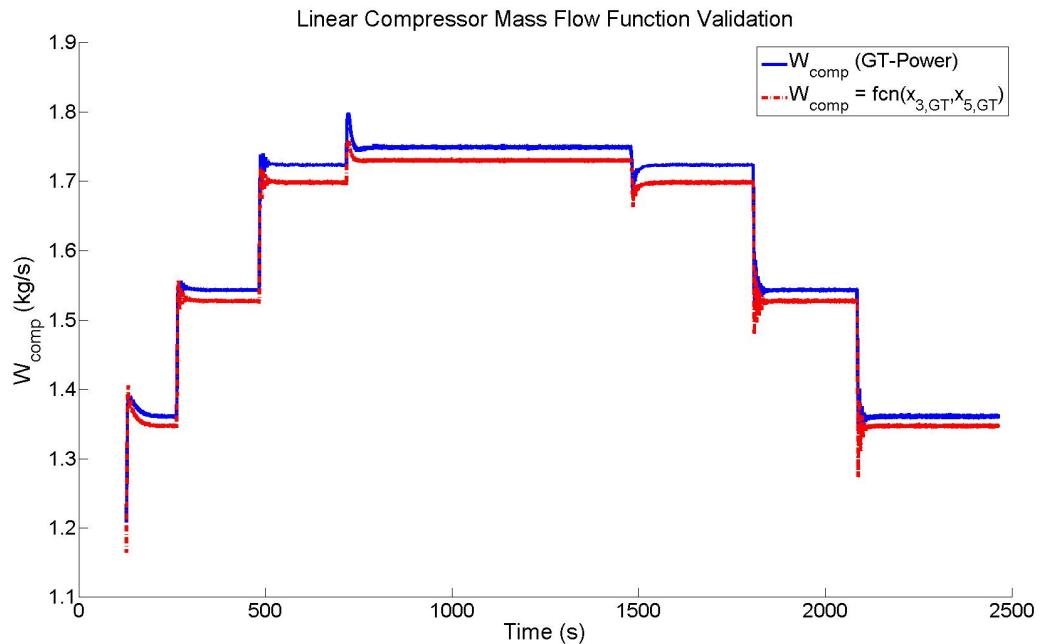


Figure 2.6. Linear compressor mass flow expression validation.

## 2.6 Turbine Mass Flow Modeling

The nonlinear turbine mass flow equation is obtained via regression on the turbine map data provided for the turbocharger in the Caterpillar G3500 natural gas engine. Assumptions for the turbine mass flow model include constant turbine efficiency, constant exhaust manifold temperature, constant ambient air pressure, turbine inlet

pressure equal to exhaust manifold pressure, constant thermodynamic properties for gases, and an approximated turbine blade tip diameter.

### 2.6.1 Nonlinear Turbine Mass Flow Equation

The turbine mass flow equation is a polynomial function of exhaust manifold pressure, $x_4$, and is expressed as:

$$W_{turb}(x_4) = \frac{2x_4}{T_{em}^{0.5}}(b_1 PR_t^7 + b_2 PR_t^6 + b_3 PR_t^5 + b_4 PR_t^4$$
$$+ b_5 PR_t^3 + b_6 PR_t^2 + b_7 PR_t + b_8) \tag{2.14}$$

where,

$$PR_t(x_4) = \frac{x_4}{P_a} \tag{2.15}$$

The turbine map data used to obtain the nonlinear relationship above between $PR_t$ and $W_{turb}$ is distinct from the truth-reference data obtained by co-simulation of the GT-Power/Simulink model.

### 2.6.2 Nonlinear Turbine Mass Flow Equation Validation

The nonlinear turbine mass flow term of Equation (2.14) is validated against reference data that spans all load factors between 0.0 and 1.0. Validation is done by substituting truth-reference values of $x_4$ into the nonlinear turbine mass flow equation and comparing with the GT-Power simulation data for $W_{turb}$ at each time step as shown in Fig. 2.7. The nonlinear turbine mass flow model matches the truth-reference data very well during transient load factor changes and steady-state, with a maximum of 2.0% steady-state error in the operating range of interest.
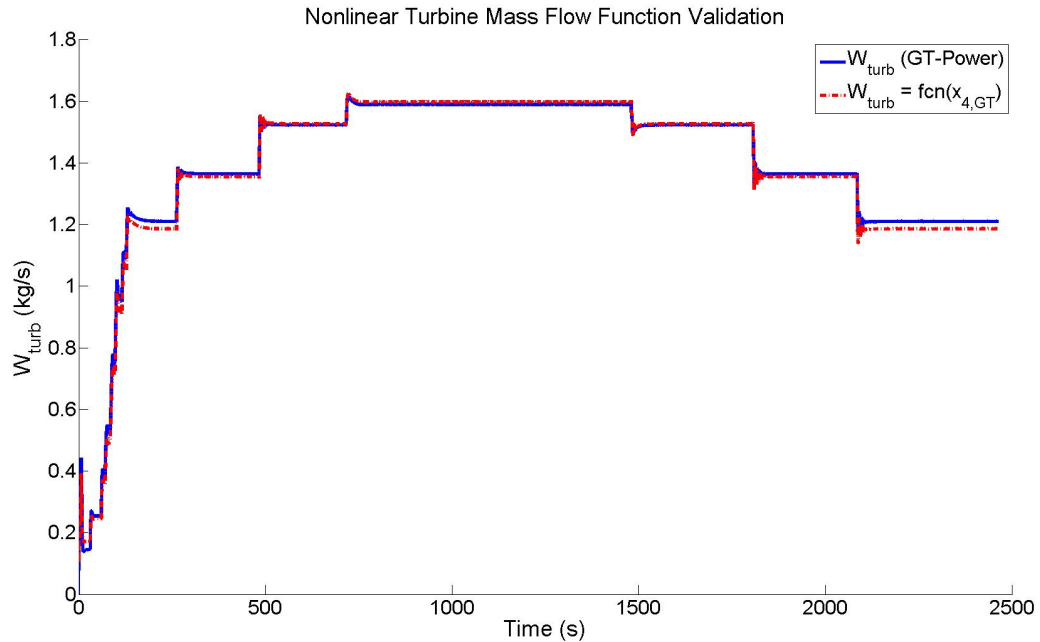
Figure 2.7. Nonlinear turbine mass flow expression validation.

### 2.6.3 Linear Turbine Mass Flow Equation

The turbine mass flow equation is a nonlinear function of exhaust manifold pressure. To simplify the control model, it is made a linear function of $x_4$ as follows:

$$W_{turb}(x_4) = C_1 x_4 + C_2 \tag{2.16}$$

The coefficients $C_1$ and $C_2$ are obtained via regression on the truth-reference data corresponding to the operating range of interest (LF = 0.7 - 1.0). Though this linearization method relies on the truth-reference data, it was by means of first-principles that turbine mass flow was made a function of $x_4$ in the first place.

### 2.6.4 Linear Turbine Mass Flow Equation Validation

The linear turbine mass flow model is validated in the same manner as the non-linear model, except that it is only compared to truth-reference data in the operating

range of interest (LF = 0.7 - 1.0). Fig. 2.8 shows that the linear mass flow model matches the reference data for $W_{turb}$ very well in both transient load factor step changes and in steady-state ($e_{ss} < 0.2\%$). Therefore, Equation (2.16) is considered a satisfactory model of turbine mass flow in the engine.
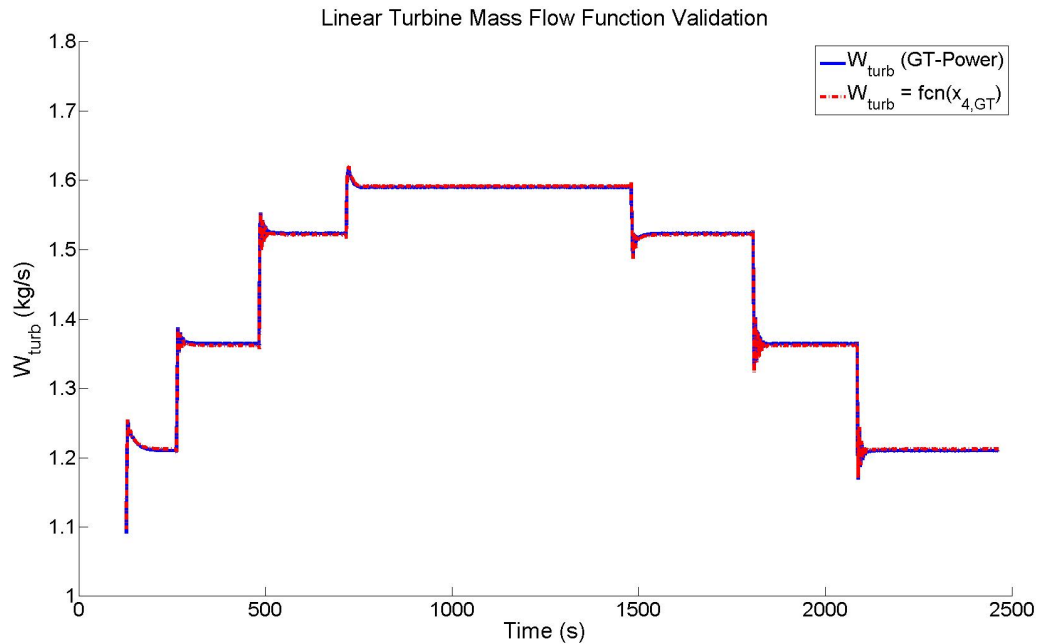


Figure 2.8. Linear turbine mass flow expression validation.

## 2.7 Wastegate Valve Mass Flow Modeling

The wastegate valve featured in this engine architecture is passive. When the boost pressure reaches a threshold value, the wastegate valve opens. This causes the exhaust gases to bypass the turbine. Assumptions for the wastegate valve mass flow model include constant thermophysical properties for exhaust gases, constant exhaust manifold temperature, and constant ambient air pressure. A schematic of the passive wastegate is shown in Figure 2.9.
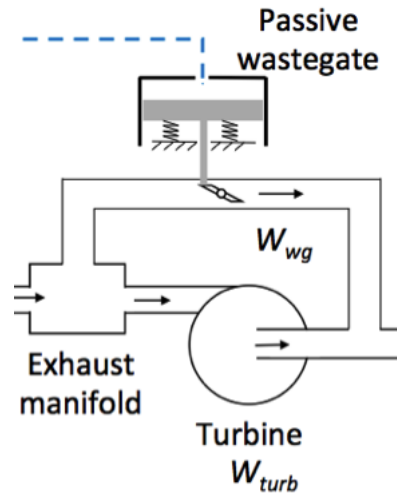
Figure 2.9. Passive wastegate schematic.

The purpose of the wastegate is to reroute exhaust gases so they bypass the turbine. This is important to prevent compressor surge which happens when boost pressure gets too high and all compressor blades stalls. Compressor surge can result in reverse flow through the compressor. When the pressure in the boost manifold reaches a threshold value, the diaphragm in the wastegate housing is pushed down with enough force to overcome pretension force in the springs and open the wastegate valve.

### 2.7.1 Wastegate Mass Flow Equation

The wastegate mass flow equation is highly nonlinear and is composed of several terms which are explained later. The equation itself is a function of exhaust manifold pressure ($x_4$) and wastegate valve lift ($x_6$):

$$W_{wg}(x_4, x_6) = CD * A_{wg} * \rho_{is} * U_{is} \qquad (2.17)$$

The term $CD$ is the coefficient of discharge for the wastegate valve, and a linear coefficient of discharge relationship is derived based on the raw engine model data for

this particular engine. The equation for $CD$ is a linear function of wastegate valve lift:

$$CD = 4.0821(\frac{x_6}{d_{wg}})$$ (2.18)

The term $\rho_{is}$ is the gas density at the throat and is expressed by the following equation:

$$\rho_{is} = (\frac{x_4}{R_{exh}T_{em}})(\frac{P_a}{x_4})^{\frac{1}{\gamma_{exh}}}$$ (2.19)

The term $U_{is}$ is the isentropic velocity at the throat and its equation is:

$$U_{is} = \sqrt{R_{exh}T_{em}} * (\frac{2\gamma_{exh}}{\gamma_{exh} - 1}[1 - (\frac{P_a}{x_4})^{\frac{\gamma_{exh}-1}{\gamma_{exh}}}])^{\frac{1}{2}}$$ (2.20)

Geometric data for the wastegate ($A_{wg}$, $d_{wg}$, etc.) is provided by Caterpillar for this particular engine. The source of the equations for wastegate mass flow, coefficient of discharge ($CD$), density at the throat ($\rho_{is}$), and isentropic velocity ($U_{is}$) are all directly taken from the documentation on flow past an orifice from the GT-Power model of the engine provided by Caterpillar. To be clear, the raw engine data used for the $CD$ regression is not the same as the truth-reference data obtained by running the GT-Power co-simulation.

### 2.7.2   Wastegate Mass Flow Equation Validation

The nonlinear wastegate mass flow model is validated against the reference data for load factors between 0.7 and 1.0. This is done by substituting truth-reference values of $x_4$ and $x_6$ into Equation (2.17) and comparing that with truth-reference GT-Power values of $W_{wg}$ at every time step, as shown in Fig. 2.10. During real engine operation, the passive wastegate valve only opens at the highest load factor (LF = 1.0). The model presented in Equation (2.17) is quite accurate as it predicts near zero mass flow through the wastegate valve at lower load factors. In the reference data, however, the wastegate valve leaks at lower load factors and wastegate valve mass flow is non-trivial. At the highest load factor, nonlinear model values and reference data values of wastegate mass flow are similar. Therefore, the nonlinear wastegate

mass flow model is considered satisfactory because of its physical accuracy at lower load factors and similarity to reference values at a load factor of 1.0 ($e_{ss} < 6.3\%$).
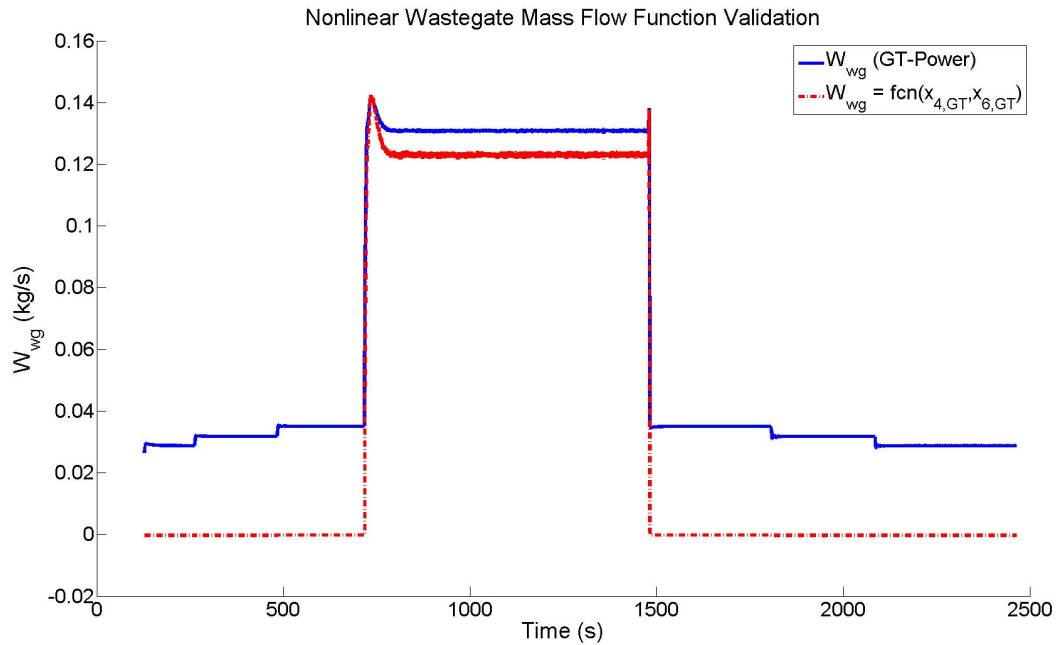


Figure 2.10. Nonlinear wastegate mass flow expression validation.

### 2.7.3 Linear Wastegate Mass Flow Equation

The wastegate mass flow expression is linearized to simplify the linearization process of the nonlinear state equations. The linear function is expressed as:

$$W_{wg} = f_1 x_6 \tag{2.21}$$

While the nonlinear expression is a function of $x_4$ and $x_6$, the linear function is made solely a function of $x_6$ because the contour graph for $W_{wg}$ in the operating range of interest suggests a stronger dependency on wastegate valve lift. Note that the nonlinear expression is valid for the entire operating range while the linear function is only valid for the operating range of interest.

### 2.7.4    Linear Wastegate Mass Flow Equation Validation

The linear wastegate mass flow model is validated against GT-Power reference data in Fig. 2.11. Unlike the nonlinear model, the linear wastegate mass flow model is only a function of $x_6$. At lower load factors when the wastegate valve should be closed in the actual engine, the linear mass flow function is more realistic than the reference data because it predicts flow values of approximately zero. At a load factor of 1.0, the linear mass flow model matches the truth-reference mass flow almost perfectly ($e_{ss} < 0.4\%$). In fact, the linear mass flow model matches the reference data better than the nonlinear mass flow model at the highest load factor. This is because the nonlinear mass flow model is based on first-principles while the linear mass flow model is based on regression in the operating range of interest.
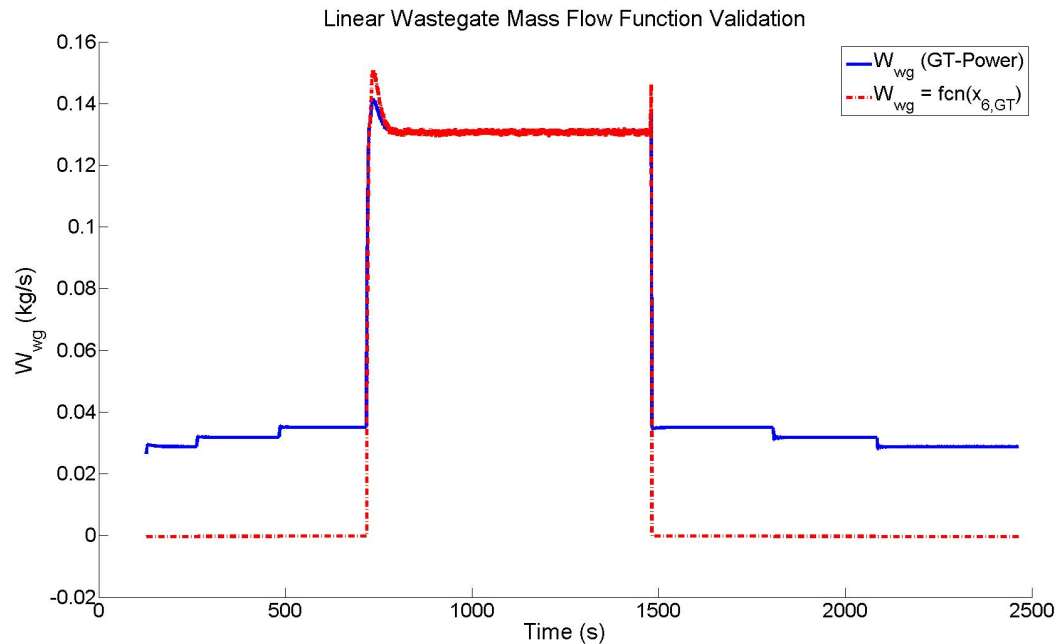


Figure 2.11.   Linear wastegate mass flow expression validation.

## 2.8   Compressor Power Modeling

A term for compressor power output ($P_{comp}$) does not appear in the original dynamic equations for the engine, but it is necessary in deriving a differential equation for turbocharger speed, one of the state variables. The strategy for modeling compressor power output is based on the approach taken in [17]. Assumptions for the compressor power output model are the same as those for the compressor mass flow rate model.

### 2.8.1   Compressor Power Equation

The compressor power equation is a function of intake manifold pressure ($x_2$) and compressor mass flow rate. The compressor mass flow rate is a function of states $x_3$ and $x_5$, which means compressor power is a function of three state variables: $x_2$, $x_3$, and $x_5$.

$$P_{comp}(x_2, x_3, x_5) = \frac{W_{comp}(x_3, x_5)c_{p,a}T_a}{\eta_{comp}}[(\frac{x_2}{P_a})^{\frac{\gamma}{\gamma-1}} - 1] \qquad (2.22)$$

### 2.8.2   Compressor Power Equation Validation

The GT-Power/Simulink model that was used to obtain truth-reference data does not have compressor power measurements built into the model. Therefore, the expression in Equation (2.22) can not be validated directly with truth-reference data. Compressor power does play a role in turbocharger speed dynamics, so if the compressor and turbine power modeling strategies are accurate, the state equation for turbocharger speed should match the reference data for $x_5$ in steady-state.

### 2.8.3   Linear Compressor Power Equation

The compressor power equation is highly nonlinear and so it is linearized in the operating range of interest to make it easier to eventually linearize the state-space model. Reference [17] provided the physical intuition to make $P_{comp}$ a function of

$W_{comp}$ and $x_2$. Using the previously linearized compressor mass flow expression in Equation (2.13), compressor power is linearized as:

$$P_{comp}(x_2, x_3, x_5) = h_1 x_2 + h_2 W_{comp} + h_3 = h_1 x_2 + h_2(g_1 x_3 + g_2 x_5 + g_3) + h_3 \quad (2.23)$$

### 2.8.4 Linear Compressor Power Equation Validation

Since compressor power is not a logged quantity in the GT-Power/Simulink model, the linear compressor power equation can not be validated against reference data. It can, however, be validated against the original nonlinear expression for compressor power as shown in Fig. 2.12. In this figure the nonlinear compressor power term is expressed by Equation (2.22), where it is a function of $x_2$ and the nonlinear $W_{comp}$ model shown in Equation (2.11). The linear compressor power term is expressed by Equation (2.23), where it is a function of $x_2$ and linear $W_{comp}$ model shown in Equation (2.13). During transient load factor step changes, both the linear and nonlinear models display very similar transient behavior. In steady-state, percent difference between the nonlinear and linear models is approximately 15% at all load factors. The nonlinear and linear compressor power models are therefore considered very close.
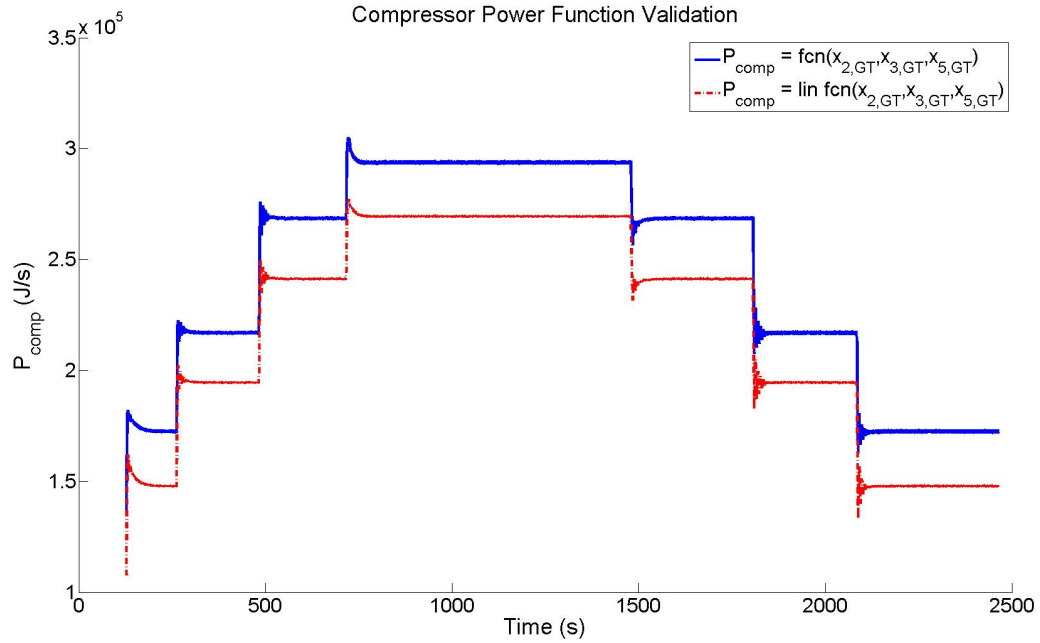
Figure 2.12.   Compressor power expression validation.

## 2.9   Turbine Power Modeling

A term for turbine power generation ($P_{turb}$) does not appear in the original dynamic equations for the engine, but it is necessary in deriving a differential equation for turbocharger speed ($x_5$), one of the state variables. The strategy for modeling turbine power generation is based on the approach taken in [17]. Assumptions for the turbine power generation model are the same as those for the turbine mass flow rate model.

### 2.9.1 Turbine Power Equation

The turbine power equation is a function of exhaust manifold pressure and turbine mass flow rate. Since turbine mass flow rate is a function of $x_4$ in this study, turbine power is strictly a function of $x_4$ in this model.

$$P_{turb} = W_{turb}(x_4)c_{p,exh}\eta_{turb}T_{em}[1 - \frac{P_{atm}}{x_4}]^{\frac{\gamma_{exh}-1}{\gamma_{exh}}} \qquad (2.24)$$

### 2.9.2 Turbine Power Equation Validation

As with compressor power, the GT-Power/Simulink model that was used to obtain truth-reference data does not have turbine power measurements built into the model. Therefore, the expression in Equation (2.24) can not be validated directly with truth-reference data. However, if the compressor and turbine power modeling strategies are accurate, the state equation for turbocharger speed should match the reference data for $x_5$ in steady-state.

### 2.9.3 Linear Turbine Power Equation

The turbine power equation is linearized in the operating range of interest as follows:

$$P_{turb}(x_4) = e_1x_4 + e_2 \qquad (2.25)$$

This is done to simplify the linearization process of the state-space model.

### 2.9.4 Linear Turbine Power Equation Validation

The linear turbine power function of Equation (2.25) is validated against the original nonlinear turbine power expression of Equation (2.24) in Fig. 2.13. Both models display nearly identical transient and steady-state behavior. At the lowest load factor of LF = 0.7, there is approximately a 3% difference in steady-state value.
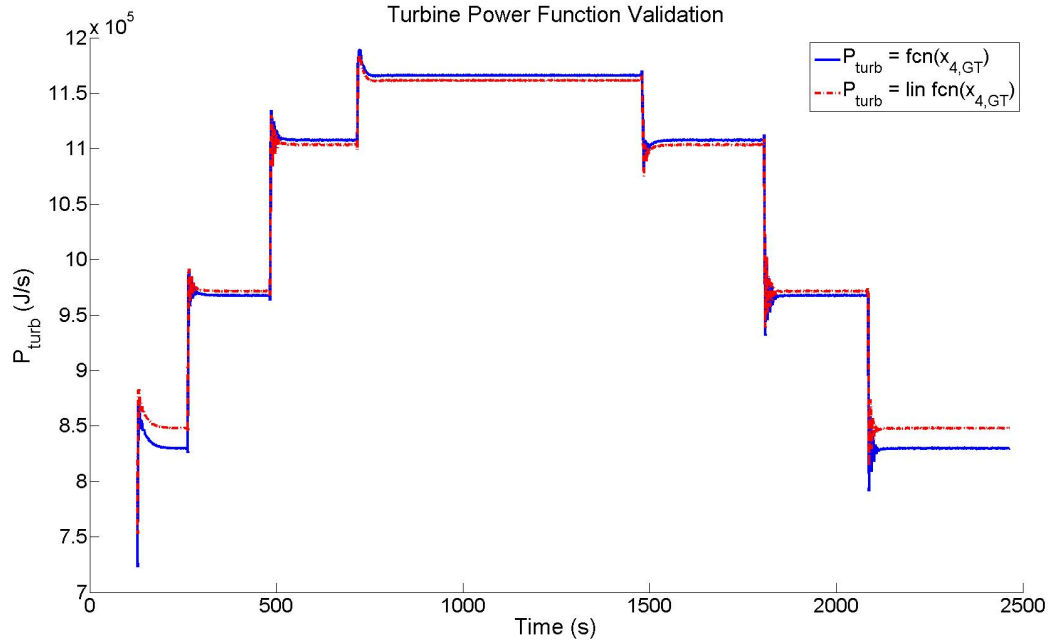
Figure 2.13. Turbine power expression validation.

## 2.10 Summary

This chapter accomplished the following tasks with regard to physics-based modeling of mass flow and power terms of the engine model:

1. Declared state variables that are later used in the formulation of a complete state-space model that characterize engine dynamics.

2. Used first-principles to model engine torque gain ($C_{trq}$) as a function of state variables and compared this expression against reference data.

3. Ultimately chose a constant value of $C_{trq}$ which effectively enslaves fueling control to air mass flow due to the assumption of constant AFR.

4. Used first-principles to model cylinder mass flow ($W_{cyl}$) as a nonlinear function of state variables and validated the expression against reference data.

5. Used first-principles and compressor map data to model compressor mass flow ($W_{comp}$) as both a nonlinear and linear function of state variables and validated both expressions against reference data.

6. Used turbine map data to model turbine mass flow ($W_{turb}$) as both a nonlinear and linear function of state variables and validated both expressions against reference data.

7. Used first-principles to model wastegate mass flow ($W_{wg}$) as both a nonlinear and linear function of state variables and validated both expressions against reference data.

8. Modeled compressor power ($P_{comp}$) as a function of state variables.

9. Modeled turbine power ($P_{turb}$) as a function of state variables.

# 3. STATE-SPACE EQUATION FORMULATION AND MODEL VALIDATION DURING STEADY-STATE AND TRANSIENT OPERATING CONDITIONS

The previous chapter focused on modeling individual mass flow rates and power terms as functions of state-space variables and validating them. This chapter derives a dynamic equation for each of the seven state variables via a physics-based approach. Starting from the fully nonlinear state equations, simplifications are applied until the equations are fully linearized state-space equations. The three modeling cases presented in this chapter are intended to be representative of the actual iterative modeling process that was completed for this engine architecture, and they are all validated in simulation and compared with reference data.

As a reminder, the truth-reference data was obtained in a closed-loop simulation on a GT-Power/Simulink engine model provided by Caterpillar. During the simulation, the Simulink controller works to select control input values that maintain the desired engine speed and other control targets in the presence of step changes in load factor. Load factor is increased from 0.0 to 1.0 in increments of 0.1 and subsequently decreased back down. The system is allowed to reach steady-state with each load factor change. The time interval of interest is the period when load factors are between 0.7 and 1.0. Validation is done by exercising the truth-reference control input data for $u_1$ and $u_2$ on the state-space models during the entirety of the time interval of interest. Truth-reference values of the state variables at the first time step in the time interval of interest are used as initial conditions for the state-space models during validation. Fueling ($u_3$) is no longer considered an independent control input to the model due to the constant AFR assumption of the engine torque gain term. The state-space model predictions of $x_1$ to $x_7$ are compared with truth-reference data for these state variables in the time interval of interest.

## 3.1 Dynamic Equations Derivation

There are seven dynamic equations, one for each state variable. A physics-based approach is taken to derive each of these equations. The derivation for each of these dynamic equations is shown in the following subsections.

### 3.1.1  $x_1$ State Equation Derivation

The differential equation for engine speed is based on a torque balance of the crankshaft of the natural gas engine, as shown in Equation (3.1).

$$J\alpha = Trq_{eng} - Trq_L \tag{3.1}$$

The torques acting on the crankshaft are the torque generated by combustion in the engine and the load-torque demand from the electrical grid. $J$ is the moment of inertia of the engine, while $\alpha$ is the angular acceleration of the engine, which can be written as $\alpha = \dot{\omega}$. The engine torque can be expressed as a product of engine torque gain and intake manifold pressure.

$$Trq_{eng} = C_{trq}P_{im} \tag{3.2}$$

Engine torque gain was assumed to have a constant value of 0.0256, as discussed in Chapter 2. Load torque was defined as a function of the disturbance variable, $w$, in Equation (2.5). By substituting Equation (2.5) and Equation (3.2) into the torque balance of Equation (3.1), the dynamic equation for engine speed can be written as:

$$\dot{\mathbf{x}_1} = \frac{1}{\mathbf{J}}[\mathbf{C_{trq}x_2} - \mathbf{T_{max}w}] \tag{3.3}$$

Equation (3.3) is the same as the dynamic equation for engine speed provided by Caterpillar in Equation (2.1), except that all terms are written explicitly as state-space variables or as functions of state-space variables. As a reminder, $x_1$ is the state variable for engine speed, $x_2$ is the state variable for intake manifold pressure, and $w$ is the disturbance variable for load factor. The fuel mass flow, $u_3$, is no longer considered

an input in this model because of the constant engine torque gain assumption. This means a lower level controller is assumed to control fueling to maintain a constant AFR.

### 3.1.2 $x_2$ State Equation Derivation

The derivation of the state equation for $x_2$ begins with applying the ideal gas law to the intake manifold. The ideal gas law is normally written as $PV = MRT$, and if both sides of the equation are divided by volume it can be written as $P = \frac{RT}{V}M$. For the intake manifold, the ideal gas law is:

$$P_{im} = \frac{R_{im}T_{im}}{V_{im}}M_{im} \tag{3.4}$$

Taking the time derivative of Equation (3.4) yields the dynamic equation for intake manifold pressure, $P_{im}$.

$$\frac{dP_{im}}{dt} = \dot{P}_{im} = \frac{R_{im}T_{im}}{V_{im}}\frac{dM_{im}}{dt} \tag{3.5}$$

Intake manifold volume, $V_{im}$, is fixed and the values of $R_{im}$ and $T_{im}$ are assumed constant in the operating range of interest. The only remaining term of Equation (3.5) is the derivative of the intake manifold mass term, $\frac{dM_{im}}{dt}$ which can be written as:

$$\frac{dM_{im}}{dt} = \dot{M}_{im} = W_{thr} - W_{cyl} \tag{3.6}$$

Equation (3.6) is found by performing a mass balance on the intake manifold. Flow into the intake manifold is throttle mass flow while flow out of the intake manifold is cylinder mass flow. Substituting Equation (3.6) into Equation (3.5) yields the original dynamic equation for intake manifold pressure of Equation (2.2). In the state-space, throttle mass flow corresponds to control input $u_1$ and cylinder mass flow was expressed as a function of state variables $x_1$ and $x_2$ in Equation (2.7). Therefore, the state equation for intake manifold pressure is found by writing all terms in Equation (2.2) as state-space variables or functions of state-space variables:

$$\dot{\mathbf{x}}_\mathbf{2} = \frac{\mathbf{R_{im}T_{im}}}{\mathbf{V_{im}}}[\mathbf{u_1} - \mathbf{W_{cyl}(x_1, x_2)}] \tag{3.7}$$

### 3.1.3  $x_3$ State Equation Derivation

To derive a state equation for $x_3$, the ideal gas law is applied to the boost manifold control volume as follows:

$$P_{bm} = \frac{R_{bm}T_{bm}}{V_{bm}}M_{bm} \tag{3.8}$$

Taking the time derivative of Equation (3.8) yields the following differential equation for $P_{bm}$:

$$\frac{dP_{bm}}{dt} = \dot{P}_{bm} = \frac{R_{bm}T_{bm}}{V_{bm}}\frac{dM_{bm}}{dt} \tag{3.9}$$

The boost manifold volume is fixed and the values of $R_{bm}$ and $T_{bm}$ are assumed constant in the operating range of interest. The mass time derivative term of Equation (3.9) is derived via a mass balance in the boost manifold.

$$\frac{dM_{bm}}{dt} = \dot{M}_{bm} = W_{comp} - W_{thr} - W_{byp} \tag{3.10}$$

Flow into the boost manifold is represented by the term $W_{comp}$. When the turbocharger operates, the compressor inducts fuel-air mixture into the boost manifold. Flow out of the boost manifold is accounted for by the terms $W_{thr}$ and $W_{byp}$. When the throttle valve is open, mass flows out of the boost manifold and into the intake manifold. When the bypass valve is open, flow leaves the compressor and goes back to the compressor inlet. The compressor bypass valve in this engine architecture is utilized when the turbocharger is operating near the surge margin and opening it reduces the boost pressure. Substituting Equation (3.10) into Equation (3.9) yields the original dynamic equation for boost pressure in Equation (2.3). $W_{thr}$ corresponds to input $u_1$ and $W_{byp}$ corresponds to input $u_2$ in the state-space. Additionally, the compressor mass flow term, $W_{comp}$ was made a function of $x_3$ and $x_5$ in Equation (2.11). The state equation for boost manifold pressure is then found by writing all terms in Equation (2.3) as state-variables or functions of state-space variables:

$$\dot{\mathbf{x}}_3 = \frac{\mathbf{R_{bm}T_{bm}}}{\mathbf{V_{bm}}}[\mathbf{W_{comp}(x_3, x_5)} - \mathbf{u_1} - \mathbf{u_2}] \tag{3.11}$$

### 3.1.4 $x_4$ State Equation Derivation

The ideal gas law is applied to the exhaust manifold control volume to derive a state equation for $x_4$:

$$P_{em} = \frac{R_{em}T_{em}}{V_{em}}M_{em} \tag{3.12}$$

A differential equation for $P_{em}$ is obtained by taking a time derivative of Equation (3.12) as follows:

$$\frac{dP_{em}}{dt} = \dot{P}_{em} = \frac{R_{em}T_{em}}{V_{em}}\frac{dM_{em}}{dt} \tag{3.13}$$

The exhaust manifold volume, $V_{em}$, is fixed. The terms $R_{em}$ and $T_{em}$ are assumed constant in the operating range of interest. The term $\frac{dM_{em}}{dt}$ is derived via a mass balance in the exhaust manifold.

$$\frac{dM_{em}}{dt} = \dot{M}_{em} = W_{cyl} - W_{turb} - W_{wg} \tag{3.14}$$

Flow into the exhaust manifold is represented by $W_{cyl}$ because charge mixture goes into the exhaust manifold after undergoing combustion in the cylinders. Flow out of the exhaust manifold is represented by the terms $W_{turb}$ and $W_{wg}$. Exhaust gases that flow into the turbine are represented by the term $W_{turb}$, and they power the turbine causing the compressor to induct more air. Since this engine architecture features a passive wastegate valve, when the boost pressure reaches a threshold value the wastegate valve opens causing gases represented by the term $W_{wg}$ to bypass the turbine.

Substituting Equation (3.14) into Equation (3.13) results in the original dynamic equation for $P_{em}$ given by Equation (2.4). Cylinder mass flow was made a function of state variables $x_1$ and $x_2$ in Equation (2.7). Turbine mass flow was made a nonlinear function of $x_4$ in Equation (2.14) and a linear function of $x_4$ in Equation (2.16). Wastegate mass flow was made a nonlinear function of $x_4$ and $x_6$ in Equation (2.17) and a linear function of only $x_6$ in Equation (2.21). Therefore, there are two possible expressions for the state equation of exhaust manifold pressure depending on the wastegate mass flow relationship that is used.

The state equation for exhaust manifold pressure obtained by substituting state-variables into Equation (3.13), and using the nonlinear function for wastegate mass flow is:

$$\dot{\mathbf{x}}_4 = \frac{\mathbf{R_{em}T_{em}}}{\mathbf{V_{em}}}[\mathbf{W_{cyl}}(\mathbf{x_1}, \mathbf{x_2}) - \mathbf{W_{turb}}(\mathbf{x_4}) - \mathbf{W_{wg}}(\mathbf{x_4}, \mathbf{x_6})] \qquad (3.15)$$

The state equation for exhaust manifold pressure obtained by substituting state-variables into Equation (3.13), and using the linear function for wastegate mass flow is:

$$\dot{\mathbf{x}}_4 = \frac{\mathbf{R_{em}T_{em}}}{\mathbf{V_{em}}}[\mathbf{W_{cyl}}(\mathbf{x_1}, \mathbf{x_2}) - \mathbf{W_{turb}}(\mathbf{x_4}) - \mathbf{W_{wg}}(\mathbf{x_6})] \qquad (3.16)$$

Note that the turbine mass flow term in Equation (3.15) and Equation (3.16) can be either nonlinear or linear, but in either case $W_{turb}$ is solely a function of $x_4$.

### 3.1.5 $x_5$ State Equation Derivation

The first step in obtaining a dynamic equation for $x_5$, is performing a torque balance on the turbocharger shaft as follows:

$$\sum T_{tc} = I_{tc}\alpha_{tc} = Trq_{turb} - Trq_{comp} \qquad (3.17)$$

In Equation (3.17), $I_{tc}$ is the turbochargers shaft inertia, $\alpha_{tc}$ is the angular acceleration of the turbocharger shaft, $Trq_{turb}$ is the torque produced by gases flowing through the turbine, and $Trq_{comp}$ is the torque produced by the compressor. The turbine and compressor torque terms can be written out in terms of power and angular velocity.

$$Trq_{turb} = \frac{P_{turb}}{\omega_{tc}} \qquad (3.18)$$

$$Trq_{comp} = \frac{P_{comp}}{\omega_{tc}} \qquad (3.19)$$

Substituting Equation (3.18) and Equation (3.19) into Equation (3.17) and dividing both sides by $I_{tc}$ yields an expression for angular acceleration of the turbocharger shaft.

$$\alpha_{tc} = \frac{P_{turb} - P_{comp}}{I_{tc}\omega_{tc}} \qquad (3.20)$$

In reality, not all of the power generated by exhaust gases flowing through the turbine are transmitted to the compressor, so a turbocharger mechanical efficiency term is introduced into Equation (3.20) as $\eta_{mech}$.

$$\alpha_{tc} = \frac{\eta_{mech}P_{turb} - P_{comp}}{I_{tc}\omega_{tc}} \tag{3.21}$$

In addition to the mechanical efficiency between the turbine and the compressor, there is also inherent damping in a turbocharger. Damping is proportional to angular velocity, so as the turbocharger shaft rotates faster damping increases. Damping is accounted for by adding a term, $b_{tc}$ to Equation (3.21).

$$\alpha_{tc} = \frac{\eta_{mech}P_{turb} - P_{comp}}{I_{tc}\omega_{tc}} - \frac{b_{tc}}{I_{tc}}\omega_{tc} \tag{3.22}$$

Both turbocharger mechanical efficiency and turbocharger damping values were not explicitly provided for the turbocharger in this engine architecture, so they were estimated. Turbine power was made a nonlinear function of $x_4$ in Equation (2.24) and a linear function of $x_4$ in Equation (2.25). Likewise, compressor power was made both a nonlinear and linear function of $x_2$, $x_3$, and $x_5$ in Equations (2.22) and (2.23) respectively. Therefore, the state equation for turbocharger speed can be found by substituting state-space variables into Equation (3.22) and writing out the power terms as functions of state-space variables.

$$\dot{\mathbf{x}}_5 = \frac{\eta_{mech}\mathbf{P}_{turb}(\mathbf{x}_4) - \mathbf{P}_{comp}(\mathbf{x}_2, \mathbf{x}_3, \mathbf{x}_5)}{\mathbf{I}_{tc}\mathbf{x}_5} - \frac{\mathbf{b}_{tc}}{\mathbf{I}_{tc}}\mathbf{x}_5 \tag{3.23}$$

### 3.1.6   $x_6$ State Equation Derivation

The state equation for wastegate valve lift is found by taking the time derivative of wastegate valve lift:

$$\frac{dL_{wg}}{dt} = 1000V_{wg} \tag{3.24}$$

The units of $L_{wg}$ are mm and the units of $V_{wg}$ are m/s, which is why velocity is multiplied by one-thousand in Equation (3.24). Substituting $x_6$ for wastegate valve

lift and $x_7$ for wastegate valve velocity in Equation (3.24) results in the state equation for $x_6$.

$$\dot{\mathbf{x}}_{\mathbf{6}} = \mathbf{1000x_7} \tag{3.25}$$

### 3.1.7  x$_7$ State Equation Derivation

The dynamic equation for wastegate valve velocity is derived via a force balance on the wastegate diaphragm. Since this engine architecture features a passive wastegate, the displacement of the diaphragm dictates the lift of the wastegate valve. The forces acting on the diaphragm are the spring displacement force, spring pretension force, damping force, and forces resulting from pressures acting on the wastegate diaphragm area. The following equation describes force balance on the wastegate diaphragm:

$$\sum F_{wg} = m_{wg} a_{wg} = \frac{A_d}{10}(P_{bm} - P_a) - k_{wg} L_{wg} - F_p - b_{wg} V_{wg} \tag{3.26}$$

Figure 3.1 shows a zoom-in of the wastegate valve and diaphragm housing. $F_{P_{bm}}$ is the force resulting from boost pressure, $F_{P_a}$ is the force resulting from ambient air pressure, $F_P$ is the pretension force from the springs, $F_S$ is the resulting force from compressing the wastegate springs, and $F_{damp}$ is the damping force when the wastegate valve moves.
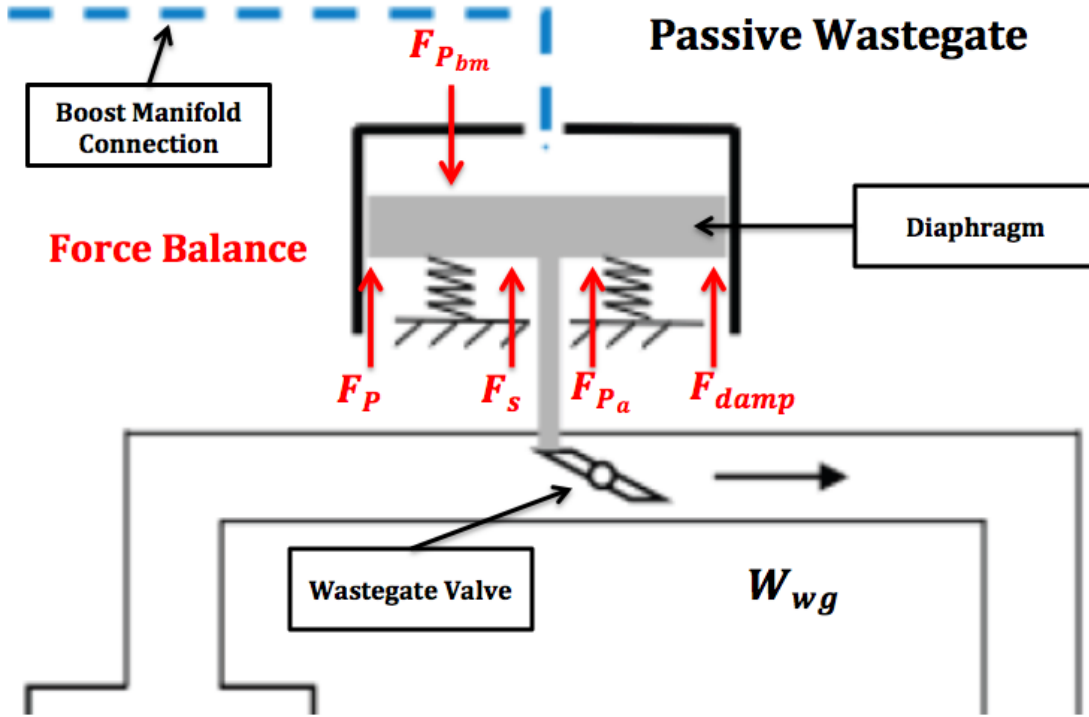
Figure 3.1. Wastegate schematic zoom-in.

In Equation (3.26) $A_d$ is the diaphragm area, $k_{wg}$ is the wastegate valve spring constant, and $b_{wg}$ is the wastegate valve damping constant. The equation above can be rearranged by dividing both sides by the wastegate diaphragm mass.

$$a_{wg} = \dot{V}_{wg} = \frac{1}{m_{wg}}[\frac{A_d}{10}(P_{bm} - P_a) - k_{wg}L_{wg} - F_p - b_{wg}V_{wg}] \qquad (3.27)$$

Boost pressure, wastegate valve lift, and wastegate valve lift velocity are all variables in the state-space domain, so the state equation for $x_7$ is found by substituting state variables into Equation (3.27).

$$\dot{x}_7 = \frac{1}{m_{wg}}[\frac{A_d}{10}(x_3 - P_a) - k_{wg}x_6 - F_p - b_{wg}x_7] \qquad (3.28)$$

Note that when the wastegate valve is closed shut, the right hand side of Equation (3.28) becomes zero and both states $x_6$ and $x_7$ have values of zero. Therefore by

applying steady-state conditions to the dynamic equation for $x_7$, the threshold boost pressure to open the valve can be expressed symbolically:

$$P_{bm,crit} = \frac{10F_p}{A_d} + P_a \tag{3.29}$$

Despite being a linear dynamic equation, the state equation for $x_7$ is conditional in reality. In the actual engine, the valve only opens when the boost pressure reaches the threshold value of Equation (3.29) and stays closed otherwise. Wastegate valve lift can not be negative, even when boost pressure is really low in the real engine.

## 3.2 Model Case Definitions

This section defines the three physics-based modeling cases that are validated against the GT-Power engine model. The first case consists of a set of nonlinear state equations whose mass flow and power terms are nonlinear functions of state variables. The second case consists of a simplifying the nonlinear state equations by linearizing most of the mass flow and power expressions. The third case shows how the simplified nonlinear state equations are linearized about an equilibrium point and expressed in a true state-space form, which is the ultimate goal of control-oriented modeling.

### 3.2.1 Case A Model Definition: Nonlinear Expressions

In this modeling case the state equations are as follows:

$$\dot{x}_1 = \frac{1}{J}[C_{trq}x_2 - T_{max}w] \tag{3.30}$$

$$\dot{x}_2 = \frac{R_{im}T_{im}}{V_{im}}[u_1 - W_{cyl}(x_1, x_2)] \tag{3.31}$$

$$\dot{x}_3 = \frac{R_{bm}T_{bm}}{V_{bm}}[W_{comp}(x_3, x_5) - u_1 - u_2] \tag{3.32}$$

$$\dot{x}_4 = \frac{R_{em}T_{em}}{V_{em}}[W_{cyl}(x_1, x_2) - W_{turb}(x_4) - W_{wg}(x_4, x_6)] \tag{3.33}$$

$$\dot{x}_5 = \frac{\eta_{mech}P_{turb}(x_4) - P_{comp}(x_2, x_3, x_5)}{I_{tc}x_5} - \frac{b_{tc}}{I_{tc}}x_5 \tag{3.34}$$

$$\dot{x}_6 = 1000x_7 \tag{3.35}$$

$$\dot{x}_7 = \frac{1}{m_{wg}}[\frac{A_d}{10}(x_3 - P_a) - k_{wg}x_6 - F_p - b_{wg}x_7] \tag{3.36}$$

The value of $C_{trq}$ is assumed to be 0.0256, and Equation (2.7) expresses $W_{cyl}$ as a function of state variables. The mass flow terms $W_{comp}$ and $W_{turb}$ are defined in Equations (2.11) and (2.14), respectively, while the power terms $P_{comp}$ and $P_{turb}$ are defined in Equations (2.22) and (2.24), respectively. Wastegate mass flow, $W_{wg}$, is defined by Equation (2.17). All mass flow terms and power terms are nonlinear expressions in this modeling case.

### 3.2.2 Case B Model Definition: Linearized Mass Flow and Power Terms

The difference between this case and the previous case A (Equations (3.30) - (3.36)) is that the terms $W_{comp}$, $W_{turb}$, $W_{wg}$, $P_{comp}$, and $P_{turb}$ are simplified to be linear functions of state variables. Compressor mass flow, $W_{comp}$, is now a linear function of $x_3$ and $x_5$ as defined in Equation (2.13). Turbine mass flow, $W_{turb}$, is a linear function of $x_4$ as defined in Equation (2.16). Wastegate mass flow, $W_{wg}$, is a linear function of $x_6$ as defined in Equation (2.21). Compressor power is a linear function of $x_2$, $x_3$, and $x_5$ as defined in Equation (2.23), and turbine power is a linear function of $x_4$ and defined in Equation (2.25). Cylinder mass flow ($W_{cyl}$) is still a nonlinear function of states $x_1$ and $x_2$ as per Equation (2.7).

The state equations for this case are simplified and written out in expanded form, where a constant value of 0.0256 is substituted for $C_{trq}$, Equation (2.13) is substituted for $W_{comp}$, Equation (2.16) is substituted for $W_{turb}$, Equation (2.7) is substituted for $W_{cyl}$, Equation (2.21) is substituted for $W_{wg}$, Equation (2.23) is substituted for $P_{comp}$, and Equation (2.25) is substituted for $P_{turb}$:

$$\dot{x}_1 = \frac{1}{J}[0.0256x_2 - T_{max}w] \tag{3.37}$$

$$\dot{x}_2 = \frac{R_{im}T_{im}}{V_{im}}[u_1 - \frac{\eta_v V_D}{2RT_{im}}x_1x_2] \tag{3.38}$$

$$\dot{x}_3 = \frac{R_{bm}T_{bm}}{V_{bm}}[g_1x_3 + g_2x_5 + g_3 - u_1 - u_2] \tag{3.39}$$

$$\dot{x}_4 = \frac{R_{em}T_{em}}{V_{em}}[\frac{\eta_v V_D}{2RT_{im}}x_1 x_2 - C_1 x_4 - C_2 - f_1 x_6] \tag{3.40}$$

$$\dot{x}_5 = \frac{\eta_{mech}e_1}{I_{tc}}\frac{x_4}{x_5} + \frac{\eta_{mech}e_2 - h_2 g_3 - h_3}{I_{tc}}\frac{1}{x_5} - \frac{h_1}{I_{tc}}\frac{x_2}{x_5} - \frac{h_2 g_1}{I_{tc}}\frac{x_3}{x_5} - \frac{h_2 g_2}{I_{tc}} - \frac{b_{tc}}{I_{tc}}x_5 \tag{3.41}$$

$$\dot{x}_6 = 1000 x_7 \tag{3.42}$$

$$\dot{x}_7 = \frac{A_d}{10 m_{wg}}x_3 - \frac{k_{wg}}{m_{wg}}x_6 - \frac{b_{wg}}{m_{wg}}x_7 - \frac{A_d P_a + 10 F_p}{10 m_{wg}} \tag{3.43}$$

For simplicity of notation, lengthy expressions that are of a constant value in Equations (3.37) - (3.43) can be substituted with a single constant value as shown in Equations (3.44) - (3.50).

$$\dot{x}_1 = f_1 = m_1 x_2 + m_2 w \tag{3.44}$$

$$\dot{x}_2 = f_2 = m_3 u_1 + m_4 x_1 x_2 \tag{3.45}$$

$$\dot{x}_3 = f_3 = m_5 x_3 + m_6 x_5 + m_7 + m_8 u_1 + m_9 u_2 \tag{3.46}$$

$$\dot{x}_4 = f_4 = m_{10} x_1 x_2 + m_{11} x_4 + m_{12} + m_{13} x_6 \tag{3.47}$$

$$\dot{x}_5 = f_5 = m_{14}\frac{x_4}{x_5} + m_{15}\frac{1}{x_5} + m_{16}\frac{x_2}{x_5} + m_{17}\frac{x_3}{x_5} + m_{18} + m_{19} x_5 \tag{3.48}$$

$$\dot{x}_6 = f_6 = m_{20} x_7 \tag{3.49}$$

$$\dot{x}_7 = f_7 = m_{21} x_3 + m_{22} x_6 + m_{23} x_7 + m_{24} \tag{3.50}$$

The simplification constants are written out in Equations (3.51) - (3.74):

$$m_1 = 0.0256 \tag{3.51}$$

$$m_2 = -\frac{T_{max}}{J} \tag{3.52}$$

$$m_3 = \frac{R_{im}T_{im}}{V_{im}} \tag{3.53}$$

$$m_4 = -\frac{\eta_v V_D}{2V_{im}} \tag{3.54}$$

$$m_5 = \frac{R_{bm}T_{bm}g_1}{V_{bm}} \tag{3.55}$$

$$m_6 = \frac{R_{bm}T_{bm}g_2}{V_{bm}} \tag{3.56}$$

$$m_7 = \frac{R_{bm}T_{bm}g_3}{V_{bm}} \tag{3.57}$$

$$m_8 = -\frac{R_{bm}T_{bm}}{V_{bm}} \tag{3.58}$$

$$m_9 = -\frac{R_{bm}T_{bm}}{V_{bm}} \tag{3.59}$$

$$m_{10} = \frac{\eta_v V_D}{2V_{em}} \tag{3.60}$$

$$m_{11} = -\frac{R_{em}T_{em}C_1}{V_{em}} \tag{3.61}$$

$$m_{12} = -\frac{R_{em}T_{em}C_2}{V_{em}} \tag{3.62}$$

$$m_{13} = -\frac{R_{em}T_{em}f_1}{V_{em}} \tag{3.63}$$

$$m_{14} = \frac{\eta_{mech}e_1}{I_{tc}} \tag{3.64}$$

$$m_{15} = \frac{\eta_{mech}e_2 - h_2g_3 - h_3}{I_{tc}} \tag{3.65}$$

$$m_{16} = -\frac{h_1}{I_{tc}} \tag{3.66}$$

$$m_{17} = -\frac{h_2g_1}{I_{tc}} \tag{3.67}$$

$$m_{18} = -\frac{h_2g_2}{I_{tc}} \tag{3.68}$$

$$m_{19} = -\frac{b_{tc}}{I_{tc}} \tag{3.69}$$

$$m_{20} = 1000 \tag{3.70}$$

$$m_{21} = \frac{A_d}{10m_{wg}} \tag{3.71}$$

$$m_{22} = -\frac{k_{wg}}{m_{wg}} \tag{3.72}$$

$$m_{23} = -\frac{b_{wg}}{m_{wg}} \tag{3.73}$$

$$m_{24} = -\frac{A_dP_a + 10F_p}{10m_{wg}} \tag{3.74}$$

### 3.2.3  Case C Model Definition: Fully Linearized Case

In case B, most mass flow and power terms were made linear function of state variables, but the state equations were still nonlinear. In this case, the nonlinear state equations of case B (Equations (3.44) - (3.50)) are linearized about an equilibrium point. It is important to note that once linearized, the state variables and input variables are perturbations of the states and inputs from equilibrium values. After linearization, the model is expressed in the standard state-space form:

$$\dot{x} = Ax + Bu$$

The schematic in Figure 3.2 shows a block diagram representation of the linearized physics-based state equations.
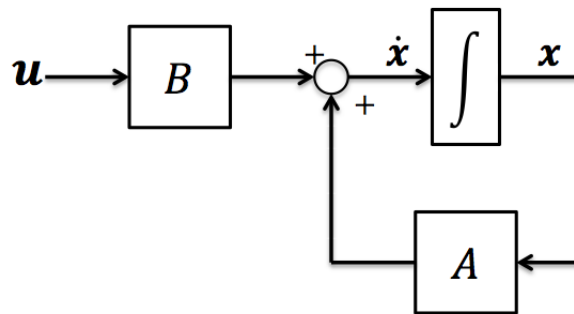


Figure 3.2.  Block diagram representation of linearized physics-based engine model.

The symbolic $A$ and $B$ matrices are obtained by taking partial derivatives of the nonlinear state equations as follows:

$$A_{7\times7} = \begin{bmatrix} \frac{df_1}{dx_1} & \frac{df_1}{dx_2} & \cdots & \frac{df_1}{dx_7} \\ \vdots & \cdots & \ddots & \vdots \\ \frac{df_7}{dx_1} & \frac{df_7}{dx_2} & \cdots & \frac{df_7}{dx_7} \end{bmatrix} \qquad B_{7\times3} = \begin{bmatrix} \frac{df_1}{du_1} & \frac{df_1}{du_2} & \frac{df_1}{dw} \\ \vdots & \vdots & \vdots \\ \frac{df_7}{du_1} & \frac{df_7}{du_2} & \frac{df_n}{dw} \end{bmatrix}$$

Because there are 7 state variables and 3 input variables (2 control inputs and 1 disturbance variable), $A$ is a $7 \times 7$ matrix and $B$ is a $7 \times 3$ matrix. The functions $f_1$ through $f_7$ in the matrices above refer to Equations (3.44) - (3.50). Element $(a, b)$

in $A$ is found by symbolically differentiating $f_a$ with respect to state $x_b$. Matrix $B$ is found by differentiating $f_1$ through $f_7$ with respect to the inputs symbolically, and element $(a, b)$ in B is found by symbolically differentiating $f_a$ with respect to $u_b$. In this case, the disturbance variable, $w$, is treated as an input variable so the last column of matrix $B$ corresponds to $f_1$ through $f_7$ being differentiated with respect to $w$.

Numeric $A$ and $B$ matrices are found by substituting equilibrium point values of states and inputs into the symbolic matrices. The equilibrium point is the values of states ($x_1$ - $x_7$) that cause all the dynamic equations given by $f_1$ through $f_7$ to equal zero. The equilibrium point values depend on the point of linearization. In this case, the linearization point is chosen to correspond to a load factor of 0.85 ($w = 0.85$). Since the GT-Power model is never actually run at a load factor of $w = 0.85$, the equilibrium point input values of $u_1$ and $u_2$ are found by averaging their respective steady-state values in the truth-reference data at load-factors of 0.8 and 0.9. After the equilibrium input and disturbance values are substituted into $f_1$ through $f_7$, the equilibrium point values of the states are found algebraically by setting $f_1$ through $f_7$ equal to zero so there are seven equations and seven unknowns ($x_1$ - $x_7$). These numeric matrices are shown below.

$$A_{SS} = \begin{bmatrix} 0 & 2.6e-4 & 0 & 0 & 0 & 0 & 0 \\ -4.9e4 & -4.3 & 0 & 0 & 0 & 0 & 0 \\ 0 & 0 & -17 & 0 & 2e4 & 0 & 0 \\ 3e5 & 26 & 0 & -28 & 0 & -2.7e5 & 0 \\ 0 & -0.23 & 0.14 & 1.1 & -488 & 0 & 0 \\ 0 & 0 & 0 & 0 & 0 & 0 & 1.0e3 \\ 0 & 0 & 5e-3 & 0 & 0 & -28 & -699 \end{bmatrix}$$

$$
B_{SS} = \begin{bmatrix}
0 & 0 & -88 \\
7.4e5 & 0 & 0 \\
-3.2e6 & -3.2e6 & 0 \\
0 & 0 & 0 \\
0 & 0 & 0 \\
0 & 0 & 0 \\
0 & 0 & 0
\end{bmatrix}
$$

## 3.3 State-Space Model Validation: $x_1$

This section compares the engine speed responses of Models A, B, and C against the GT-Power reference data during the time interval of interest. Models A and B match the reference values for $x_1$ quite well throughout the time interval, with steady-state error increasing with load factor. Model C tends to match the reference data for engine speed better with increasing load factor. Table 3.1 highlights steady-state error at each load factor for each of the Models A, B, and C compared to the reference data for $x_1$.

Table 3.1.  Steady-state error of $x_1$ in Models A, B, and C

| $x_1$ Deviation from Reference | Model A | Model B | Model C |
|:---:|:---:|:---:|:---:|
| Error (%) for $LF = 0.7$ | 1.9 | 1.9 | 14.8 |
| Error (%) for $LF = 0.8$ | 3.3 | 3.3 | 11.7 |
| Error (%) for $LF = 0.9$ | 4.0 | 4.0 | 8.9 |
| Error (%) for $LF = 1.0$ | 4.6 | 4.6 | 6.2 |

Figure 3.3. $x_1$ vs. time.

(a) Step from $LF = 0.7$ to $0.8$

(b) Step from $LF = 0.8$ to $0.9$

(c) Step from $LF = 0.9$ to $1.0$

(d) Step from $LF = 1.0$ to $0.9$

(e) Step from $LF = 0.9$ to $0.8$

(f) Step from $LF = 0.8$ to $0.7$
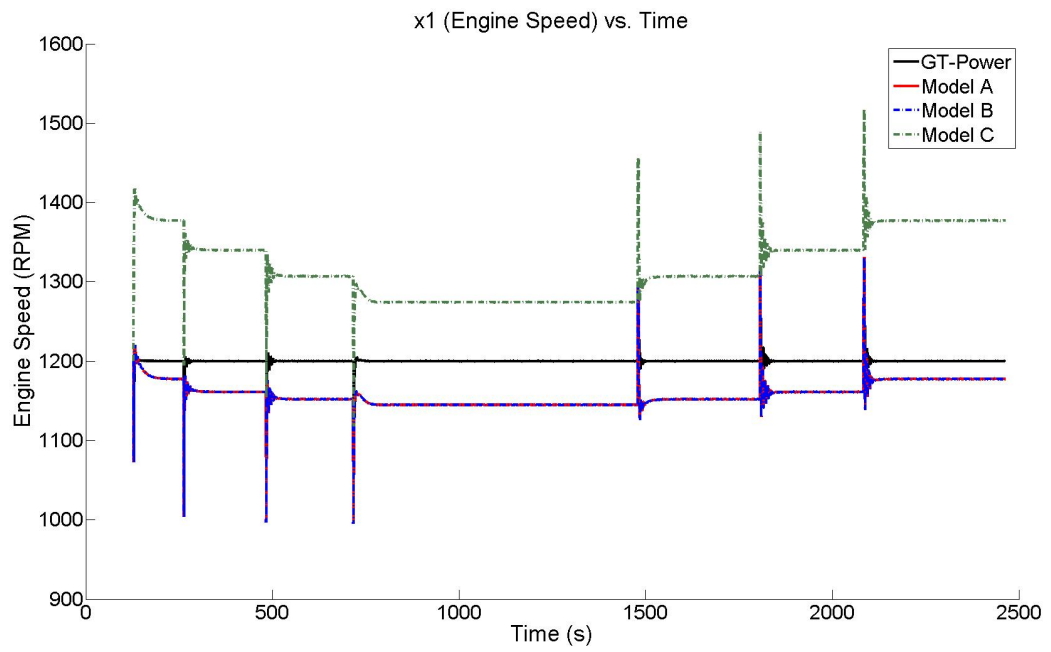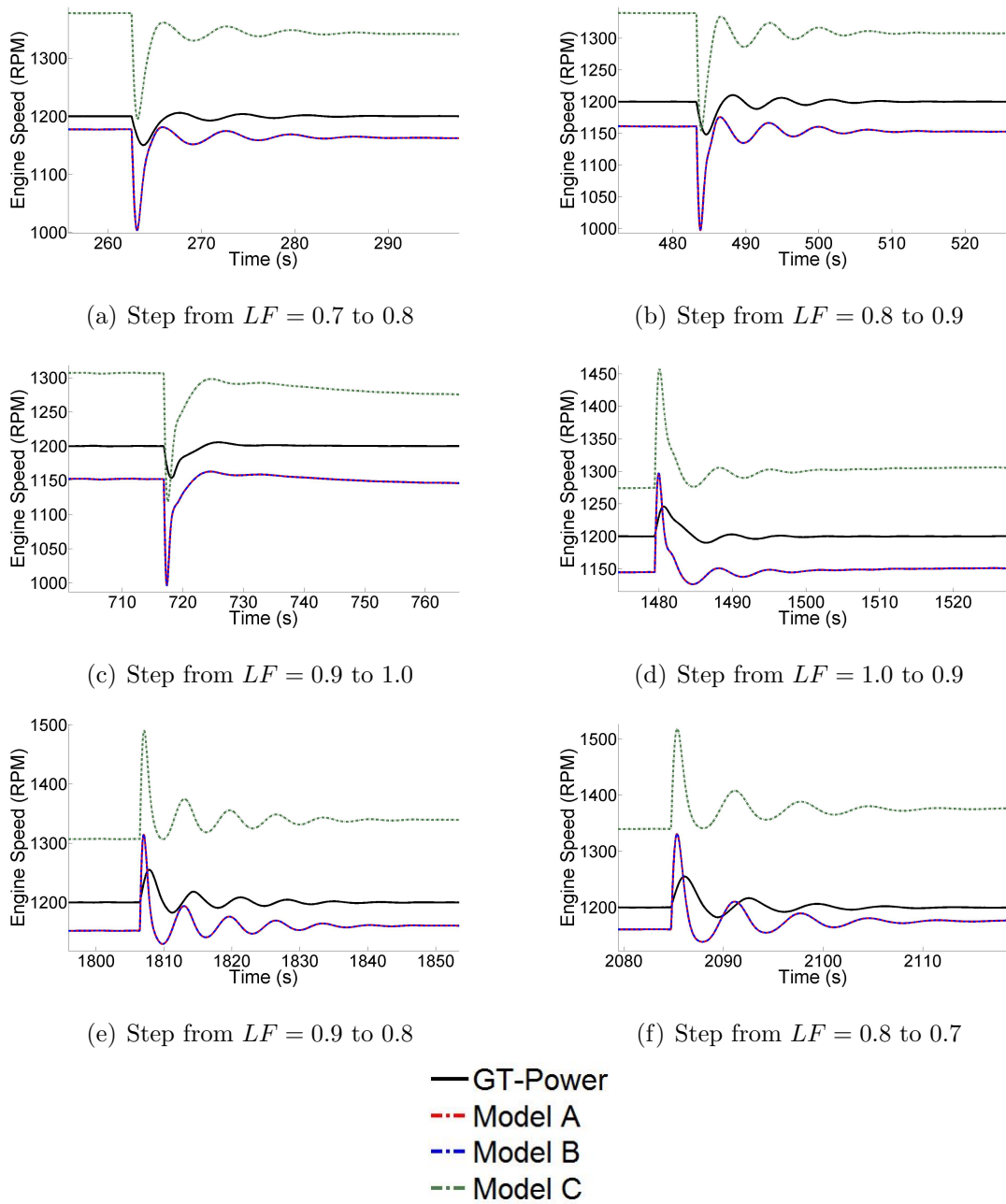
Figure 3.4. Zoom-ins for $x_1$ vs. time.

Figure 3.3 shows the engine speed responses for Models A, B, and C compared to the truth-reference GT-Power data for $x_1$. Subfigures 3.4(a) - 3.4(f) show zoomed-in views of transient behavior during load factor step changes. The fully linearized Model C shows higher steady-state error than Models A and B, which have an identical engine speed response. The zoomed in subfigures show that Models A, B, and C tend to have exaggerated initial peaks for $x_1$ compared to the truth-reference GT-Power data. Additionally the transient $x_1$ responses of Models A, B, and C have a slightly different phase than that of the reference data.

## 3.4   State-Space Model Validation: $x_2$

This section compares the intake manifold pressure responses of Models A, B, and C against the GT-Power reference data during the time interval of interest. The nonlinear Models A and B tend to match the reference data very well, with the highest steady-state error being under 3% at the highest load factor. The linearized Model C tends to underestimate $x_2$ particularly at load factors of 0.7 and 0.8. Table 3.2 highlights steady-state error at each load factor for each of the Models A, B, and C compared to the reference data for $x_2$.

Table 3.2.  Steady-state error of $x_2$ in Models A, B, and C

| $x_2$ **Deviation from Reference** | **Model A** | **Model B** | **Model C** |
|:---:|:---:|:---:|:---:|
| **Error** (%) for $LF = 0.7$ | 1.9 | 1.9 | 17.0 |
| **Error** (%) for $LF = 0.8$ | 0.3 | 0.3 | 13.7 |
| **Error** (%) for $LF = 0.9$ | 0.6 | 0.6 | 11.4 |
| **Error** (%) for $LF = 1.0$ | 2.8 | 2.8 | 8.2 |

Figure 3.5. $x_2$ vs. time.

(a) Step from $LF = 0.7$ to $0.8$

(b) Step from $LF = 0.8$ to $0.9$

(c) Step from $LF = 0.9$ to $1.0$

(d) Step from $LF = 1.0$ to $0.9$

(e) Step from $LF = 0.9$ to $0.8$

(f) Step from $LF = 0.8$ to $0.7$
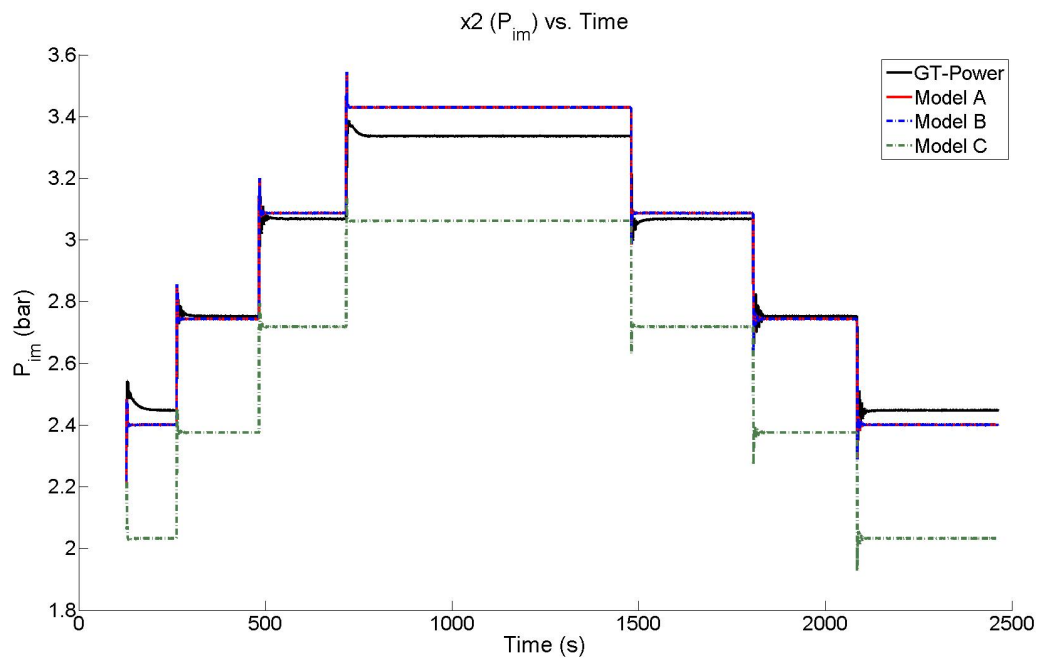
— GT-Power
–·– Model A
–·– Model B
–·– Model C
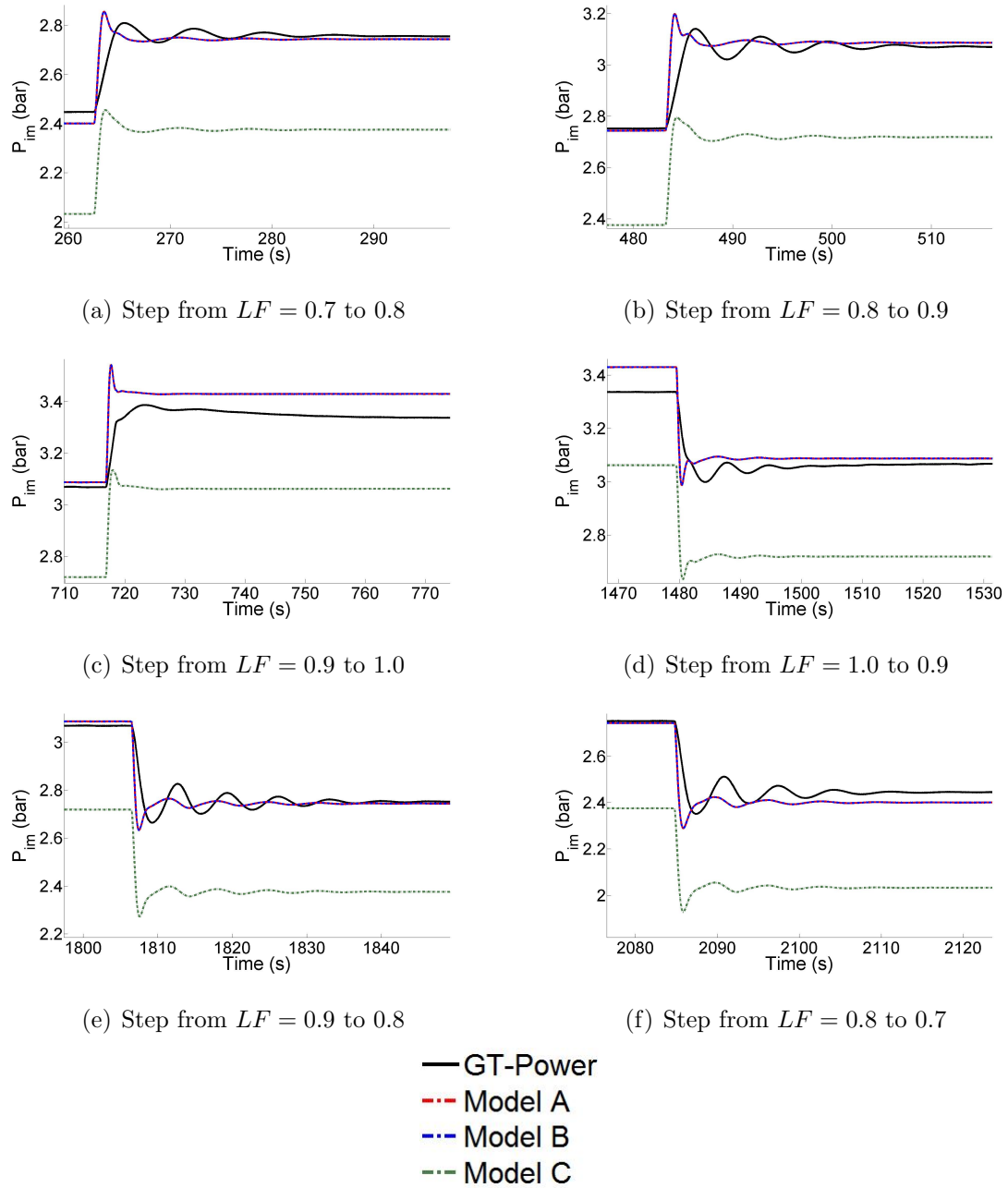
Figure 3.6.   Zoom-ins for $x_2$ vs. time.

Figure 3.5 shows the intake manifold pressure responses for Models A, B, and C compared to the truth-reference GT-Power data for $x_2$. Subfigures 3.6(a) - 3.6(f) show zoomed-in views of transient behavior during load factor step changes. Models A and B are nearly identical in their transient response. All three models have a slightly different phase than the reference $x_2$ response.

## 3.5   State-Space Model Validation: $x_3$

This section compares the boost manifold pressure responses of Models A, B, and C against the GT-Power reference data during the time interval of interest. All of the state-space models tend to overestimate boost pressure at steady-state, especially at the lower load factors of 0.7 and 0.8. This is most likely because of the overestimation of turbocharger speed, $x_5$. The compressor mass flow term that appears in the dynamic equation of $x_3$ in Equation (3.11) is a function of both $x_3$ and $x_5$. The boost pressure is highly sensitive to turbocharger speed dynamics because the highest steady-state error for $x_5$ is under 11% whereas the highest steady-state error for boost pressure is over 30%. Table 3.3 highlights steady-state error at each load factor for each of the Models A, B, and C compared to the reference data for $x_3$.

Table 3.3.   Steady-state error of $x_3$ in Models A, B, and C

| $x_3$ Deviation from Reference | Model A | Model B | Model C |
|---|---|---|---|
| Error (%) for $LF = 0.7$ | 30.8 | 31.2 | 32.7 |
| Error (%) for $LF = 0.8$ | 19.94 | 19.2 | 20.6 |
| Error (%) for $LF = 0.9$ | 10.6 | 9.2 | 10.2 |
| Error (%) for $LF = 1.0$ | 5.0 | 3.5 | 4.7 |

Figure 3.7. $x_3$ vs. time.

(a) Step from $LF = 0.7$ to $0.8$

(b) Step from $LF = 0.8$ to $0.9$

(c) Step from $LF = 0.9$ to $1.0$

(d) Step from $LF = 1.0$ to $0.9$

(e) Step from $LF = 0.9$ to $0.8$

(f) Step from $LF = 0.8$ to $0.7$
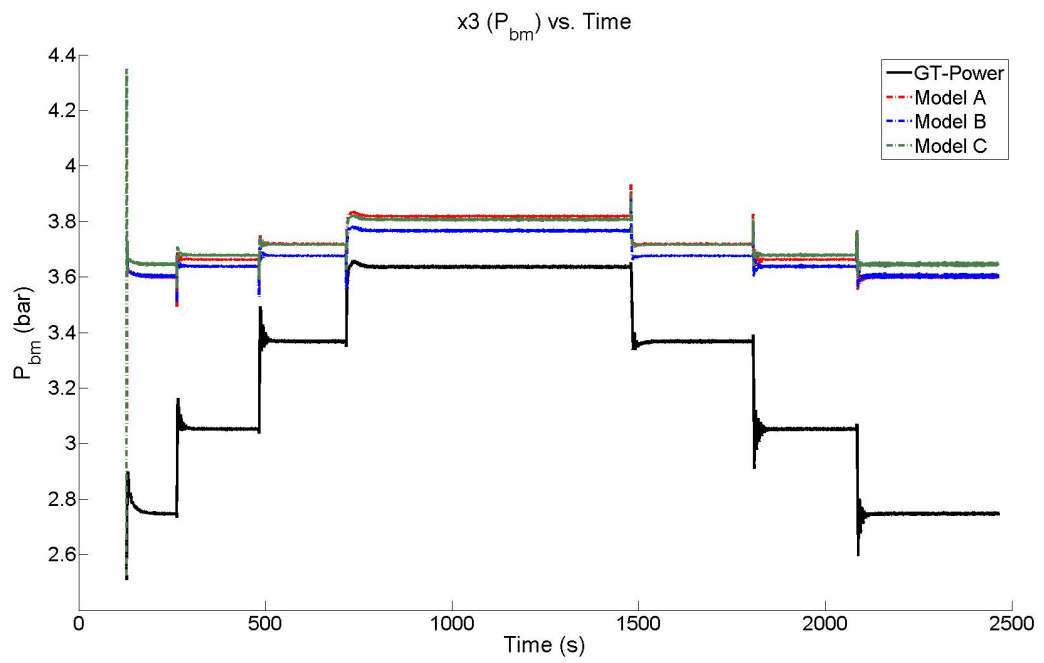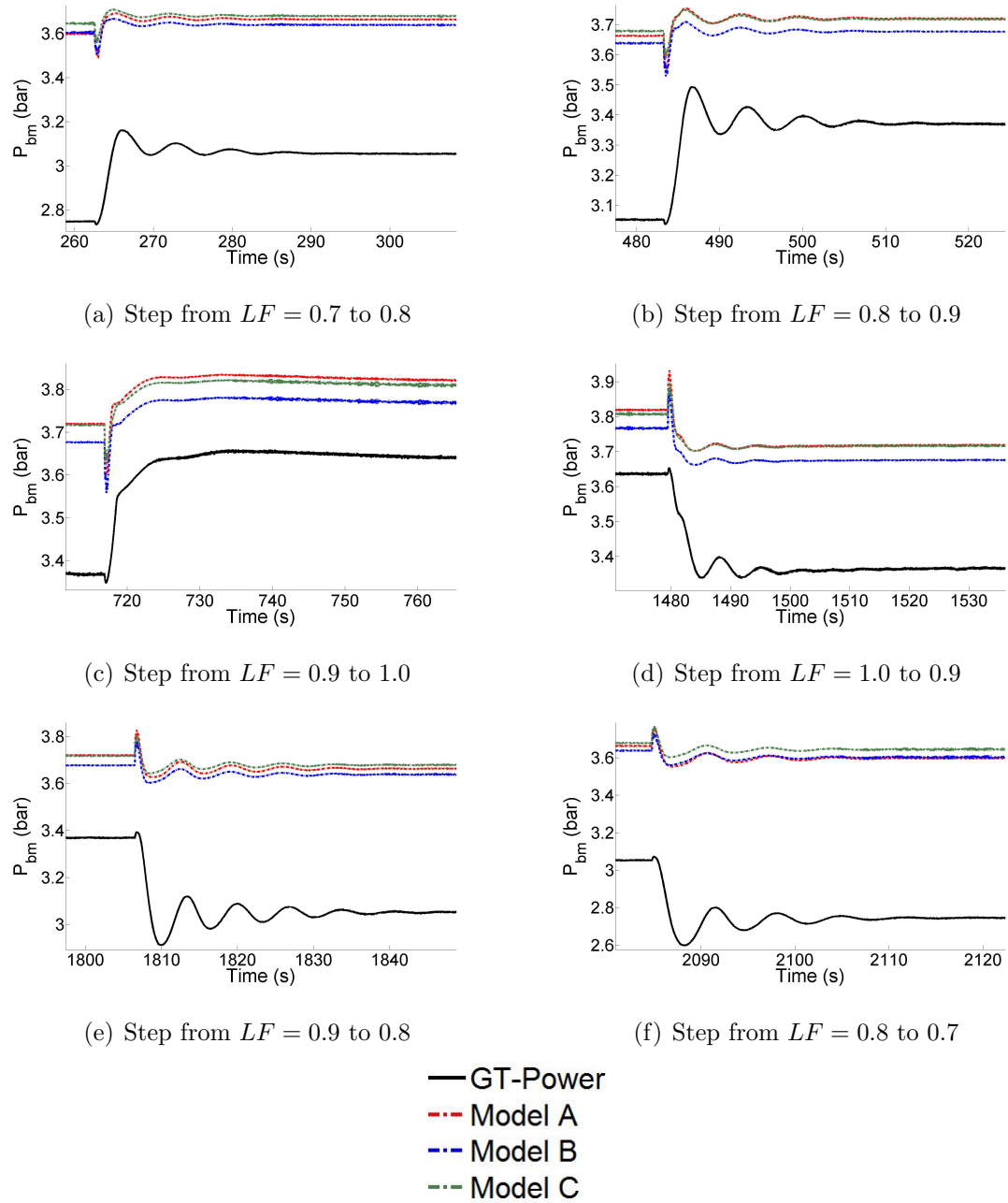
Figure 3.8.   Zoom-ins for $x_3$ vs. time.

Figure 3.7 shows the boost manifold pressure responses for Models A, B, and C compared to the truth-reference GT-Power data for $x_3$. Subfigures 3.8(a) - 3.8(f) show zoomed-in views of transient behavior during load factor step changes. Models A, B, and C display very similar transient behavior, though they have a slightly different phase than the reference $x_3$ response.

## 3.6  State-Space Model Validation: $x_4$

This section compares the exhaust manifold pressure responses of Models A, B, and C against the GT-Power reference data during the time interval of interest. All of the state-space models tend to underestimate exhaust manifold pressure when compared to the reference. Table 3.4 highlights steady-state error at each load factor for each of the Models A, B, and C compared to the reference data for $x_4$.

Table 3.4.  Steady-state error of $x_4$ in Models A, B, and C

| $x_4$ **Deviation from Reference** | **Model A** | **Model B** | **Model C** |
|---|---|---|---|
| **Error (%) for** $LF = 0.7$ | 1.1 | 5.1 | 8.3 |
| **Error (%) for** $LF = 0.8$ | 5.2 | 6.5 | 9.2 |
| **Error (%) for** $LF = 0.9$ | 8.7 | 8.1 | 10.6 |
| **Error (%) for** $LF = 1.0$ | 8.9 | 7.9 | 10.2 |

Figure 3.9. $x_4$ vs. time.

(a) Step from $LF = 0.7$ to $0.8$

(b) Step from $LF = 0.8$ to $0.9$

(c) Step from $LF = 0.9$ to $1.0$

(d) Step from $LF = 1.0$ to $0.9$

(e) Step from $LF = 0.9$ to $0.8$

(f) Step from $LF = 0.8$ to $0.7$
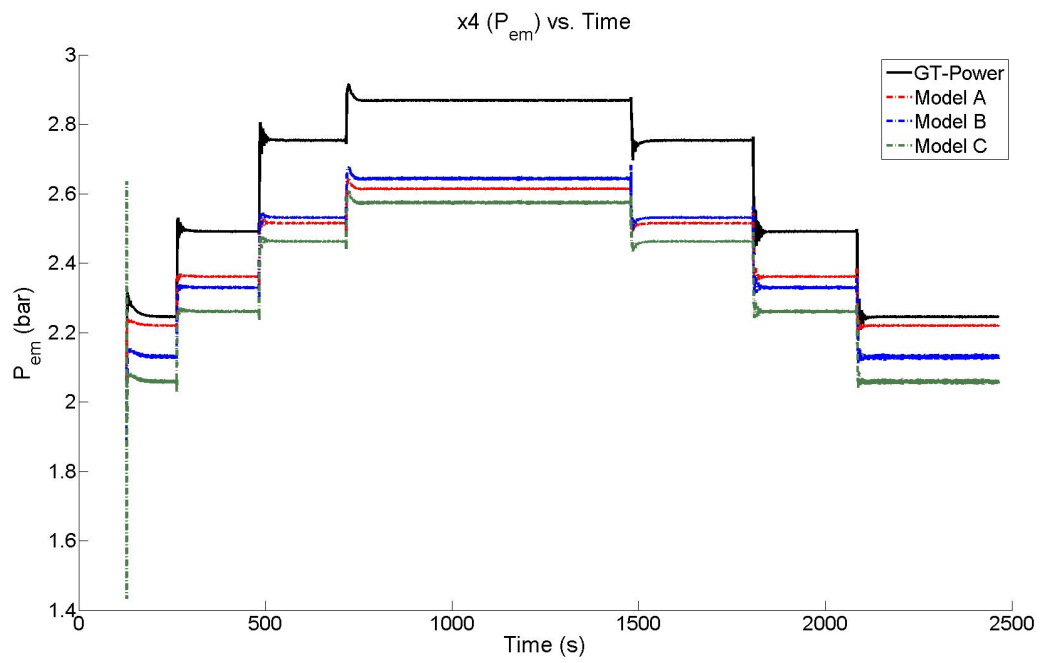
GT-Power
Model A
Model B
Model C
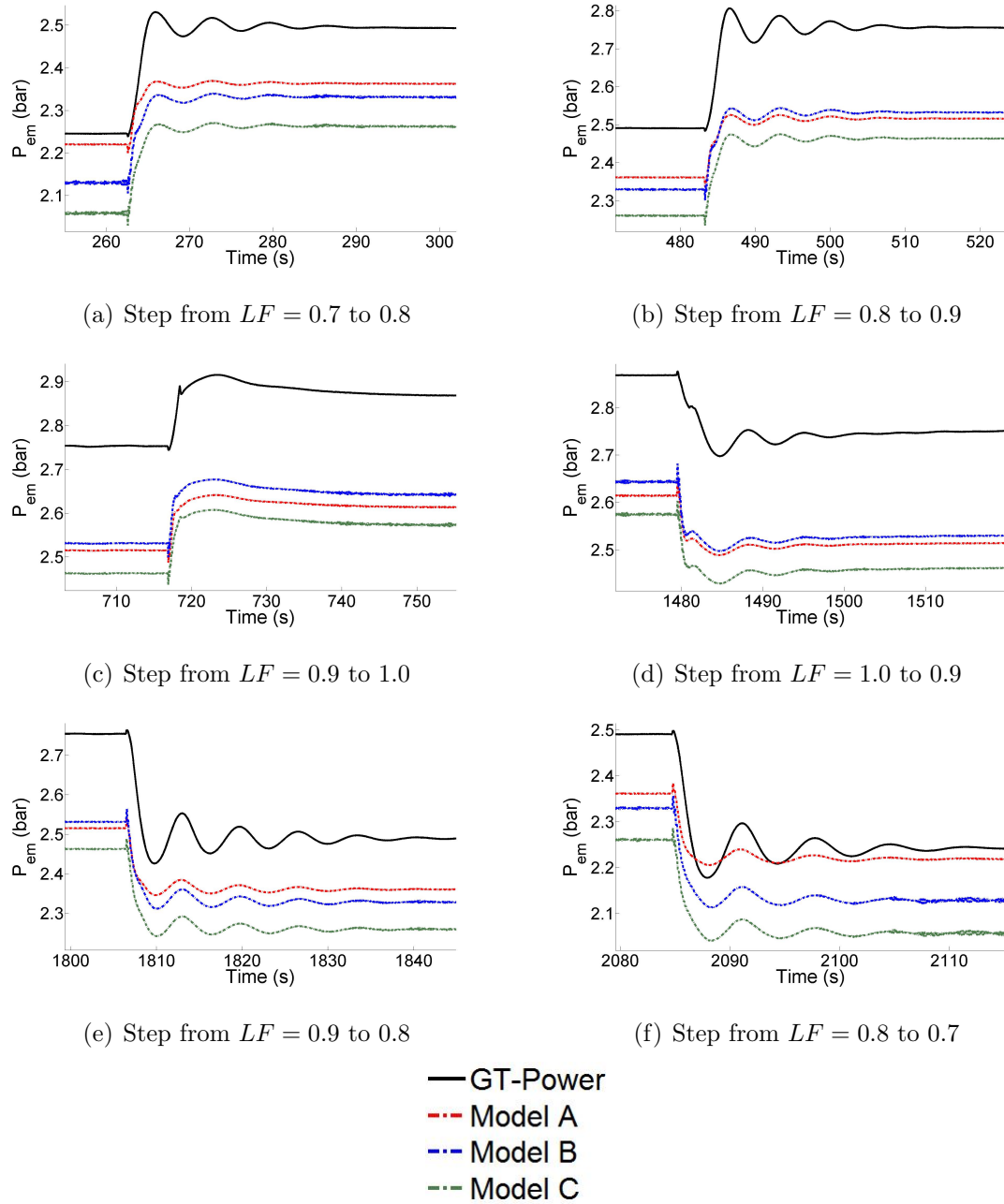
Figure 3.10. Zoom-ins for $x_4$ vs. time.

Figure 3.9 compares the exhaust manifold pressure response of Models A, B, and C with the truth-reference GT-Power data for $x_4$. Subfigures 3.10(a) - 3.10(f) show zoomed-in views of transient behavior during load factor step changes. The phases of all three models match that of the GT-Power truth-reference well. There is steady-state error in all three models which was addressed in Table 3.4.

## 3.7 State-Space Model Validation: $x_5$

This section compares the turbocharger speed responses of Models A, B, and C against the GT-Power reference data during the time interval of interest. Models A, B, and C tend to overestimate turbocharger speed but match reference data better at higher load factors. Table 3.5 highlights steady-state error at each load factor for each of the Models A, B, and C compared to the reference data for $x_5$.

Table 3.5.  Steady-state error of $x_5$ in Models A, B, and C

| $x_5$ **Deviation from Reference** | **Model A** | **Model B** | **Model C** |
|:---:|:---:|:---:|:---:|
| **Error (%) for** $LF = 0.7$ | 10.7 | 8.5 | 9.0 |
| **Error (%) for** $LF = 0.8$ | 6.1 | 5.6 | 6.0 |
| **Error (%) for** $LF = 0.9$ | 2.2 | 3.1 | 3.4 |
| **Error (%) for** $LF = 1.0$ | 0.6 | 1.4 | 1.8 |

Figure 3.11. $x_5$ vs. time.

(a) Step from $LF = 0.7$ to $0.8$

(b) Step from $LF = 0.8$ to $0.9$

(c) Step from $LF = 0.9$ to $1.0$

(d) Step from $LF = 1.0$ to $0.9$

(e) Step from $LF = 0.9$ to $0.8$

(f) Step from $LF = 0.8$ to $0.7$
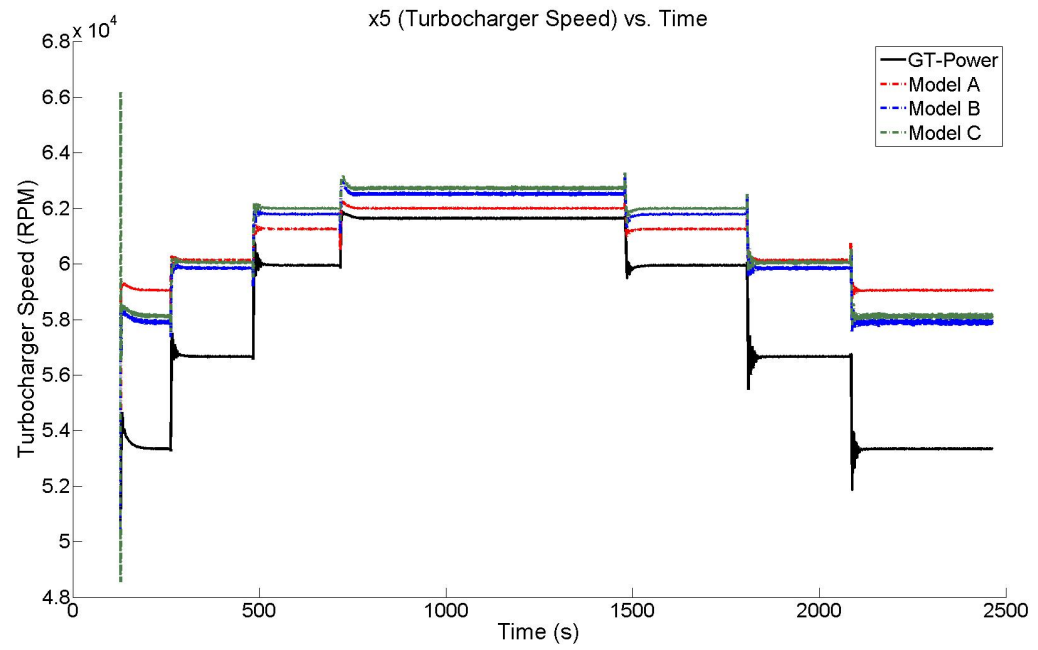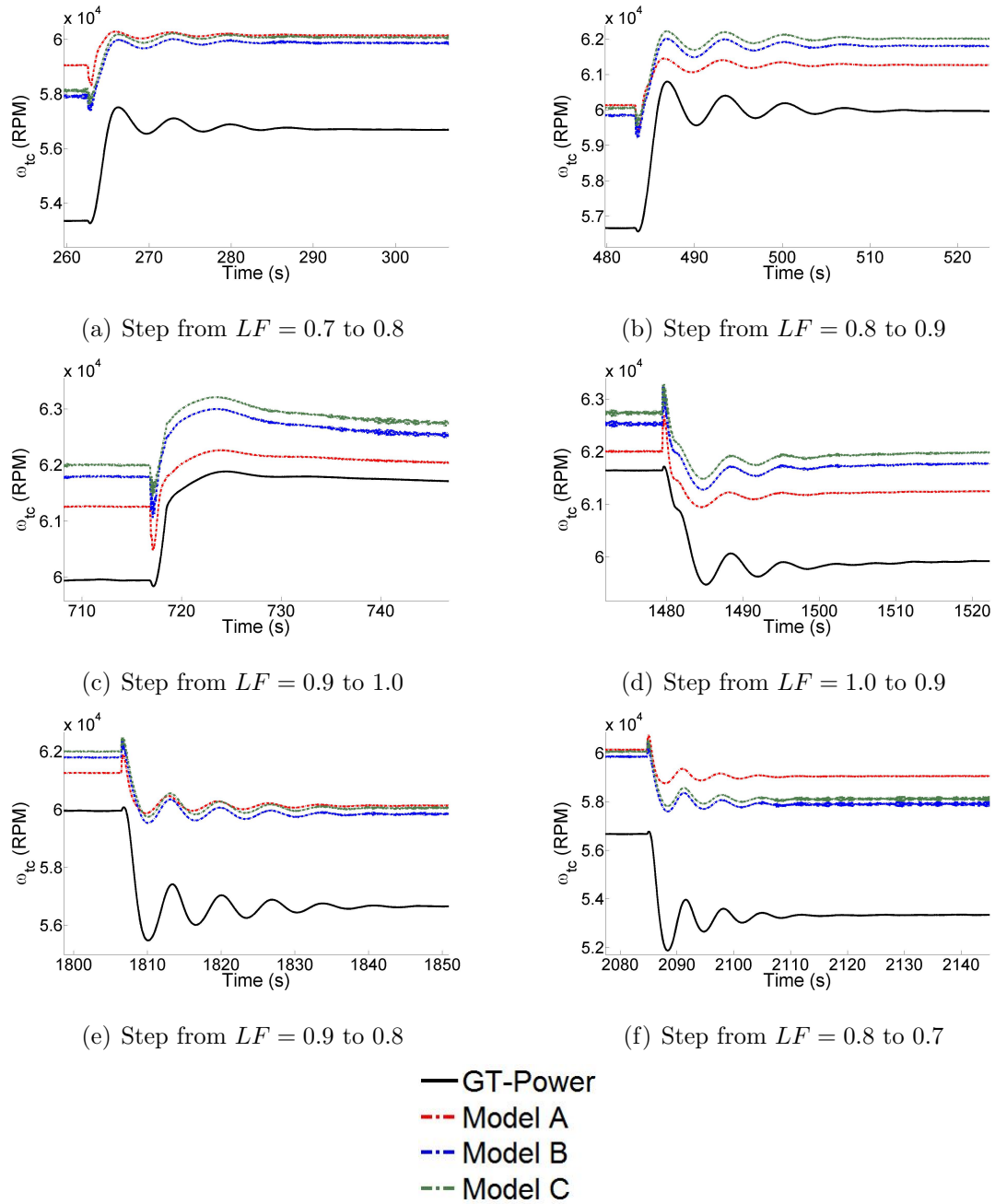
Figure 3.12.   Zoom-ins for $x_5$ vs. time.

Figure 3.11 compares the turbocharger speed responses for Models A, B, and C with the truth-reference GT-Power data for $x_5$. Subfigures 3.12(a) - 3.12(f) show zoomed-in views of transient behavior during load factor step changes. At the beginning of load factor step changes, the physics-based models tend to have slightly exaggerated dips that are not prominent in the truth-reference GT-Power data for $x_5$. Models A, B, and C do however match the oscillatory phase of the reference data quite well except at the load step from $LF = 1.0$ to $LF = 0.9$.

## 3.8 State-Space Model Validation: $x_6$

This section compares the wastegate valve lift responses of Models A, B, and C against the GT-Power reference data during the time interval of interest. In general, the wastegate valve lift is highly sensitive to boost pressure error. All three models tended to overestimate boost pressure, so the same is true of wastegate valve lift.
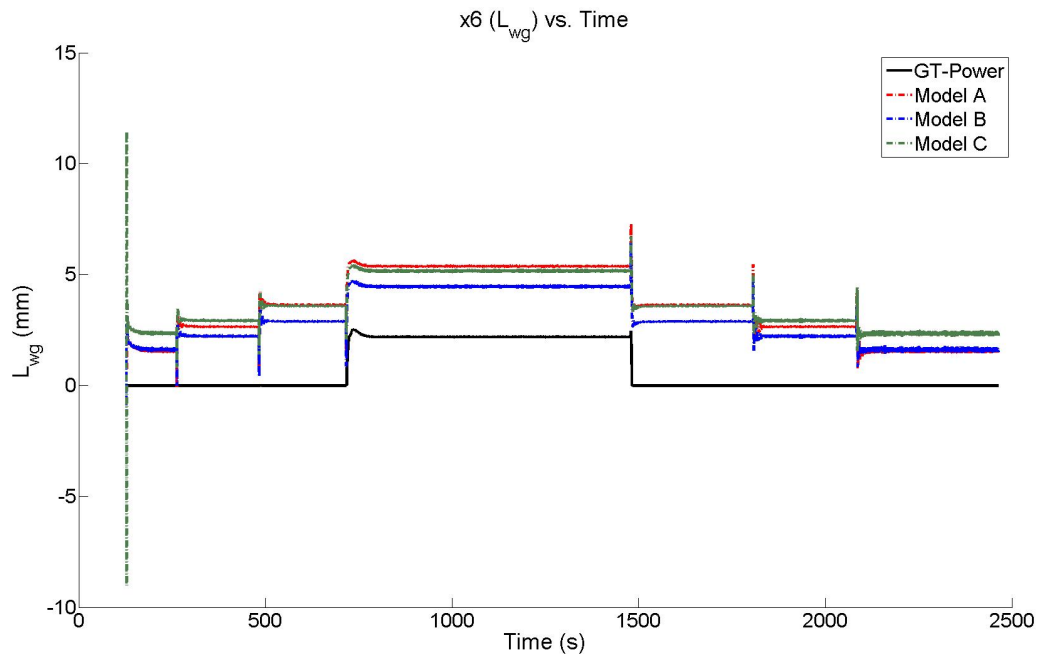


Figure 3.13. $x_6$ vs. time.

Figure 3.13 compares the wastegate valve lift responses of Models A, B, and C with the truth-reference GT-Power data for $x_6$. The steady-state error is due to overestimated boost pressure, which is why Models A, B, and C predict the wastegate opening even when it does not open in truth-reference GT-Power data. However, when the reference data shows the wastegate valve opening at $LF = 1.0$, all three of the physics-based models capture the nature of the transient behavior accurately.

## 3.9   State-Space Model Validation: $x_7$

This section compares the wastegate valve velocity responses of Models A, B, and C against the GT-Power reference data during the time interval of interest. The wastegate valve moves when the net force on the diaphragm is non-zero. As shown in Figure 3.14, Models A, B, and C tend to underestimate $x_7$ compared to the reference data during the load factor change from $LF = 0.9 \rightarrow 1.0$ and $LF = 1.0 \rightarrow 0.9$.
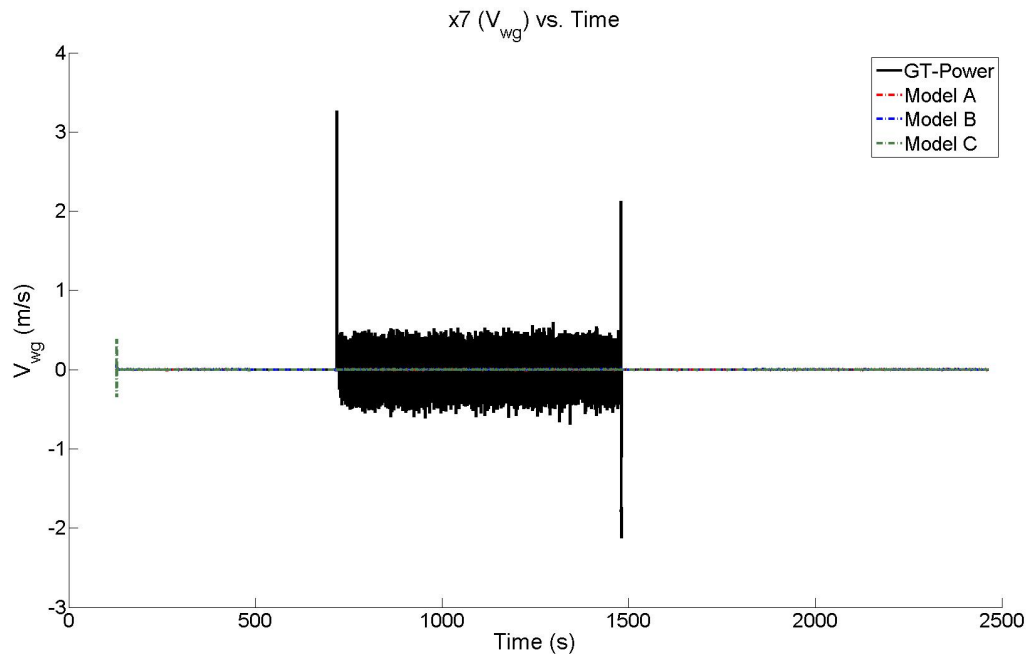


Figure 3.14.   $x_7$ vs. time.

## 3.10   Summary

This chapter accomplished the following tasks pertaining to state-space model formulation and validation:

1. Derived a dynamic equation for engine speed $(x_1)$ by performing a torque balance on the crankshaft.

2. Derived a dynamic equation for intake manifold pressure $(x_2)$ by applying the ideal gas law to the intake manifold and performing a mass balance.

3. Derived a dynamic equation for boost manifold pressure $(x_3)$ by applying the ideal gas law to the boost manifold and performing a a mass balance.

4. Derived a dynamic equation for exhaust manifold pressure $(x_4)$ by applying the ideal gas law to the exhaust manifold and performing a mass balance.

5. Derived a dynamic equation for turbocharger speed $(x_5)$ by performing a torque balance on the turbocharger shaft.

6. Derived a dynamic equation for wastegate valve lift $(x_6)$ by using a physics-based approach.

7. Derived a dynamic equation for wastegate valve velocity $(x_7)$ based on a force balance on the wastegate valve.

8. Formulated a nonlinear state-space model with all flow and power terms expressed as nonlinear functions of state variables.

9. Formulated a simplified nonlinear state-space model with all flow and power terms (except $W_{cyl}$) expressed as linear functions of state variables.

10. Linearized the simplified nonlinear model about an equilibrium point to obtain a linear engine model in conventional state-space form.

11. Compared the state trajectories of all three models against truth-reference data obtained by performing a co-simulation with GT-Power/Simulink.

## 4. CONTROL-ORIENTED ANALYSIS OF THE NATURAL GAS ENGINE STATE-SPACE MODEL

Chapters 2 and 3 comprehensively covered the physics-based modeling, linearization, and validation efforts that go into obtaining a state-space model that is amenable to controller design. A model in such a form is often necessary to apply some of the decoupled and coordinated control algorithms discussed in the introductory chapter. The physics-based models of the previous chapters assume a constant engine torque gain ($C_{trq}$) and AFR. Therefore, fueling was not an independent control input, and it was bound by air mass flow in those models. The term-by-term simplification and overall linearization of the nonlinear state equations in Chapters 2 and 3 is representative of how a physics-based control model is obtained. However, the final state-space model of Chapter 3 is not used in this chapter. Instead, Caterpillar provided a new linearized state-space model for the same engine architecture, and the new model is analyzed in this chapter. The state variables, input variables, and output variables for the new state-space model are summarized below.

- The state variables are: $x_1$ - engine speed, $x_2$ - intake manifold pressure, $x_3$ - boost manifold pressure, $x_4$ - exhaust manifold pressure, $x_5$ - turbocharger speed, $x_6$ - wastegate valve lift, $x_7$ - wastegate valve velocity, $x_8$ - fuel-air ratio (FAR).

- The control inputs are: $u_1$ - throttle valve mass flow, $u_2$ - bypass valve mass flow, and $u_3$ - fuel mass flow.

- The disturbance variable is: $w$ - load torque.

- The outputs are: $y_1$ - engine speed, $y_2$ - pressure differential across the throttle valve, and $y_3$ - FAR.

The linearized state-space model provided by Caterpillar is expressed as follows:

$$\dot{x} = Ax + Bu + Vw$$

$$y = Cx + Du$$

where,

$$x = \begin{bmatrix} x_1 & x_2 & x_3 & x_4 & x_5 & x_6 & x_7 & x_8 \end{bmatrix}^T$$

$$u = \begin{bmatrix} u_1 & u_2 & u_3 \end{bmatrix}^T$$

The block diagram in Figure 4.1 represents the system corresponding to Caterpillar's state-space model. Note that the $D$ matrix is a zero matrix which is why it is not shown in the block diagram.
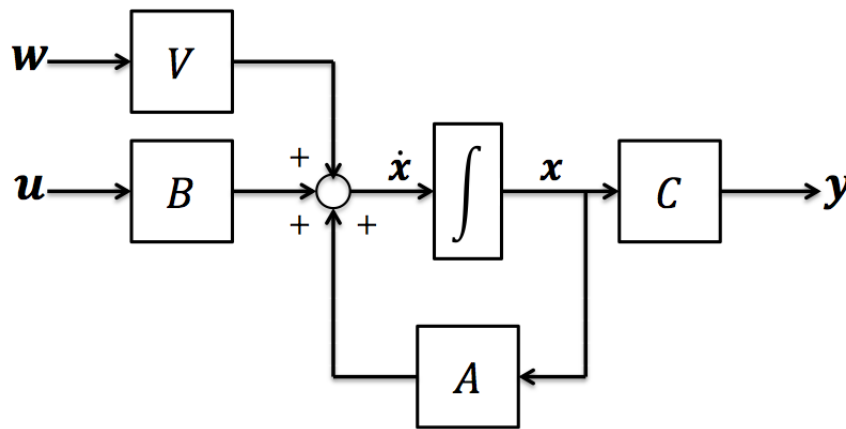


Figure 4.1. Block diagram representation of Caterpillar's state-space model.

The $A$ matrix captures internal state dynamics, the $B$ matrix captures the effect of control inputs on the state dynamics, while the $V$ matrix captures the effect of the disturbance on state dynamics. The $C$ and $D$ matrices describe the output variables in terms of states and control inputs. For this particular model, the numeric $A$, $B$, $V$, $C$, and $D$ matrices provided by Caterpillar are:

$$
A = \begin{bmatrix}
0 & 2.9e-4 & 0 & 0 & 0 & 0 & 0 & 2.8e3 \\
-9.9e3 & -3.9 & 0 & 0 & 0 & 0 & 0 & 0 \\
0 & 0 & -42 & 0 & 6.2e3 & 0 & 0 & 0 \\
5.9e4 & 23 & 0 & -29 & 0 & -1.7e8 & 0 & 0 \\
0 & 0 & 0.049 & 0.076 & -12 & 0 & 0 & 0 \\
0 & 0 & 0 & 0 & 0 & 0 & 1.0 & 0 \\
0 & 0 & 5.0e-3 & 0 & 0 & -2.8e4 & -699 & 0 \\
0 & -5e-11 & 9.9e-7 & 0 & -1.5e-4 & 0 & 0 & -3.9
\end{bmatrix}
$$

$$
B = \begin{bmatrix}
0 & 0 & 0 \\
7.2e5 & 0 & 0 \\
-3.4e6 & 0 & 0 \\
0 & 0 & 0 \\
0 & 0 & 0 \\
0 & 0 & 0 \\
0 & 0 & 0 \\
9.4e-6 & 0.079 & 2.4
\end{bmatrix}
$$

$$
V = \begin{bmatrix}
-0.01 \\
0 \\
0 \\
0 \\
0 \\
0 \\
0 \\
0
\end{bmatrix}
$$

$$C = \begin{bmatrix} 1 & 0 & 0 & 0 & 0 & 0 & 0 & 0 \\ 0 & -1 & 1 & 0 & 0 & 0 & 0 & 0 \\ 0 & 0 & 0 & 0 & 0 & 0 & 0 & 1 \end{bmatrix}$$

$$D = \begin{bmatrix} 0 & 0 & 0 \\ 0 & 0 & 0 \\ 0 & 0 & 0 \end{bmatrix}$$

## 4.1 Transfer Matrix Formulation

State-space equations are in the time-domain, but analysis in the frequency domain can provide useful information regarding the input-output relationships of the plant. A state-space system can be converted to a transfer matrix, $G(s)$, in the following manner: $G(s) = C(sI - A)^{-1}B + D$. Rows of the transfer matrix correspond to output variables, while columns of the transfer matrix correspond to input variables. Element $(i, j)$ of the transfer matrix is the transfer function between input $j$ and output $i$. The transfer matrix is used in relative gain array (RGA) analysis.

## 4.2 Relative Gain Array

As mentioned in [4], the relative gain array is a way of quantifying coupling interaction in a MIMO system such as an engine. For a square transfer matrix the RGA is defined as:

$$RGA(G) = G(s) \times (G(s)^{-1})^{T}$$

The symbol, $\times$, denotes element-by-element multiplication between the matrices. While the RGA for this particular engine plant is only a $3 \times 3$ matrix, it features elements that are $28^{th}$ degree polynomials, so the symbolic RGA matrix is not shown in this thesis. Individual elements are, however, plotted against frequency in subsequent subsections.

The elements of the RGA are functions of frequency, $\omega$. RGA rows correspond to outputs and its columns correspond to inputs, so the $(i, j)$ element of the RGA is the RGA element between input $j$ and output $i$. At a particular frequency, $\omega$, a plant is considered an ideal candidate for decentralized control if the RGA matrix can be made an identity matrix or some permutation of the identity matrix. RGA elements that have a value of approximately 1 correspond to input-output pairings that should be used for decentralized control.

Take for example the steady-state RGA matrix for Caterpillar's state-space model,

$$RGA(0) = \begin{bmatrix} -0.0346 & 0 & 1.0346 \\ 0 & 1 & 0 \\ 1.0346 & 0 & -0.0346 \end{bmatrix} \tag{4.1}$$

The matrix of Equation (4.1) can be made an approximate identity matrix by swapping the first and third rows, meaning the model is suitable for decentralized control at steady-state ($\omega = 0$ rad/s). Consequently, the ideal input-output pairings at steady-state would be: $u_1 \rightarrow y_3$, $u_2 \rightarrow y_2$, and $u_3 \rightarrow y_1$. Since RGA analysis is done on a linearized state-space model of a plant, its usefulness is contingent upon an accurate plant model. If the plant model does not accurately capture the dynamics of the real plant, the real system may not be suitable for decentralized control even if RGA analysis suggests it to be.

## 4.3   RGA Number

For square plants, the RGA number provides a single metric for how suitable a specific configuration of input-output pairings is for decentralized control. As per [4], the RGA number is a measure of diagonal dominance and is found as follows:

$$RGAN = ||RGA - I||_{sum} \tag{4.2}$$

To compute the RGA number, the identity matrix is subtracted from the relative gain array and the sum norm is taken. The sum norm of a matrix is calculated by

summing the absolute values of all its elements. RGA numbers close to zero indicate that the chosen input-output pairings are suitable for achieving decentralized control of the plant. Reference [4] says that RGA numbers between 5 to 10 or greater are considered high, and decentralized control of the plant may not be feasible for input-output configurations that yield such RGA number values. There are two important notes to make regarding the calculation of the RGA number:

1. The relative gain array is a function of frequency. Therefore, the RGA number is a function of frequency. This means that a plant that has very minimal coupling interaction at one frequency can be highly coupled at another frequency.

2. For a plant with $n$ inputs and $n$ outputs, different permutations of the identity matrix can be used for the RGA number calculation in Equation (4.2). Using the conventional identity matrix is akin to seeing how suitable a plant is for decentralized control assuming the input-output pairings are: $u_1 \rightarrow y_1$, $u_2 \rightarrow y_2$, $\cdots$, $u_n \rightarrow y_n$. Conversely, using an off-diagonal identity matrix in RGA number calculations is akin to testing the plant's suitability to decentralized control for the following input-output pairings: $u_1 \rightarrow y_n$, $u_2 \rightarrow y_{n-1}$, $\cdots$, $u_n \rightarrow y_1$.

Caterpillar's state-space model describes an engine architecture that features three control inputs and three target outputs of interest. For a 3-input 3-output plant there are six possible input-output configurations for which an RGA number can be computed as a function of frequency. Each of the six possible input-output configurations for Caterpillar's state-space model is listed explicitly below.

1. Configuration 1: $u_1 \rightarrow y_1$, $u_2 \rightarrow y_2$, $u_3 \rightarrow y_3$. The identity matrix used in the RGA number calculation of Equation (4.2) is:

$$I_1 = \begin{bmatrix} 1 & 0 & 0 \\ 0 & 1 & 0 \\ 0 & 0 & 1 \end{bmatrix}$$

2. Configuration 2: $u_1 \rightarrow y_1$, $u_2 \rightarrow y_3$, $u_3 \rightarrow y_2$. The manipulated identity matrix used in the RGA number calculation of Equation (4.2) is:

$$I_2 = \begin{bmatrix} 1 & 0 & 0 \\ 0 & 0 & 1 \\ 0 & 1 & 0 \end{bmatrix}$$

3. Configuration 3: $u_1 \to y_2$, $u_2 \to y_1$, $u_3 \to y_3$. The manipulated identity matrix used in the RGA number calculation of Equation (4.2) is:

$$I_3 = \begin{bmatrix} 0 & 1 & 0 \\ 1 & 0 & 0 \\ 0 & 0 & 1 \end{bmatrix}$$

4. Configuration 4: $u_1 \to y_3$, $u_2 \to y_1$, $u_3 \to y_2$. The manipulated identity matrix used in the RGA number calculation of Equation (4.2) is:

$$I_4 = \begin{bmatrix} 0 & 1 & 0 \\ 0 & 0 & 1 \\ 1 & 0 & 0 \end{bmatrix}$$

5. Configuration 5: $u_1 \to y_2$, $u_2 \to y_3$, $u_3 \to y_1$. The manipulated identity matrix used in the RGA number calculation of Equation (4.2) is:

$$I_5 = \begin{bmatrix} 0 & 0 & 1 \\ 1 & 0 & 0 \\ 0 & 1 & 0 \end{bmatrix}$$

6. Configuration 6: $u_1 \to y_3$, $u_2 \to y_2$, $u_3 \to y_1$. The manipulated identity matrix used in the RGA number calculation of Equation (4.2) is:

$$I_6 = \begin{bmatrix} 0 & 0 & 1 \\ 0 & 1 & 0 \\ 1 & 0 & 0 \end{bmatrix}$$

Figure 4.2 shows the RGA number versus frequency plots for each of the six input-output configurations. The RGA numbers are plotted from 0 to 5 Hz, which is the
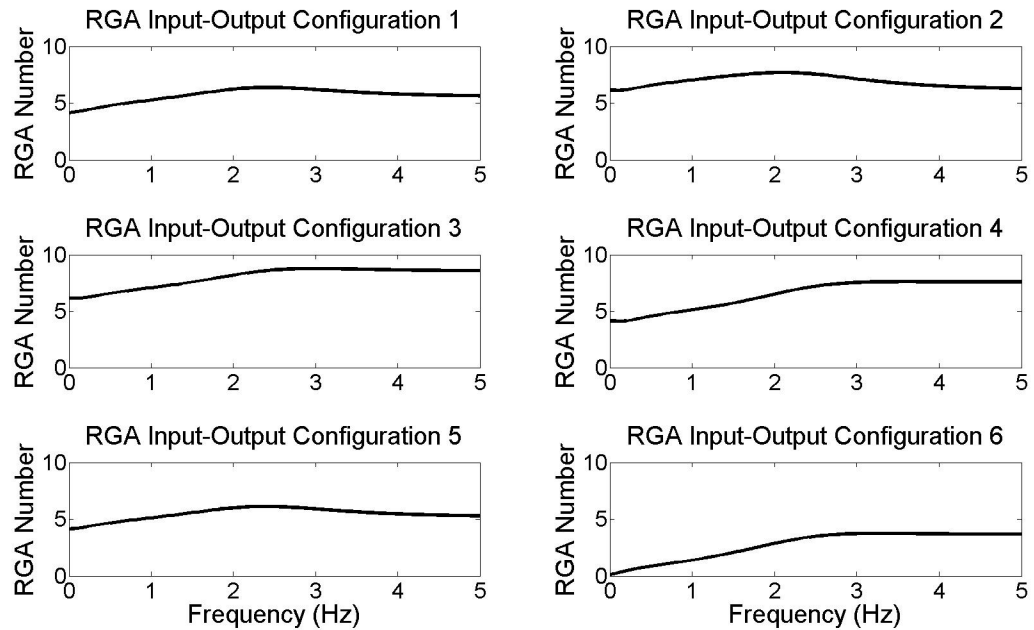
Figure 4.2. RGA number vs. frequency.

frequency when the engine becomes less responsive to control inputs. From Figure 4.2, it is apparent that configuration 6 has the lowest RGA number across all frequencies. The RGA number for configuration 6 is approximately zero at steady-state ($\omega = 0$ rad/s) and stays below a value of 4 in the entire frequency range. This means that the engine is best suited for decentralized control when using input-output configuration 6.

## 4.4 RGA Element Magnitude and Phase Analysis

RGA elements are functions of frequency in the Laplace domain ($s = j\omega$). Therefore, they are complex numbers that have a magnitude and phase. An RGA element with a phase between $-90^o$ and $+90^o$ has a positive real part, while an RGA element with a phase less than $-90^o$ or more than $+90^o$ has a negative real part. A phase of

$\pm 90^o$ indicates the real part is zero. For a 3-input 3-output system, there are nine RGA elements. As mentioned in [4], RGA elements close to a value of $+1$ are good for decentralized control. Therefore, if element $(i,j)$ of the RGA is $+1$, using input $j$ to control output $i$ is recommended. Additionally, [4] mentions that if RGA element $(i,j)$ has a negative real part, then using input $j$ to control output $i$ is not recommended, as this leads to closed-loop instability. The RGA element magnitudes and phases are plotted against frequency for every input-output pair in Figures 4.3 - 4.5.
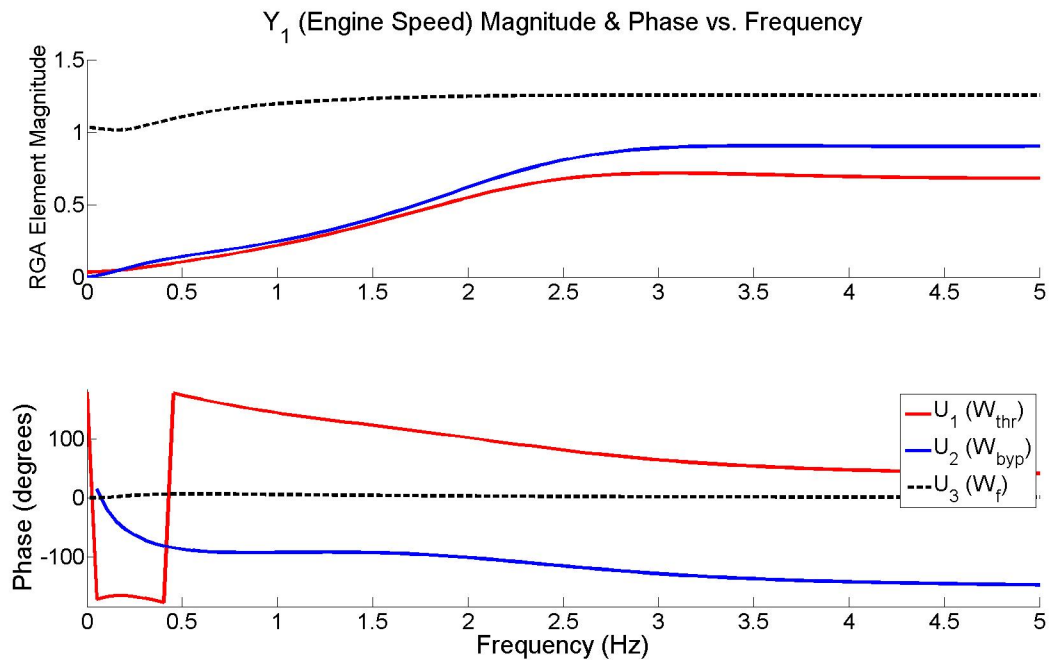


Figure 4.3. $Y_1$ RGA elements magnitude & phase vs. frequency.

Figure 4.3 features the magnitude and phase of the RGA elements between every input channel and output 1 (engine speed). It is clear that in Figure 4.3, the RGA element between $u_3 \rightarrow y_1$ has a magnitude of approximately $+1$ and a phase of 0 degrees throughout the frequency range. This means that output 1 is best controlled by input 3 (fuel mass flow). From this same figure it is also clear that at high enough frequencies, input 1 (throttle valve mass flow) becomes the second best control input
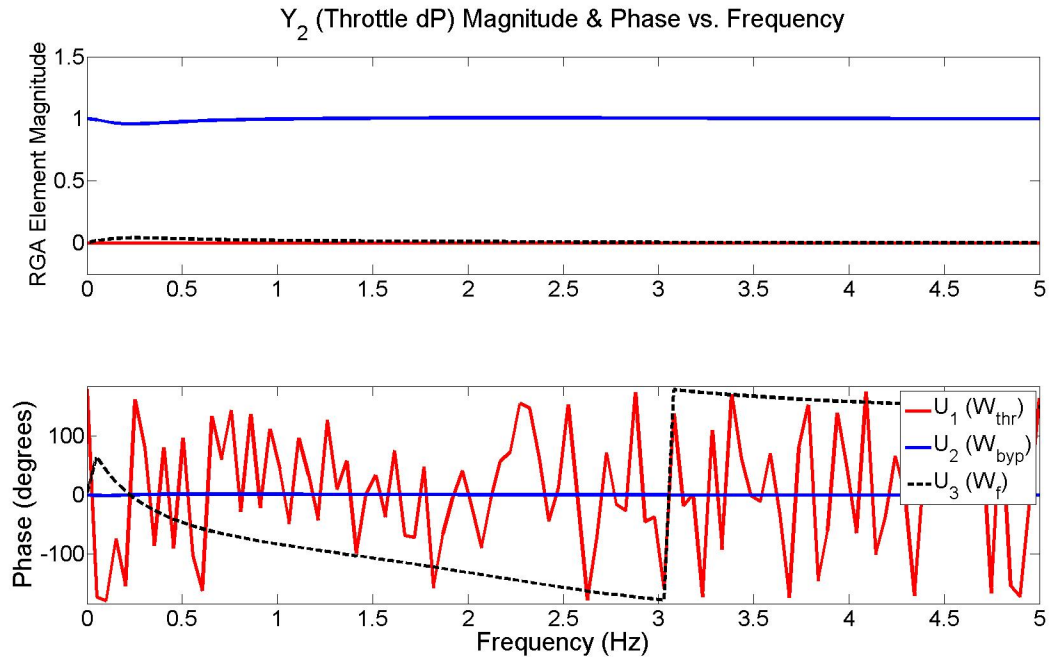
Figure 4.4. $Y_2$ RGA elements magnitude & phase vs. frequency.

to pair with output 1. At high enough frequencies, the RGA element between $u_1 \rightarrow y_1$ has a phase of less than $+90^o$, meaning it has a positive real part.

Figure 4.4 features the magnitude and phase plots for RGA elements between every input channel and output 2 (throttle valve pressure differential). It is clear from the figure that in the frequency range of interest, only the RGA element between $u_2 \rightarrow y_2$ has a magnitude of $+1$ at all frequencies and phase of about 0 degrees. Therefore, input 2 (bypass valve mass flow) should be used to control output 2 for best results in a decentralized control framework. So far for this state-space model, it has been clear which inputs should be used to control to which outputs, but in more complex plants this is not always the case. In a non-square plant with more inputs than outputs, one input may be better suited to control an output in one frequency range, while another input may be better suited to control the same output in another frequency range. This kind of information, along with information regarding phase, is not very
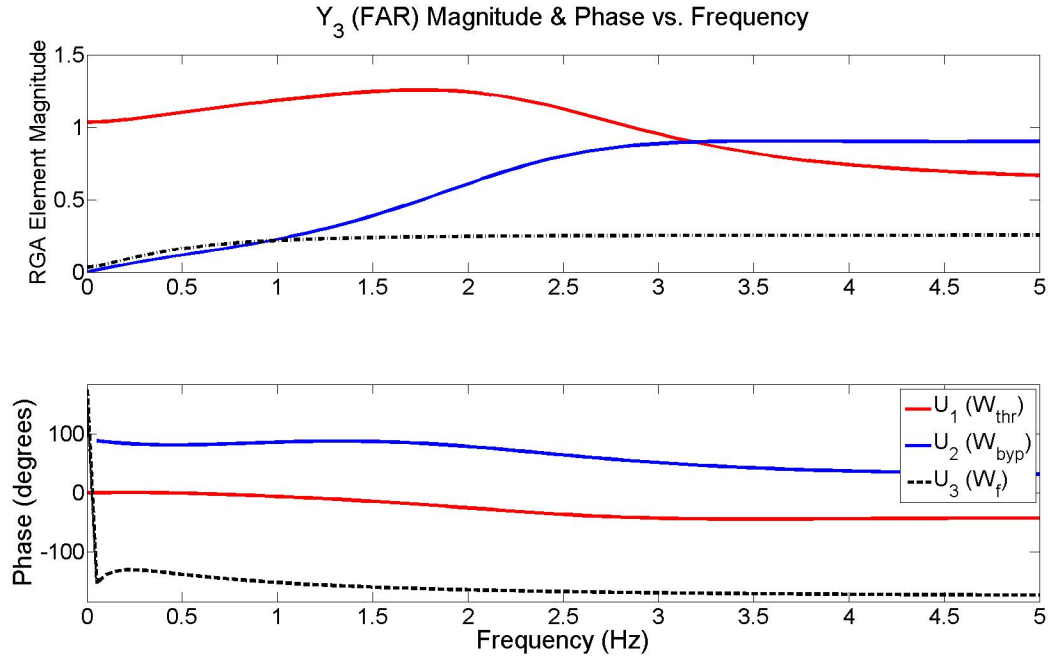
Figure 4.5. $Y_3$ RGA elements magnitude & phase vs. frequency.

transparent in the RGA number analysis, but it is in RGA element magnitude and phase plots.

Figure 4.5 shows the magnitude and phase plots for RGA elements between every input channel and output 3 (FAR). At lower frequencies, it is clear that output 3 is best controlled by input 1 (throttle valve mass flow), because the RGA element between $u_1 \rightarrow y_3$ has a magnitude of about +1 and a phase of approximately 0 degrees. At frequencies above 3.25 Hz, however, this plot shows that input 2 (bypass valve mass flow) may in fact be a better control input to pair with output 3, because the RGA element between $u_2 \rightarrow y_3$ has a magnitude of about +1 and a phase of less than $+90^o$. Solely designing a controller between $u_2$ and $y_3$ may lead to instability, particularly at lower frequencies when the RGA element between $u_2 \rightarrow y_3$ has a negative real part. However, in fast transient operations, input 2 may be a preferred way of controlling FAR, which is an important consideration in controller design.

## 4.5  Intuition from RGA Element Analysis

This section discusses how RGA element analysis can be used to make informed decisions regarding sequential loop closure in a decentralized control framework. The RGA element magnitude and phase plots of the previous section show that the input-output pairing $u_2 \to y_2$ is the most well-suited for decentralized control because its corresponding RGA element has a magnitude of $+1$ and a phase of $0$ degrees at all frequencies. Pairings $u_1 \to y_3$ and $u_3 \to y_1$ are the other optimal input-output control loops for decentralized control, but neither of the pairings has an RGA element magnitude and phase as good as that of $u_2 \to y_2$.

Reference [18] states than an RGA element $(\lambda_{ij})$ is the ratio between the "process gain for the pairing $u_j \to y_i$ in an isolated loop and the process gain when the rest of the system is under integral feedback control". This means that if an RGA element is $+1$ at all frequencies, like that of $u_2 \to y_2$, the transfer function between $u_2 \to y_2$ should have an identical frequency response in both the open-loop and closed-loop cases. The closed-loop case assumes good feedback control for the pairings $u_1 \to y_3$ and $u_3 \to y_1$, while $u_2 \to y_2$ is left uncontrolled. Figures 4.6 and 4.7 show the open-loop and closed-loop cases respectively, as they pertain to the analysis of this subsection.
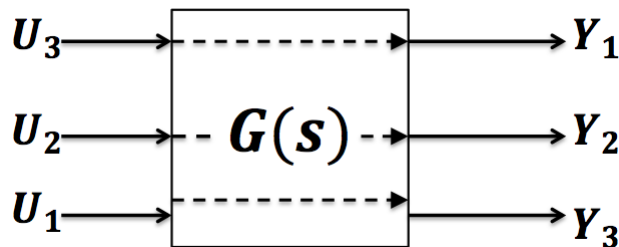


Figure 4.6.  Plant in open-loop case.

Since the RGA element of input-output pairing $u_2 \to y_2$ has a value of $+1$ at all frequencies, the relationship between $u_2$ and $y_2$ should be unaffected by implementing good feedback controllers on loops $u_1 \to y_3$ and $u_3 \to y_1$. To test this, the frequency
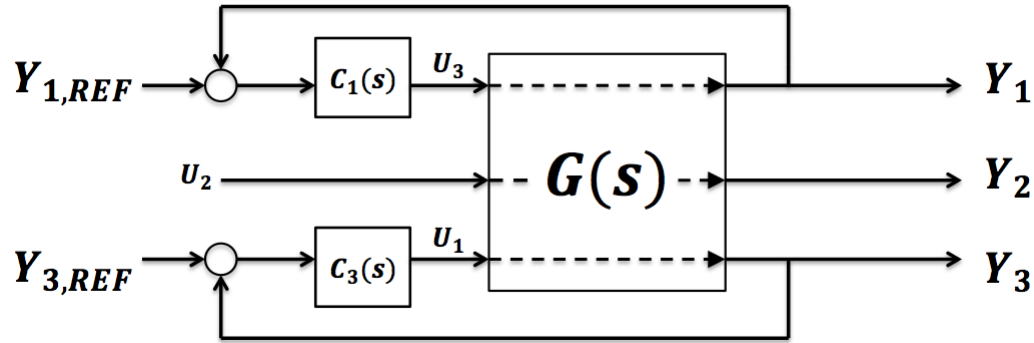
Figure 4.7. Plant in closed-loop case (controllers on two input-output pairs).

response of the transfer function between $u_2 \to y_2$ is plotted for the open-loop case (as in Figure 4.6) and two closed-loop cases (as in Figure 4.7). The two closed-loop cases are as follows:

1. Good Proportional-Integral (PI) Controllers: The control gains are $K_{P,u_1} = -30$, $K_{I,u_1} = -10$, $K_{P,u_3} = 0.75$, $K_{I,u_3} = 0.05$. These control gains achieve good reference tracking for $y_1$ and $y_3$. Negative PI gains are necessary for the loop $u_1 \to y_3$ because throttle mass flow $(u_1)$ inversely affects FAR $(y_3)$. Positive PI gains are necessary for the loop $u_3 \to y_1$ because increasing fuel mass flow $(u_3)$ increases engine speed $(y_1)$.

2. Bad PI Controllers: The control gains are $K_{P,u_1} = -1000$, $K_{I,u_1} = -5$, $K_{P,u_3} = -5e - 4$, $K_{I,u_3} = -5e - 5$. These control gains do not achieve good reference tracking on $y_1$ and $y_3$.

The results of Figure 4.8 confirm that implementing good feedback controllers on $u_1 \to y_3$ and $u_3 \to y_1$ does not affect the transfer function between $u_2 \to y_2$. The implication of this is that when performing sequential loop closure in a decentralized control framework, the input-output loop which has an RGA element value closest to +1 at all frequencies should be tuned first. For this engine model provided by Caterpillar, the control loop that should be tuned first is between $u_2 \to y_2$.
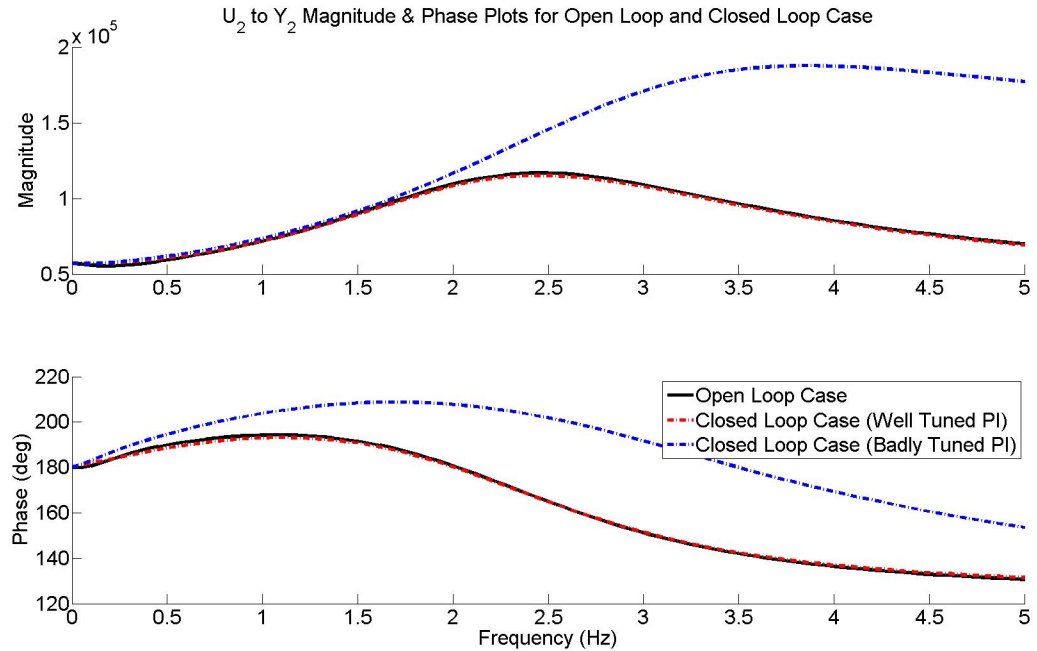
Figure 4.8. Closed-loop vs open-loop comparison of $u_2 \rightarrow y_2$ transfer function.

## 4.6 Decentralized PI Controller Design

RGA number analysis on Caterpillar's state-space model suggests that the engine is fairly well suited for decentralized control. RGA element analysis suggests that when doing sequential loop-closure, the input-output loop whose RGA element value stays closest to $+1$ throughout the frequency range should be tuned first, followed by the other loops. In this section, a decentralized controller is designed with the following PI gains on the input-output control loops:

- $u_1 \rightarrow y_3$: $K_{P,u_1} = -30$, $K_{I,u_1} = -10$

- $u_2 \rightarrow y_2$: $K_{P,u_2} = -10$, $K_{I,u_2} = -0.5$

- $u_3 \rightarrow y_1$: $K_{P,u_3} = 0.75$, $K_{I,u_3} = 0.05$

Figure 4.9 is representative of how the decentralized control structure with 3 PI compensators looks for the plant.
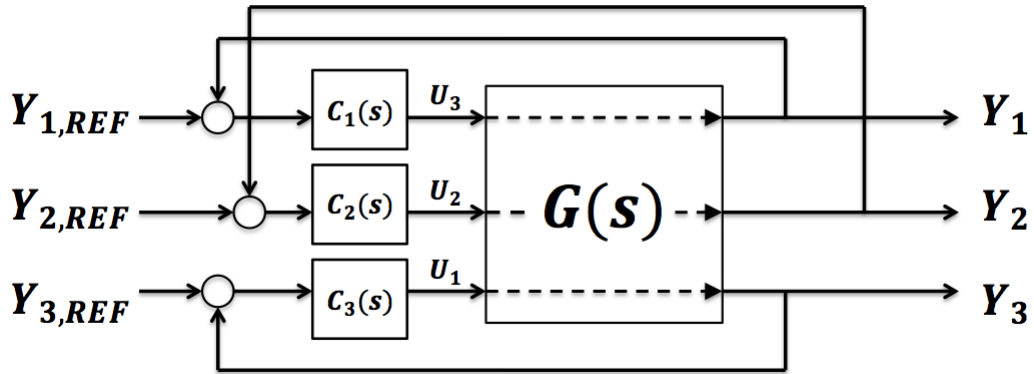


Figure 4.9. 3 decentralized controllers on plant.

### 4.6.1 Nonlinear State-Space System Augmentation

Before implementing PI controllers on the linearized state-space model, the nonlinear state equations provided by Caterpillar (not shown due to their complexity) must be augmented to include integral error states. The following states and inputs are added to the nonlinear model:

- $x_9$: Integral error for $y_1$ (engine speed).

- $x_{10}$: Integral error for $y_3$ (FAR).

- $x_{11}$: Integral error for $y_2$ (throttle valve pressure differential).

- $\hat{u}_1$: Reference FAR, $y_{3,ref}$.

- $\hat{u}_2$: Reference throttle valve pressure differential, $y_{1,ref}$.

- $\hat{u}_3$: Reference engine speed, $y_{1,ref}$.

The dynamic equations for the new integral error states are:

$$\dot{x}_9 = \hat{u}_3 - x_1 \tag{4.3}$$

$$\dot{x}_{10} = \hat{u}_1 - x_8 \tag{4.4}$$

$$\dot{x}_{11} = \hat{u}_2 - (x_3 - x_2) \tag{4.5}$$

Additionally, the control inputs ($u_1$: throttle valve mass flow, $u_2$: bypass valve mass flow, $u_3$: fuel mass flow) must be redefined for a closed-loop system. In Equations (4.6) - (4.8), the control inputs are expressed as functions of the following: PI gains, output reference values, and state variables. Doing so turns the nonlinear state-equations provided by Caterpillar into a closed-loop nonlinear model with feedback controllers on all three input-output loops:

$$u_1 = K_{P,u_1}(\hat{u}_1 - x_8) + K_{I,u_1} * x_{10} \tag{4.6}$$

$$u_2 = K_{P,u_2}(\hat{u}_2 - [x_3 - x_2]) + K_{I,u_2} * x_{11} \tag{4.7}$$

$$u_3 = K_{P,u_3}(\hat{u}_3 - x_1) + K_{I,u_3} * x_9 \tag{4.8}$$

After being augmented with the integral error state dynamics of Equations (4.3) - (4.5), the new set of nonlinear state equations is linearized about an equilibrium point to obtain closed-loop linear state-space equations. These new closed-loop linear state-equations represent the addition of three PI compensators to Caterpillar's linear state-space model. Reference-tracking tests are done on this closed-loop linear state-space model in the following subsections.

### 4.6.2   Reference Engine Speed Steps

As a reminder, the three target outputs of interest are the engine speed ($y_1$), pressure difference across the throttle valve ($y_2$), and FAR ($y_3$). The first test of the decentralized controllers involves step increments in the reference value of engine speed, $y_{1,ref}$. The values of $y_{2,ref}$ and $y_{3,ref}$ are held constant.
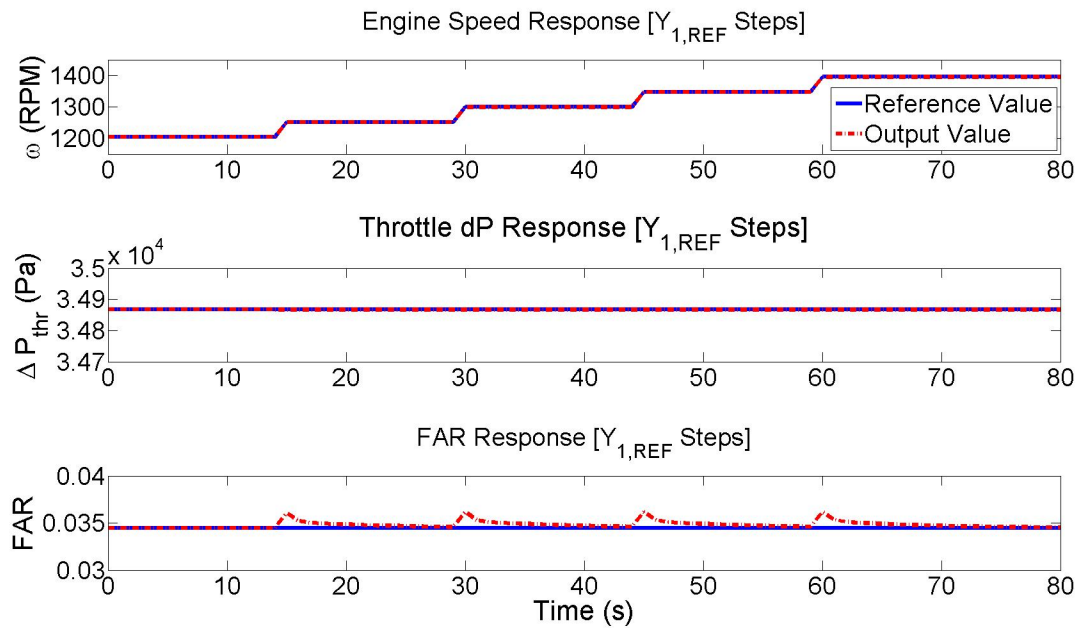
Figure 4.10.   Closed-loop system with $Y_1$ reference steps.

As shown in Figure 4.10, the decentralized control structure is able to track step changes in desired engine speed while maintaining constant reference values for throttle valve pressure differential and FAR. The reference values of throttle valve pressure differential and FAR are set to equilibrium values near the point of model linearization. Additionally, the reference engine speed steps are fairly small and stay near the point of linearization. Therefore, the decentralized control structure is only being tested for reference tracking in operating conditions near the point of linearization.

### 4.6.3   Reference Throttle Valve Pressure Differential Steps

The second test of the decentralized controllers involves step increments in $y_{2,ref}$. The values of $y_{1,ref}$ and $y_{3,ref}$ are held constant. As shown in Figure 4.11, the decentralized control structure is able to track step changes in desired throttle valve
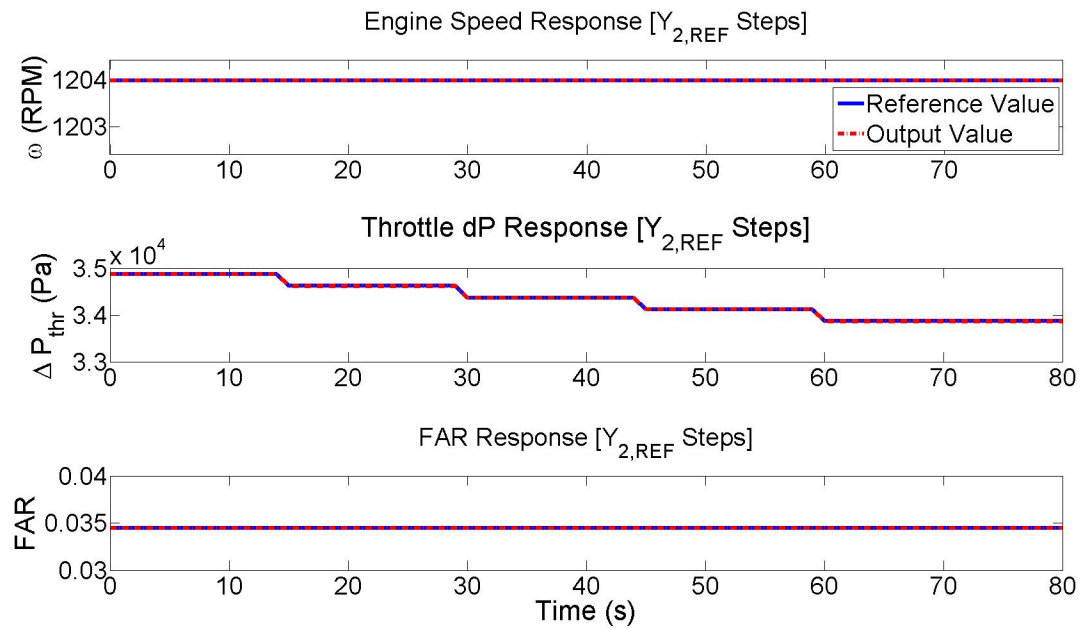
Figure 4.11.  Closed-loop system with $Y_2$ reference steps.

pressure differential while maintaining constant reference values for engine speed and FAR. The engine speed and FAR reference values are set to equilibrium values near the point of model linearization. Additionally, the reference throttle valve pressure differential steps are fairly small and stay near the point of linearization. Therefore, the decentralized control structure is only being tested for reference tracking in an operating region near the point of linearization.

### 4.6.4   Reference FAR Steps

The third test of the decentralized controllers involves step decrements in the reference value of FAR, $y_{3,ref}$. The values of $y_{1,ref}$ and $y_{2,ref}$ are held constant. As shown in Figure 4.12, the decentralized control structure is able to track step changes in desired FAR while maintaining constant reference values for engine speed
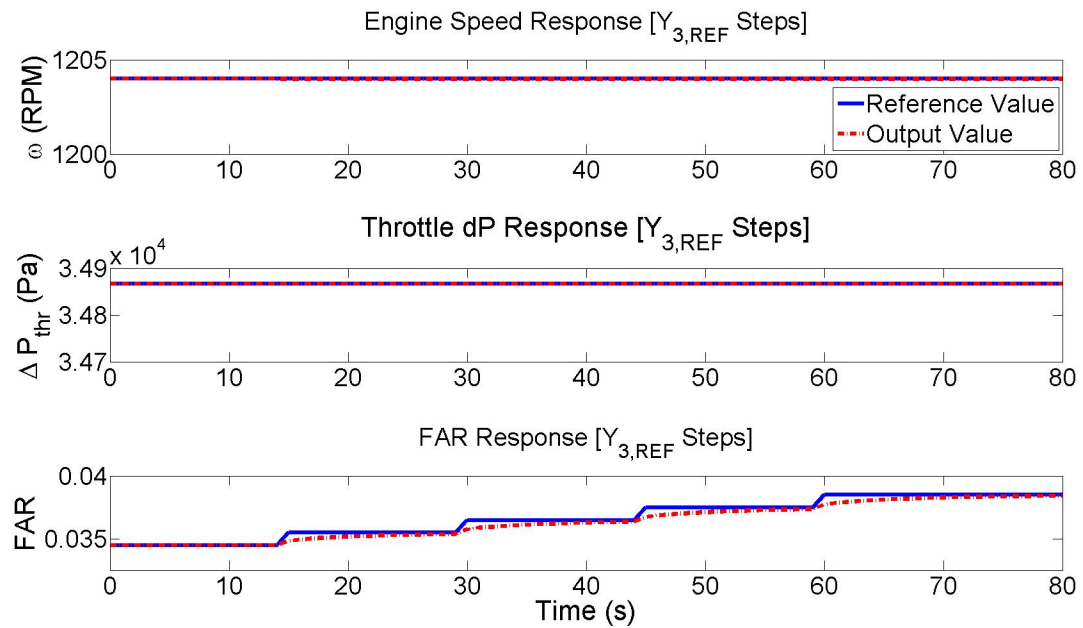
Figure 4.12.  Closed-loop system with $Y_3$ reference steps.

and throttle valve pressure differential. The engine speed and throttle valve pressure differential reference values are set to equilibrium values near the point of model linearization. Additionally, the FAR steps are fairly small and stay near the point of linearization. Therefore, the decentralized control structure is only being tested for reference tracking in operating conditions near the point of linearization.

## 4.7  Summary

This chapter accomplished the following tasks pertaining to control-oriented analysis of a state-space model provided by Caterpillar:

1. Declared the state variables, input variables, and output variables of the new state-space model.

2. Defined the $A$, $B$, $V$, $C$ and $D$ matrices of the state-space equations for the linearized model provided by Caterpillar.

3. Showed how the linearized state-space model is converted to a transfer matrix.

4. Showed how a transfer matrix can be used to calculate the relative gain array (RGA) of the plant.

5. Performed RGA number analysis to determine which input-output pairings are best for a decentralized control framework.

6. Supplemented RGA number analysis with RGA element analysis and decided the ideal input-output pairings for decentralized control are: $u_1 \rightarrow y_3$, $u_2 \rightarrow y_2$, and $u_3 \rightarrow y_1$.

7. Utilized intuition gained from RGA element analysis to make an informed decision on which order to perform loop closure in a decentralized control framework.

8. Designed a set of PI controllers that achieve good reference tracking during simulation on the closed-loop version of the Caterpillar's linear engine model.

# 5. CONCLUSIONS AND FUTURE WORK

## 5.1 Conclusions

This thesis presents a method of deriving, simplifying, and ultimately linearizing a set of state equations for the purpose of control development on an engine. The Caterpillar G3500 series engine was the system of interest, and the selected state variables were engine speed ($x_1$), intake manifold pressure ($x_2$), boost manifold pressure ($x_3$), exhaust manifold pressure ($x_4$), turbocharger speed ($x_5$), wastegate valve lift ($x_6$), and wastegate valve velocity ($x_7$). For each state variable, a first-principles approach was taken to find its corresponding dynamic equation. Additionally, a physics-based approach was taken to express terms in the nonlinear dynamic equations as functions of state variables, including the engine torque gain, mass flow rates, and power expressions. Overall, the nonlinear physics-based mass flow models matched the reference data very well. The nonlinear mass flow models also gave an insight on what state variables each mass flow term depended on. Using that insight, the mass flow models of compressor mass flow ($W_{comp}$), turbine mass flow ($W_{turb}$), and wastegate mass flow ($W_{wg}$) were made linear functions of state variables by performing regression on reference data. The nonlinear compressor and turbine power terms were also linearized, and the linear models matched the nonlinear models very well.

In the state equations developed in this thesis, the model for engine torque gain, $C_{trq}$, had satisfactory steady-state error with respect to the truth-reference data and captured transient oscillations well. However, the physics-based torque gain model showed $C_{trq}$ decreasing with load torque, while the truth-reference torque gain values increased with load torque. Therefore, $C_{trq}$ was fixed to a constant value of 0.0256, because in truth-reference data it did not vary much in the time interval of interest. This simplification implied that the engine controller must maintain a constant AFR,

effectively making the fuel control input ($u_3 = W_f$) dependent upon air mass flow. Despite this assumption, the thesis still presents a procedure representative of deriving a control-oriented model for an engine architecture.

Following the control-oriented modeling efforts, three representative state-space models were validated against the truth-reference data in simulation. This was done by exercising each of the three models with truth-reference simulation values of the control inputs ($u_1 = W_{thr}$, $u_2 = W_{byp}$). The first model (Model A) consisted of the nonlinear set of dynamic equations for $x_1$ to $x_7$, with all mass flow and power terms expressed as nonlinear functions of state variables. The second model (Model B) was a simplification of the first model and consisted of the nonlinear set of dynamic equations for $x_1$ to $x_7$, with most mass flow and power terms expressed as linear functions of state variables. The third model (Model C) was obtained by linearizing the second model about an equilibrium point and expressing the engine model in a true state-space form with $A$, $B$, $C$, and $D$ matrices. Models A and B matched the reference data fairly well, with low steady-state errors for $x_1$, $x_2$, and $x_4$. There were some minor issues with the phase of transient oscillations in all three models. Model C generally deviated more from the truth-reference reference data with regards to its predictions for $x_1$, $x_2$, and $x_4$, which is expected since it is a fully linearized state-space model. Wastegate valve lift ($x_6$) dynamics are extremely sensitive to the boost pressure dynamics, and all three state-space models tended to overestimate wastegate valve lift. This is because all three models overestimated boost pressure. Boost pressure dynamics appear to be sensitive to turbocharger speed dynamics because of the compressor mass flow term in the dynamic equation for $x_3$. All models slightly overestimated turbocharger speed, particularly at lower load factors. This highlights the fact that in a model where state dynamics are highly coupled with each other, small errors in prediction can propagate and cause large deviations from reference data.

Following control model development, control-oriented analysis was performed on a new state-space model provided by Caterpillar for the G3500 series engine. To

understand the feasibility of decentralized control for this new engine model, the thesis extensively used the frequency-valued RGA as a tool. Through RGA number analysis, it was found that certain input-output configurations of this engine model were fairly well-suited for decentralized control, with the ideal configuration consisting of the following pairings:

- $u_1 \rightarrow y_3$: Control fuel-air ratio with throttle valve mass flow.

- $u_2 \rightarrow y_2$: Control throttle pressure differential with bypass valve mass flow.

- $u_3 \rightarrow y_1$: Control engine speed with fuel mass flow.

The intuition gained from the RGA element magnitude and phase analysis was used to formulate guidelines on which control loops to tune first in a decentralized control framework.

## 5.2   Future Work

The scope for future work is extensive within the realm of physics-based modeling and state-space equation formulation. Because many efficiency and temperature terms varied only slightly in the truth-reference data, the thesis assumed constant values for them in modeling efforts. For example, the engine torque gain term is a function of volumetric efficiency, thermal efficiency, and intake manifold temperature, all of which were assumed constant because they did not vary significantly in the truth-reference data. Adding new state variables for efficiency and temperature terms would allow a state-space model to capture more physics of the engine and possibly allow for a more accurate control model. On a similar note, during the modeling efforts of Chapters 2 and 3, there were many parameters that had to be estimated such as thermal efficiency, compressor blade diameter, turbine blade diameter, and turboshaft efficiency. Obtaining more data on all unknown parameters would allow for the development of a more accurate control model.

There is also the potential for future work in control-oriented analysis and controller development. The RGA analysis conducted on the model provided by Caterpillar can also be performed for other engine architectures to make informed decisions regarding controller design. The engine that was investigated in this thesis had a passive wastegate valve. In some engines, however, there is an active wastegate valve, which would mean a fourth control input. In a 4-input 3-output plant, RGA analysis can yield useful information on what control inputs are best at certain frequencies. This type of intuition is useful in the development of cascaded control structures, where more than one control input is paired to an output and the controller decides which control inputs to use based on frequency. Additionally, some of the coordinated control strategies that were mentioned in Chapter 1 can be applied to the model provided by Caterpillar to investigate the benefits and drawbacks of centralized control strategies in simulation and ultimately in an experimental test cell.

LIST OF REFERENCES

LIST OF REFERENCES

[1] P. Dolovai et. al. H-infinity controller design for speed control of a natural gas engine. In *Chinese Control Conference*, 2008.

[2] A. Sivasubramanian and P. H. Meckl. Numerical solution for multivariable idle speed control of a lean burn natural gas engine. In *American Control Conference*, 2004.

[3] S. Nlwa, M. Kajitani, K. Sagimori, and K. Nakajima. Development of coordinated algorithm of egr and boost pressure based on the adaptive sliding mode control. *SAE International*, 2008.

[4] *Multivariable Feedback Control Analysis and Design*. John Wiley and Sons, 2001.

[5] P. Emiliano. Spark ignition feedback control by means of combustion phase indicators on steady and transient operation. In *ASME Journal of Dynamic Systems, Measurement, and Control*, 2014.

[6] System for decoupling egr flow and turbocharger swallowing capacity/efficiency control mechanisms. Technical report, Cummins, Inc., 2002.

[7] Y. Wang, I. Haskara, and O. Yaniv. Model-based quantitative feedback control of egr rate and boost pressure for turbocharged diesel engines. In *American Control Conference*, 2008.

[8] L. Guzzella and A. Amstutz. Control of diesel engines. *IEEE*, 1998.

[9] M. Iwadare, M. Ueno, and S. Adachi. Multi-variable air-path management for a clean diesel engine using model predictive control. *SAE International*, 2009.

[10] M. Wendeker, G. Baranski, and P. Magryta. Model-based control for air-fuel ratio of natural gas fueled si engines. *SAE International*, 2014.

[11] P. Lino, B. Maione, C. Amorese, and S. de Mattheis. Modeling and predictive control of a new injection system for compressed natural gas engines. In *IEEE International Conference on Control Applications*, 2006.

[12] Z. Weige, J. Jiuchun, X. Yuan, and Z. Xide. Cng engine air-fuel ratio control using fuzzy neural networks. In *IEEE International Workshop on Autonomous Decentralized System*, 2002.

[13] T. Lee and Z. Filipi. Nonlinear model predictive control of advanced engines using discretized nonlinear control oriented models. *SAE International*, 2010.

[14] M. Kaiadi et. al. Transient control of combustion phasing and lambda in a six-cylinder port-injected natural gas engine. *ASME Journal of Engineering for Gas Turbines and Power*, 2010.

[15] J. Anders and M. Franchek. Nonlinear adaptive engine speed control using an instrumental variables approach and a truncated volterra series. In *ASME International Mechanical Engineering Congress and Exposition*, 2005.

[16] K. Stricker et. al. Turbocharger map reduction for control-oriented model. In *ASME Dynamic Systems and Control Conference*, 2011.

[17] L. Kocher et. al. Control-oriented gas exchange model for diesel engines utilizing variable intake valve actuation. In *ASME Journal of Dynamic Systems, Measurement, and Control*, 2014.

[18] M. Farina and G. Trecate. Decentralized and distributed control models of large-scale systems. 2012.

[19] Closed loop diesel engine egr control including event monitoring. Technical report, International Engine Intellectual Property Company, L.L.C., 2002.